Small Scale Unmanned Aircraft for Environmental Monitoring

by

James Yuen

A thesis submitted in partial fulfillment of the requirements for the degree of

Master of Science

Department of Mechanical Engineering

University of Alberta

Abstract

Advances in sensor technology and unmanned aircraft systems (UAS) have created the opportunity for low cost aerial monitoring. As much of this development is not tailored for remote sensing applications, a custom built UAS was used to test the feasibility of inexpensive monitoring over forested and farmland case studies. This system flew autonomously at 50 m altitude above ground level, to create visual wavelength maps with 3 cm resolution and better than 5 m horizontal accuracy. Images were collected with 2 m spot size point spectrometer readings at 4 Hz, for identification of specific compounds. In test runs, approximately 15 acres were surveyed in just over 9 minutes. Methods developed can be applied to industrial monitoring applications such as tailings pond surface moisture content estimation and petroleum leak detection for pipelines.

Acknowledgements

I would like to thank Dr. Michael Lipsett for his support and guidance throughout this project, the Mechanical Engineering machine shop and support staff for their assistance, Dr. Benoit Rivard for his expertise, and my laboratory cohorts for their generous support.

In particular I thank Stephen Dwyer for his assistance in building the UAP platforms, programming and tuning the autopilot, operating the ground station, and setting up the DTMF tone generator and parser. Thank you to Derek Russell for executing a number of the laboratory soil sample tests against the ASD FieldSpec, and to Nicolas Olmedo for his assistance conducting the sand target field trials.

Most importantly I am grateful for the patience, support, and love of my wife Lauren, without whom this undertaking could not have been completed.

Contents

List of Figures

List of Tables

Chapter 1

Introduction

An aerial view can change the entire perspective on a problem. Whether it is the ability to immediately assess the extent of an oil spill, count the number of livestock in a herd, or map the productivity of farmland, an overhead view is invaluable for many tasks. In the past, it was been too difficult, expensive, or dangerous for most people to obtain this view, leaving it strictly in the domain of the military and other large, heavily funded organizations. Even the simplest method of manual photography from manned aircraft has a price point that limits when, where and how often aerial images can be taken. With recent advances in sensor technology and processing capability, this work aims to demonstrate how an airborne system can now be implemented at a low cost to collect accurate data.

1.1   Background and Motivation

1.1.1   Remote Sensing

Remote sensing can be defined as acquiring information from a distance much larger than the dimension of the sensor [61]. For practical applications, this generally refers to data collection from

satellite or airborne sensors. In this sense, remote sensing has been in widespread use throughout the military and scientific communities for many years. While initially developed for military reconnaissance and extraterrestrial exploration [39], remote sensing technology is well established for terrestrial scientific study. Canada has been actively involved in the community since the creation of the Canada Centre for Remote Sensing in 1971, and a key player in the Landsat program [50]. Terrestrial scientific applications are wide ranging, including population studies, natural resource mapping, and environmental monitoring [31].

Due to these successes, interest is growing in remote sensing for industrial applications. Aside from mining, where airborne and satellite data has been used effectively for mineral exploration [63], application has been limited, despite the potential for increased efficiency of industrial activities. This is partly due to the availability, cost and analysis requirements of traditional remote sensing missions. Although satellite data is now readily accessible commercially, many monitoring cases such as utility inspection and precision agriculture require higher resolution, lower repeat times, or both [8]. This greatly limits the utility of satellite data for these cases, and requires low altitude airborne data collection. Due to the complexity and risk associated with launching a satellite or flying a full scale, manned aircraft to carry large, expensive sensors, this high cost has simply been required to build remote sensing datasets.

With the ongoing miniaturization and cost reduction of computing technologies, high processing capability is now available to accomplish data reduction and sensor fusion on small systems. Just as crucial, sensor capability, mass, and cost have also improved significantly in recent years. For example, Headwall Photonics now manufactures the Micro-Hyperspec sensor which squeezes an imaging spectrometer and full Inertial Measurement Unit (IMU) with Global Positioning System (GPS) into a package under 2 lbs [33]. At the low end of the price spectrum, Ocean Optics now offers the STS spectrometer which fits a point spectrometer into a 50 mm cube weighing just over two ounces for under $2000 [52].

This has generated interest in applying this technology to remote sensing. It is now possible to construct small scale, low cost Unmanned Aircraft Systems (UAS) that are capable of carrying

simplified remote sensing payloads. Since the size and cost of these systems is a small fraction of the investment required for conventional remote sensing, it is economical to deploy UAS to collect data in areas and applications where it was not possible before [31]. This results in not only reduced cost and risk, but can also improve the efficiency of the monitored processes. The application to the oil, utility, agriculture and forestry industries is of particular interest, as they represent a large sector of economic activity in Alberta. These industries also require the location of assets distributed across large areas of land which has made them difficult and costly to monitor in the past.

1.1.2   Unmanned Aircraft Systems

Although manned and unmanned kites and balloons were first used for remote sensing, military development of manned aircraft rendered them obsolete [6, 39]. With recent developments in miniature electronics UAS use has exploded. In 2004, the US Department of Defence completed more than 50,000 UAS flight hours[1] for the first time [80]. Just six years later, over 550,000 hours[2] were achieved in 2010 [80]. Similar growth is now occurring in the civilian sector due to the availability of inexpensive and high performance microchips, sensors, and aircraft. There is an ever expanding online community of hobbyist UAS developers that is driving the growth of a low cost UAS component marketplace. In 2008, ten months after its launch, the website `diydrones.com` had 1000 members and 5000 daily page views [4]. As of March 14, 2013, those numbers were up to 36,000 members and over 70,000 page views every day [5]. Along with user blogs and forums, DIY Drones also operates a web-store with over 300 UAS products. This well established community shows that the UAS market is here and ready to expand into the commercial sector.

One major reason this expansion has not occurred en masse is that, as with many new technologies, regulations surrounding UAS use are lagging behind development. The International Civil Aviation Organization held meetings starting in 2005 with member states including Australia, Canada,

---

[1]These figures do not include UAS 20 lbs and under, of which the Department of Defence had 6810 in their possession in July 2011 [80].

[2]See above footnote.

3

Finland, Italy, Malaysia, Sweden, UK and the US to implement special operating procedures for UAVs [13]. In many of these countries there are now procedures in place that allow for UAS implementations, and commercial operations are becoming more and more common. A notable exception is the US, where at the time of writing federal, state and local government agencies can apply for a UAS Certificate of Authorization, but there is still no legal process to fly a UAS for profit. This is in stark contrast to other countries such as Japan that "had more than 2,000 Yamaha Rmax unmanned helicopters in service for agricultural purposes by 2002" [13]. The US FAA has been mandated to integrate UAS into the national airspace system by 2015 [22], at which point the US market will explode as there is already a well established base of commercial UAS suppliers.

Since the technology is still new, the risk evaluation and liability analysis process is still being improved. In Canada UAS operation requires the receipt of a Special Flight Operations Certificate (SFOC) from Transport Canada, which is issued upon review of a risk analysis and contingency management plan prepared by the UAS operator. Although turnaround time on the SFOC can vary, the regulatory process is continually improving as UAS become more common, and soon will be well established process that does not hinder deployment. For example, the governments of Alberta and Nevada signed a Memorandum of Understanding on July 29, 2013 to encourage opportunities in unmanned vehicles [26], which should aid in the development of UAS.

As with other robotic systems, it is the ability of UAS to excel in dull, dirty, or dangerous tasks that has made them so suitable for military service. Remote sensing, particularly in certain environments, meet these criteria which makes UAS a good candidate technology for industrial monitoring. By using an autonomous system, survey lines can be flown more consistently while people remain in a safe location. One example of a recently introduced small UAS is the Gatewing X100 aerial mapping system, which is a 2 kg, 100 cm wingspan system for easily creating orthophoto mosaics and digital surface models (DSM) [73]. Although not adaptable to other payloads, this type of system is actively used for land surveying after it was acquired by Trimble and released as the UX5.

1.1.3   Industrial Monitoring and Distributed Asset Management

Within the broad field of environmental monitoring, this work aims to evaluate the use of UAS technology to support the remote monitoring of the large oil and forestry industries operating in Alberta. Of particular interest is the early detection of leaks along pipeline corridors and monitoring of oilsands tailings ponds.

All pipeline corridors operated in Canada are required to be visually inspected [12] every two weeks for erosion, leaks, and vegetation or construction encroachment [74]. The traditional method used is human visual inspection from aircraft, truck, ATV, or foot. While this is sufficient to monitor vegetation or construction encroachment along the right of way, it is not efficient at detecting subtle features and is vulnerable to human error. Pipeline weeping leaks can go undetected for some time if the flow rate is below the resolution of the flow-rate based electronic process monitoring systems [74] used to control the pipeline. By Alaska state code, pipeline leak detection systems must be able to detect leaks larger than 1% of daily throughput if technically feasible [72]. In Canada, CSA Z662 [12] defines time periods that flow calculations must be made in and restricts uncertainty to 5% per 5 minutes, 2% per week, or 1% per month [12]. On pipelines that can easily carry over 500,000 barrels of oil a day [11], weeping leaks are still significant and even with regular aerial surveillance can be difficult to detect. Pilots visually inspecting the corridor have difficulty spotting these leaks until a large surface pool has formed. About 30% of hazardous liquid pipeline leaks in the US from January 1, 2010 to July 7, 2012 were first reported by members of the public who came across a spill [68], which indicates that there is room for improvement in this monitoring procedure. The lower cost of owning and operating a small UAS compared to manned surveillance allows a larger fraction of the monitoring budget to be put towards advanced sensors that can more efficiently detect leaks or other targeted features. It would then be possible to monitor more frequently, efficiently, and effectively.

Another area that has proven challenging to monitor with traditional means are the oilsands tailings ponds in northern Alberta. A byproduct of the oilsand refining process is a mixture of water, sand, silt, clay, and small amounts of bitumen [21]. Tailings mineralogy and water content result in

5

slow consolidation, caused in part by thixotropic properties [70], which leads to an extremely long duration before the tailings regain enough strength to support the load of people and equipment. This is extremely important, as until heavy equipment can be deployed the reclamation process cannot be completed. The most important factors effecting this process are the water content and mineralogy of the tailings [70]. As ore sources are variable, the makeup of each tailings pond can vary by location. To date, the unstable nature of these ponds has severely limited the ability to monitor the settling process. Occasional monitoring can be done during the summer with a hovercraft [20] or amphibious barge, and some ponds can support the weight of people and equipment in the winter. Aside from the long time requirements of these methods, they are also fairly high risk to the personnel who are sent out onto the unstable surface. Again, the application of small UAS to this monitoring task would reduce risk to people and provide useful data that is currently too difficult or expensive to collect. With over 170 km^2 [27] of tailings ponds currently in Alberta, an airborne system equipped with the correct sensors could efficiently monitor the area by providing high resolution data from a low altitude. This data could be used for the mapping of tailings pond surface mineralogy and predicted trafficability, greatly aiding in the reclamation process.

Industrial monitoring is generally high cost, and in some cases even high risk to personnel. High cost has also prevented the use of remote sensing and UAS in industry to date. By applying new technology, this cost and risk is greatly reduced and can result in improved efficiency.

1.2 Objective of the Thesis

This thesis will attempt to demonstrate the feasibility of a small scale, low cost UAS for monitoring the environmental impacts of industrial facilities. It will contribute a practical design methodology and provide an affordable procedure for obtaining aerial remote sensing data. Monitoring applications in the pipeline, oilsands, and forestry industries will be addressed in more detail. Of particular focus will be the measurement of tailings pond stability and hydrocarbon leak detection around industrial facilities. To study this a small UAS will be developed and used in a number of field

trials to evaluate its effectiveness in observing a number of known targets. Differences between this system and the requirements of an industrially deployed version will also be discussed.

1.3   Organization of the Thesis

Following this introduction is a literature review in Chapter 2 of recent work in remote sensing and civilian UAS development pertaining to this thesis. Chapter 3 covers the methodology followed in this study, including details on sensors, the UAS platform, software, and test plan. The results of lab and field testing are presented in Chapter 4, along with an assessment of overall performance, uncertainty, and current limitations. Finally, Chapter 5 summarizes the conclusions of this work and areas for future laboratory development and industrial application.

Chapter 2

Literature Review

Recent literature relevant to remote sensing of industrial installations is presented in this chapter. Developments in remote sensing, civilian UAS development, observation of mines and pipelines, and sensor fusion and registration are covered. Previous monitoring solutions and their limitations are discussed.

2.1 Remote Sensing

First, developments in 'traditional' remote sensing are covered, which in the context of this work refers to the large scale satellites and aircraft that have been commonly used for earth observation studies.

2.1.1 Soil Moisture

An important characteristic of engineered tailing soils is the water content, as this is directly related to their stability and trafficability [70]. The specific application of remote sensing for water content of tailings ponds is just beginning [21], but there has been extensive work in measuring soil water

content. Bryant [10] provides a good overview of remote sensing techniques for monitoring soil moisture content: hyperspectral, thermal infrared, and radar.

Hyperspectral methods look for the typically higher albedo of dry soils. Landsat TM bands 5/7 and 5/4 have been used with some success in the past to develop good correlations with soil moisture [10], particularly if the type of soil is known. Finn [24] tested the correlation between airborne hyperspectral and ground moisture readings in northern Florida. It was shown using the SWIR HyperSpectral Imaging sensor that bands in the 1000-1600 nm range can be used to estimate soil moisture to a 2 in depth. Entezari [21] has done lab spectral characterization for some tailings samples from mines in northern Alberta and was able to correlate spectral measurements and moisture content with R^2 above 0.8. It was found that the absorption depth at 1450 nm was able to achieve the best accuracy in samples above 15% moisture content. Below 15%, the depth at 1925 nm gave the best result.

Thermal infrared measurements over a diurnal cycle can be used to estimate water content if air temperature is also accounted for. This is due to the high heat capacity of water which causes water logged soils to change temperature more slowly than drier soil in the same area. In ground testing Bryant [10] found similar results for 3 tested soils, indicating this method may be fairly independent of soil type. Minacapilli [47] evaluated the ATM Daedalus 1268 airborne sensor (11 bands between 0.42 - 13 µm) and got good results using the Johansen model of the relationship between soil thermal conductivity and soil volumetric water content. Minacapilli was able to confirm the results of previous laboratory studies, showing that the Johansen model can be applied to remote sensing applications.

Radar methods measure the moisture varying dielectric constant of soil. Due to the added complexity of implementing a radar system on a small UAS, this method was not pursued in this work. It is worth noting that as technology continues to evolve it may soon be practical to deploy a small airborne radar system at which time this work can be extended.

The success of these methods in measuring soil moisture suggests that it will be possible to implement a combination or variation of the above methods to give remote measurements of tailings

moisture.

2.1.2 Surface Hydrocarbon Detection

To locate leaks along pipelines it is essential to have a robust method for identifying the presence of hydrocarbons. In a series of experiments, Allen [1, 3] characterized the reflectance spectra of common hydrocarbons (crude oils, gasoline, diesel, motor oil) on various substrates including concrete, gravel, grass, sands and clays. He found it was possible to distinguish these hydrocarbons from each other and water using an ASD FieldSpec Pro-FR2 (350-2500 nm). Airborne hyperspectral sensing was shown to be very effective at determining the presence of hydrocarbons by identifying small adsorption features at 1730 nm and 2310 nm [35]. Using the Hymap[37] sensor, colour composite images were generated without atmospheric correction that vividly highlighted areas with hydrocarbons present. Some preliminary work was also done to apply this spectral library to identify oil spills from airborne SpecTIR HST-3 imagery over some recent spills caused by Hurricane Katrina [2], with encouraging results. Lammoglia [41] also conducted some lab and field measurements of 17 hydrocarbon samples with an ASD Fieldspec Pro (350-2500 nm) to develop a library for characterizing offshore hydrocarbon seeps from remote sensing data.

At a much larger scale, satellite data from ASAR, MERIS and SPOT-5 was used in an earth observation trial of the Shell and Albian oil sands mines in northern Alberta [15]. Data sets were produced showing land cover and the percentage of leased land and watershed with active mining activity of the region. This successfully demonstrated the potential of earth observation to support sustainable development practices.

This shows that with appropriate sensor selection it is possible to identify the presence of hydrocarbons, and it may be possible to classify the hydrocarbon with sufficient resolution. Although satellite systems already exist, UAS allow for much higher resolution, adaptable payloads, and user determined repeat measurement periods. This work aims to show it is even possible from a small, low-cost UAS.

2.1.3 Small Scale Sensors

As much of the remote sensing literature uses large scale sensors and aircraft, it is also important to note some development that has used sensors that could be flown on a small UAS. For the purposes of this work, a small UAS will be defined as having a takeoff weight between 1-10 kg, similar to the definitions of *Mini UAV* by Weibel [79], and *Group 1 UAS* by the US Department of Defence [80].

Edmonds [18] used a small Ocean Optics S2000 spectrometer and fore-optic to take atmospheric measurements from ground stations. Although no longer available for purchase, the S2000 was 143 mm x 104 mm x 40 mm, weighed 200 grams, and required 130 mA at 5 VDC, making it suitable for airborne use. A USB2000 was also used from a helicopter to monitor SO_2 volcanic emissions. These measurements were made from a 100 m standoff distance and required a 200-1000 ms integration time. In a similar SO_2 application, McGonigle [46] used a USB2000 from a standoff distance of approximately 2500 m and a 130-1000 ms integration time. With a similar setup for UV SO_2 measurement, Horton [36] required an integration time of 300-1000 ms. The equipment used in these applications are similar in size, weight and standoff to what would be required for a UAS deployment, but the long integration time would be difficult to accommodate on a UAS.

Although larger than the scale considered in this work, Groeneveld [28] demonstrated that it is possible to fly a commercial point spectrometer without much integration and get results accurate enough to perform empirical line correction of satellite hyperspectral data. With an ASD spectrometer and inexpensive handheld GPS, they were able to collect spectra from 500 ft with a 2.7 x 16.1 m ground spot. This corresponds to half a Landsat TM pixel, so it can be used for correction.

One of the major unknown factors in using small spectrometers on a UAS is the integration time that will be required to achieve a sufficient signal to noise ratio. No previous work was found that used a point spectrometer without custom manufactured fore-optics for airborne earth observation.

2.1.4 Petroleum Mining and Pipelines

Although not remote, Syncrude has been using sensors at 2220 nm and 2230 nm on their incoming slurry pipeline for process control. Friesen [25] showed that it is possible to use near infrared (NIR) spectroscopy from 1100-2300 nm to identify specific conditions in upstream slurry pipelines, such as transitions between and departures from steady states. A principal component analysis (PCA) was used to determine specific ore type and water content compared to initial measurements. This could be used to further enhance the refinery process control to increase efficiency.

Work has also been done to estimate the bitumen content of oil sand from infrared reflectance spectra [60]. Rivard was able to develop predictive models with less than 1.5% error compared to laboratory analysis. In another study, hyperspectral reflectance spectra between 300-2500 nm was used to predict the bitumen and fines content of oil sand ore samples [59]. A good correlation was found using wavelet analysis of the spectral measurements. This is encouraging as some of the same principles may be applied to remote sensing of oil sand ore and tailings.

Some remote sensing work has been done on monitoring mine sites and utility corridors. Since there has not been much remote sensing work on oilsands tailings (our work), results from monitoring other mine sites is looked at. Zabcic [82] used the Hymap hyperspectral sensor to map the pH of acid mine drainage from the Sotiel-Migollas mine in Spain. Using a partial least squares method to determine the relationship between recorded spectra and pH, an r^2 value of 0.71 was obtained.

In a preliminary study to test the effectiveness of vegetation stress for detecting pipeline leaks, Meijde [75] was able to find small leaks. In areas with a red edge shift (711-716 nm) due to reduced chlorophyll, core samples were taken to confirm the presence of hydrocarbon contamination. No airborne testing was done, but Meijde indicated that aerial trials would be the next step.

Some work has been done by Dimitrova [16] to classify and test the strength of tailings from the Clarabelle Copper Mine in Sudbury, Ontario. These silty sand tailings were mixed to form a 180% water content mixture and left to settle over 3 days. The shear strength was then tested with a fall cone device. A similar procedure could be applied to characterize oilsands tailings and evaluate the

performance of remote sensing techniques.

2.2   Civilian UAS Development

With the reduction in cost and size of electronic components, it has become affordable for hobby-ists to build simple UAVs. The commercial introduction of MEMS accelerometer and gyroscopes greatly accelerated this process, and low cost autopilot systems with good performance can now be affordably had. Many people have identified the opportunity to use this technology to develop versatile sensor platforms for research. Small UAS are very attractive as environmental remote sensing platforms for several important reasons:

- low cost - the entire UAP3 UAS that was built for this work cost less than $6000, which is less than the typical cost of manned aerial orthophoto acquisition [39]. Nagai's [49] $43,000 UAV mapping payload is relatively 'low cost' in the realm of aerial imaging. UAP3 has a 1.7 m wingspan, maximum takeoff weight of 2.7 kg, and further details are presented in Section 3.2.

- easily portable - can be transported and deployed at a field site with one or two people and a regular vehicle

- low operating altitudes of less than 400 ft can easily give centimetre resolution compared to the meter resolution of other methods (satellite, manned aircraft) [40]

- reduced risk - no pilot onboard, and the small size and weight limit damage in event of a malfunction or crash.

Suzuki [71] showed that a hobby type aircraft equipped with an autopilot and consumer off-the-shelf point and shoot cameras can create a very low cost vegetation monitoring system. By putting two cameras on the UAV, one with its IR filter removed, an inexpensive multispectral imaging system was created and NDVI maps were created that could identify vegetation types. Many similar systems have been built by RC aircraft hobbyists. For their extremely low cost these systems got very good results, but for detailed research or commercial work more advanced sensors are

required.

Schwarzbach [66] was responsible for the development of a UAS for environmental remote sensing using the Paparazzi [57] open source autopilot, Avantes point spectrometer, Dias thermal camera, and Vision Components CCD. This system used the SIFT algorithm [44, 42] for image matching and the Bi-directional Reflectance Distribution Function (BRDF) to analyze the data. Although the system flew successfully with its payload, it was found that the integration time of the spectrometer was around 300 ms [65] which made geolocating measurements very difficult.

There are also now many UAV manufacturers and service providers who can provide UAV platforms with various sensors. The Trimble UX5 [73] is very popular for land surveying due to is small 2 kg weight, easy portability, and completely automated workflow. Companies like ING Robotic Aviation [38] can integrate various sensor into their UAVs and run the actual data collection operation. This is attractive for people who do not have the time or expertise to operate a UAV, but would still like to take advantage of the technology.

2.2.1 Environmental Monitoring

The European PRESENSE [32] project studied the use of UAVs to monitor pipeline installations. In particular they were concerned with third party interference along the corridor and detection of gas leaks in the range of 0.01-10 m^3/h. A mix of optical, infrared and SAR sensing methods were used, and although some promising initial results were found a complete system was never demonstrated in this project.

Using RC helicopters as sensor platforms has been done to good effect in volcanic plume and vegetation monitoring. McGonigle [45] used Thunder Tiger Raptor 90 which was flown under RC to monitor the plume of the La Fossa crater with spectrometers for airborne measurements. The results were encouraging and enabled measurements to be taken from inside the plume which before had been too dangerous and expensive. Berni [8] used a Benzin helicopter outfitted with the Tetracam MCA-6 multispectral and a FLIR thermal camera for vegetation monitoring. They were

able to produce ground verified maps of chlorophyll concentration and water stress levels.

2.2.2 Archaeology

Another field of researchers who have been quick to incorporate UAS into their work are field archaeologists. It is very important to document an excavation site, and the best vantage point to do so is often from above. In the past people have used pole and tower mounted cameras to get this vantage point, but for large areas this is difficult and time consuming.

Aircraft are commonly used as aerial camera platforms, but archaeologists have found that kites provide a low cost platform that covers the relatively small area of most sites with ease [6]. Verhoeven [77] was recently able to obtain sub-meter accuracy with a kite, Nikon D80 camera, and Agisoft PhotoScan structure from motion (SfM) software. This resulted in a map and Digital Elevation Model (DEM) of a Roman quarry site with 0.137 m horizontal and 0.310 m vertical accuracy using the National Standard for Spatial Data Accuracy.

Oczipka [53] used an octocopter platform with a Leica M8 camera to collect aerial imagery over sites in central Mongolia. The imagery had about 5 cm resolution and the location was verified with a Trimble DGPS unit. Eisenbeiss [19] completed an investigation on the use of UAVs for archaeological documentation with a series of case studies in Peru, Honduras and Bhutan. Using the Copter 1B, MD4-200 and Falcon 8 with Canon, Nikon and Panasonic consumer cameras, they were able to achieve image resolution around 1-3 cm and DSM and accuracy in the sub-10 cm range. These commercial rotorcraft cost in the 20-40k Euro range, which it is noted is low compared to manned alternatives, which is important to fit low-budget projects. The handling of these systems can also generally be learned in only 3-4 days.

2.3 Sensor Fusion and Registration

When using a system with multiple sensors it is crucial to have a method for synchronizing data from each sensor with one another and an external reference. Sensor fusion is the process of taking this data from multiple sources and combining it to create a product that is more valuable than using the data separately [34]. For UAV applications, this typically requires the timestamping and geolocating of sensor measurements. With the prevalence of GPS, an accurate time and position source is readily available and used in most systems.

Rodriguez [62] developed a system architecture for synchronizing video and telemetry data on a small UAV. This method aligns all sensor data to GPS data using known sensor delays and interpolation where required. Matching to GPS data ensures that the most accurate position data is used and reduces offset errors due to the motion of the vehicle. Rodriguez also used an analog camera to allow telemetry matching to be done onboard and transmitted to the ground control station (GCS) in a realtime video feed.

To register and mosaic data from multiple cameras on a UAV, Orduyilmaz [54] used software to align images with automatic control point detection. The system used green, red, and NIR sensors to allow the generation of normalized difference vegetation index (NDVI) products from the mosaics. Heterogeneous regions of interest were selected for control point detection to reduce errors in processing. This shows that photo alignment using automatic control point detection can be effective, which is crucial to developing a feasible UAV imaging system.

Most automatic control point detection algorithms have difficulty or fail on image scenes without distinctive features. Du [17] developed methods for mosaicking multispectral images with large homogenous areas. The strategy involves using regions with higher variability for control point selection followed by identification and removal of control point outliers. Manual and automatic evaluations were conducted and misregistrations of approximately one pixel were found across the image. This type of approach will be helpful for processing imagery of agricultural fields that are of industrial interest but have large homogenous areas.

Nagai [49] developed a UAV mapping system consisting of digital cameras, IR cameras, a laser scanner, IMU, and GPS. Sensor fusion in this system was a challenge; the procedure involved differential GPS processing, a GPS and IMU Kalman filter for sensor trajectory, and a bundle block adjustment of the images. This workflow produced a sensor package path that the laser scanner data could then be matched with. A similar procedure of using image data to help correct and register other sensor data shows promise in lower cost applications as well and was pursued in this work.

2.4   Concluding Remarks

There has been rapid development in the remote sensing field with the introduction of readily available, low cost, MEMS accelerometers and gyroscopes. This has led to the development of small measuring equipment, and UAVs which have the potential to carry advanced payloads. Many people have taken interest in using small-scale civilian UAS for remote sensing and many theoretical studies have concluded this would be an economical and efficient method. Despite this, there have only been a few practical demonstrations of the technology at a price point that would make it economical for widespread use. Currently available systems are too expensive for the majority of potential users to afford, and typically do not allow for integration of custom payloads by the user. This work gives a framework for developing low-cost UAS for remote sensing that can be reconfigured to carry specific payloads. The key design issues addressed are the integration of low cost sensors and components into a UAS, and the commissioning steps required to produce a functional and useful system for remote sensing of hydrocarbons, vegetation and surface moisture content. While many UAS are now available, the process of developing a low cost system for a specific mission objective has not been well documented.

17

Chapter 3

Methodology

3.1   General Methodology

As the research goal is to develop a framework for low cost remote sensing, the system was custom built in-house for sensing of vegetation, surface moisture and hydrocarbons. The UAS was used to test the ability of low cost sensors and components to perform remote sensing tasks that are typically not possible with a small budget. By conducting the design and development of the UAS in-house, the system could be tailored to this study and all components selected and customized for it. While some pre-built systems are available, they are generally more costly and do not allow for the level of customization required to develop the framework. Most importantly, this allowed the system to be low cost, lightweight, and tested to emulate an industrial application. Case studies involving field testing were done for the forestry and oil industries. Although the exact system used for this testing would not be suitable for direct industrial deployment, the design methodology and test procedures are general enough to be used for a specific industry requirement. An upgraded payload and airframe may be enough to meet many industrial needs by measuring specific target wavelengths from a ruggedized and weatherproofed package. More detail on the design and development of the UAS can be found in Section 3.2.

3.1.1 General System Concept

The system consists of a small hobby aircraft outfitted with an autopilot and sensory payload, as shown in Figure 3.1. This creates a UAS capable of remote or automatic operation from a field
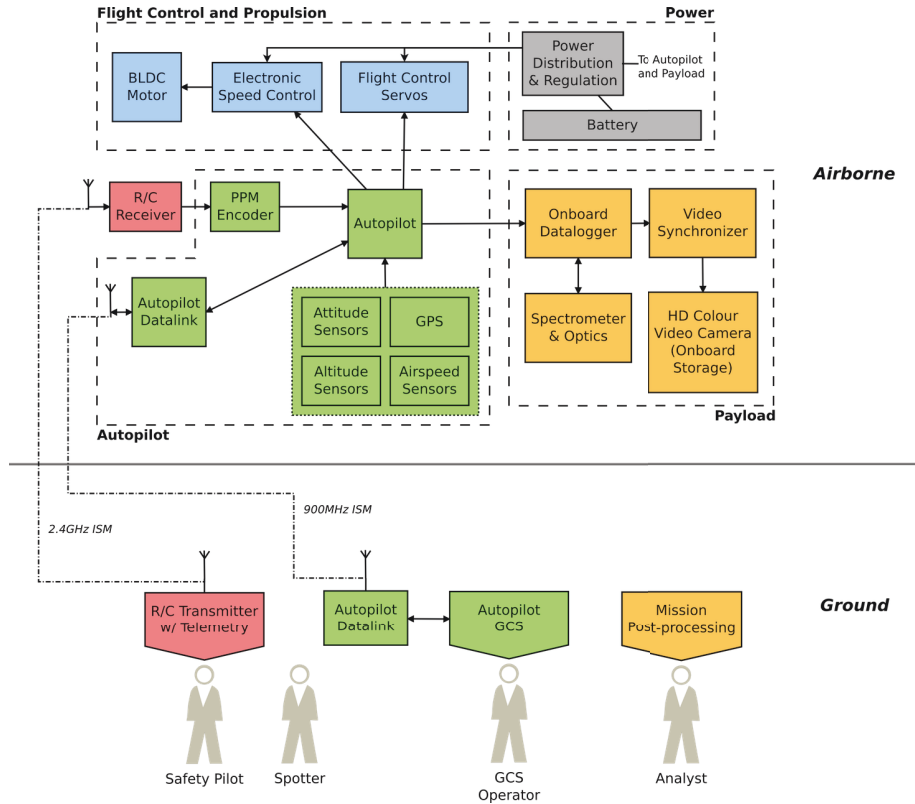
Figure 3.1: UAS architecture block diagram

deployed ground station while carrying a light payload. Autonomously following GPS waypoints allows the system to conduct user defined survey patterns with greater accuracy and repeatability than even an experienced remote pilot. Building the UAS and ground station keeps the cost low and allows customization for the purposes of this demonstration. For simplicity the aircraft records all data onboard which will be offloaded for processing post-flight.

3.1.2 Sensory Options

Selecting a sensor first requires detailing the mission profile to determine goals and observation requirements. This then leads to the assessment of sensor options. The goal of this work is to fly mapping missions over remote terrain while taking measurements to aid in detecting oil spills, vegetation health, and moisture content. Although the ideal sensor would be a full imaging spectrometer, the purpose of this work was to determine the feasibility of producing a useful dataset at a price point that would be commercially attractive. As small imaging spectrometers cost in the $50,000 – $100,000 range, other solutions had to be found to remain light weight, inexpensive, and able to emulate an industrial application. To be useful, all sensor measurements must be georectified to match data with a real-world coordinate system. This georectification process is detailed in Section 3.3.

Visible

In the most basic application, only a visible light camera is required to produce aerial maps of the area being monitored or surveyed. The purpose of this study is to go further and demonstrate a procedure for collecting data not visible to the naked eye without significantly increasing cost. With a full imaging spectrometer a dedicated visible camera would not be required, but low cost point sensors can be paired with a camera for mapping and context of their measurements. In general a camera with a full frame shutter is preferred as this reduces the effect of vibration. If vibration levels are low, it may be possible to use cheaper and more readily available alternatives. As the camera market is very large, the general camera categories that were considered for this work are listed with their advantages and disadvantages in Table 3.1.

To keep the cost and size of the system low, sensor selection focussed on small consumer cameras. Although a point-and shoot camera would also produce good quality imagery, the GoPro Hero2 camera was selected. This was primarily due to its small size and video recording capability as it can easily be mounted on any aircraft and the video provides an additional data product. The

Table 3.1: Basic camera options for visible imaging.

Camera Type	Advantages	Disadvantages	Cost
Remote Sensing Metric (Trimble Aerial Camera)	Fully calibrated, low distortion, high image quality, external control	Expensive, 15 cm cube, 1.5 kg	$100k-$150k
Machine Vision Camera (Teledyne Dalsa Falcon)	Low distortion, high image quality, external control	Expensive, typically require control computer	$7000
DSLR - (Nikon D300S)	Low distortion, high image quality	Large, 840 grams	$1500
Consumer Point-and-shoot (Canon PowerShot)	Small, inexpensive, 195 grams	Triggering usually requires custom work	$500
Consumer Mini Video (GoPro)	Small, inexpensive, 100 grams	Synchronization with flight data required, lens distortion	$300

development effort associated with integrating the point-and-shoot or video camera was thought to be similar as work would be required for the triggering or synchronization. Lens distortion in the GoPro cameras is significant, which may have required calibration to correct during post-processing and rectification. If a procedure could be developed to handle this worst case scenario, then other sensors should produce better results. A working process for the GoPro would also drastically reduce the entry requirements in system cost, size, weight and complexity to collect airborne imagery.

Spectral

Spectrometers can be used to measure reflectance spectra and identify targets based on absorption features. For a pipeline monitoring application, the detection of hydrocarbons is particularly important and there are distinctive hydrocarbon absorption features at 1730 nm and 2310 nm. Horig [35] achieved particularly good results with the Hymap [37] sensor using bands 21 (1668.22 nm), 26 (1729.31 nm), and 31 (1788.98 nm). Table 3.2 shows the specifications of suitable spectrometers considered for this study.

Headwall Photonics manufactures the High Efficiency Hyperspec® SWIR (900 - 2500nm), which

covers the range used by Horig. This is a full imaging spectrometer which is ideally suited to this application other then its $100,000 price range. A more affordable solution was to use a point spectrometer with a visible camera to collect low spatial resolution data. Small point spectrometers from Ocean Optics covering these wavelengths are in the $20,000 range. The unknown was that these sensors have not been used in airborne earth observation applications, so testing was required. To reduce risk and enable this testing, a visible wavelength range spectrometer costing $3,000 was used to evaluate the feasibility of an airborne point spectrometer and camera pairing.

Thermal

A wide selection of thermal imaging cameras are available to be flown on a small UAS for surface temperature measurement. While extremely useful for detecting people and under-watered crops, they can also be used for thermal inertia methods by taking measurements over a diurnal cycle. This approach has been successful to remotely measure soil water content and could likely be applied to tailings pond monitoring as well. Since a large contributing factor to tailings stability is simply water content, these methods could be easily adapted. A UAS would also be well suited to this task as multiple measurements over the ponds are required over an entire day which would be very expensive with traditional manned sensing techniques. This work focussed on spectral sensing, but the thermal option is a promising area for future research in tailings monitoring. One of the key factors in determining tailings stability is the water content, and diurnal thermal measurements have been effective in estimating soil moisture concentration [10, 47].

Table 3.2: Survey of available spectrometers.

Sensor	Wavelength Range (nm)	Spectral Resolution (nm)	Spatial Resolution (bands)	Mass (kg)	Price
Headwall High Efficiency Hyperspec NIR	900 -1700	12	640	3.3	$175,000
Headwall High Efficiency Hyperspec SWIR	900 - 2500	14	320	3	
Headwall Hyperspec SWIR	1000 - 2500	8 - 12	320	4.1	$95,000
Headwall Micro Hyperspec	380 - 1000	5	1000 - 1500	0.45	
Headwall Micro Hyperspec	900 - 1700	7 - 12	320 - 400	0.45	
Resonon Pika II	400 - 900	2.1	640	1	$30-40K
Resonon Pika NIR	900 -1700	5.4	320	1.5	$30-40K
Specim AsiaEAGLE	400 - 970	3.3	1024	6.5	
Specim AsiaEAGLET	400 - 1000	3.3	1600	3.5	
Electrophysics IRE320S	800 - 2500	1700	320	4	
Electrophysics MicronViewer 7290	400 - 1900	1500	650	1.4	
Cri VariSpec Filter	850 - 1800	6		1	
Ocean Optics NIRQuest256	900 - 2500	9.5	Point	1.2	$23,000
Ocean Optics USB2000+	350 - 1100	10	Point	0.2	$3000
Required Spec	1700	10		4.5	

3.2 UAS Testing Platform

Key specifications and notes on development and operation of the Unmanned Aerial Platforms (UAP) developed as part of this work are covered here. More details on the UAPs are given in Appendix C. The final UAP-3 system undergoing a field white reference calibration is shown in Figure 3.2.

Figure 3.2: UAP-3 during field white reference calibration

3.2.1 Performance Specifications

Three UAS were developed for this project, and their specifications are shown in Table 3.3. To have more flexibility in payload size, capacity and longer endurance, UAP-1 was developed with a larger airframe and gasoline engine. UAP-2 is a large body version of UAP-1 that has more room for payload and avionics integration and was not flown in this work. The start of this study coincided with the founding of the University of Alberta UAS Group, which was to share use of the UAP developed for this work. This requirement led to the selection of larger aircraft with more payload capacity for UAP-1 and UAP-2. As particular mission requirements and payloads were identified

for this study, it was found that a smaller electric powered system was sufficient and could be much more easily transported to field locations, so UAP-3 was used for most of the experiments.

Table 3.3: Key specifications for the UAS developed during this study

	UAP-1/UAP-2	UAP-3
Airframe	Hobby Lobby Senior Telemaster	Multiplex Mentor
Propulsion	26cc 2-stroke	Electric
Fuel	gasoline/oil mixture	lithium polymer batteries
Wingspan (m)	2.4	1.7
Length (m)	1.6	1.2
Max Speed (km/h)	110	90
Payload Capacity (kg)	6	2
Max Takeoff Weight (kg)	12	2.7
Max Endurance (min)	60	20

3.2.2 Development

Early in the project a custom system was determined to have the required flexibility to integrate various payloads. To speed the development of this system, effort was made to design and build it using as many off the shelf components as possible. The most crucial parts of any UAS are the airframe and autopilot. Each UAP was based on a commercially available hobby aircraft as they are readily available, inexpensive, and have proven flight characteristics. Once the payload size and mass was determined, the specific airframe was selected based on its ability to carry the desired payload. More details on the selection and development of the UAPs is included in Appendix C. The Paparazzi autopilot was chosen for its customizability and proven record, and is detailed in Section 3.2.4.

3.2.3 EO Sensors

The UAP was outfitted with a visible camera and point spectrometer for data collection. This is an affordable option to an imaging spectrometer while still providing useful spectra with visual context.

Spectrometer

An extended range spectrometer to cover the hydrocarbon absorption feature at 1700 nm is out of the budget of this work, and so a visible-NIR spectrometer was used for initial testing of the system architecture. A product review found that Ocean Optics point spectrometers were the lowest cost on the market, and were also small and light enough to easily carry on any of the UAP. Since cost was the primary constraint in this work, the USB2000+ was chosen, which is a 400-1000 nm point spectrometer. These spectrometers are typically used for lab or contact field measurements, so another unknown was the effectiveness of the available lenses from Ocean Optics for aerial sensing. The work done by Edmonds, McGonigle, and Horton [18, 36, 46] shows that the USB2000 can be used for standoff distances of over 2 km, but Edmonds and McGonigle used custom manufactured telescopes on ground based sensors. Edmonds was able to take volcanic plume measurements with a collimating lens directly attached to a USB2000, and a similar approach was taken during the initial testing of this work.

To evaluate the performance of the spectrometer, it was first tested separately from the rest of the system against a known good ASD FieldSpec spectrometer. Available Ocean Optics off-the-shelf fore-optics were tested to find an effective, low cost solution. After this stage of testing the spectrometer was integrated into the UAS and several stages of testing followed to characterize the performance of the system, including ground and flight testing. Details of this testing and its results can be found in Section 4.1.1.

Camera

A GoPro Hero2 camera was chosen to record visible light video and imagery during the flights. This camera has several advantages, including being inexpensive, small, light, and robust with the capability to record high definition pictures and video. It is also fully self-contained, which made it easy to integrate on testing flights. One disadvantage with the GoPro is that it has a wide angle lens which introduces significant barrel distortion. As the intention of this work is to produce low

cost aerial data, this distortion provided a worst case scenario for the data processing workflow developed. The GoPro also uses a CMOS sensor with rolling shutter which introduces further error as the entire image frame is not recorded simultaneously. Using a typically more expensive CCD sensor with full frame capture would remove this error, but if workable results could be obtained with the GoPro it would significantly lower the entry barriers for UAS monitoring. For future flights a camera with less lens distortion will make image registration simpler and should produce images with higher resolution and better geolocation accuracy. To provide an additional data product, it was decided to record video during each flight and use video frames to provide context for the spectrometer measurements. This required the development of a method to synchronize the spectrometer measurements with a video frame, which was accomplished with a microcontroller attached to the autopilot. At each spectrometer trigger a DTMF tone is fed into the first audio channel on the GoPro, which is later analyzed by a custom python script to extract the timing and automate image synchronization. The second audio channel records ambient noise to provide additional situational awareness. While the synchronization was not quantitatively verified, image extraction was tested in the lab by taking multiple exposures of various targets, and flight testing later showed the image and spectral data matched well. A simple test with an LED in frame could be done to verify this timing, but this was not done for this work as the system worked effectively during testing. Initial flights were done to test the image processing and geolocation workflow. Once this was demonstrated, testing moved to the fusion of spectral and image data.

After testing was completed, the GoPro Hero3 and Hero3+ line of cameras was released. These cameras are available with wifi control and up to 4k video resolution, which would make it possible to more tightly integrate a GoPro into the UAS. Triggering the camera from a wifi module on the aircraft may remove the need for DTMF synchronization as used here.

3.2.4 Autopilot

The open source Paparazzi [57] Lisa/M v2.0 autopilot [55] was selected for this system. It is a mature project with GPS waypoint navigation, GCS, failsafes, flexible system architecture, and its open

27

nature allows for modifications and additions required to integrate various payloads. Numerous PID loops, summarized in Figure 3.3, are used to generate actuator control signals from the IMU, GPS, pitot tube, flight plan, and pilot inputs. The Lisa/M v2.0 was purchased from `https:`
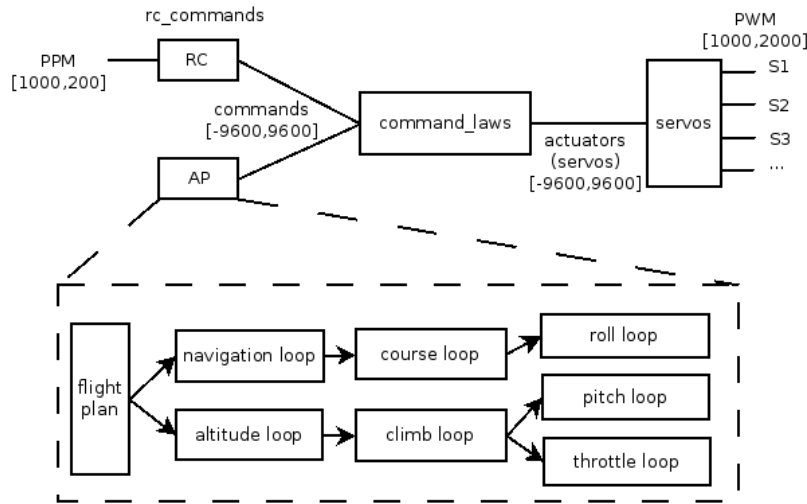
Figure 3.3: Overview of paparazzi control loops [56]

`//ppzuav.com/`, and at the end of development was running a branch of paparazzi v5.0 which is available at `https://github.com/scdwyer/paparazzi/tree/uasgroup-v5.0`. An Eagle Tree Airspeed Microsensor V3 pitot tube and sensor is used to provide the autopilot with airspeed data.

Navigation

The Paparazzi system uses a GPS receiver to drive all navigation routines. Several PID control loops use the GPS input to control the course, altitude, and speed of the aircraft. The course loop is shown in Figure 3.4, and details of all control loops are shown in Appendix C.4. The paparazzi energy-based controller was used for the latter half of flight testing as it was found to produce more stable flight. On the UAP the speed is also augmented with airspeed input from the pitot tube, which is particularly useful to ensure airspeed is maintained in windy conditions. More accurate altitude measurements can be taken by incorporating a barometer or ultrasonic
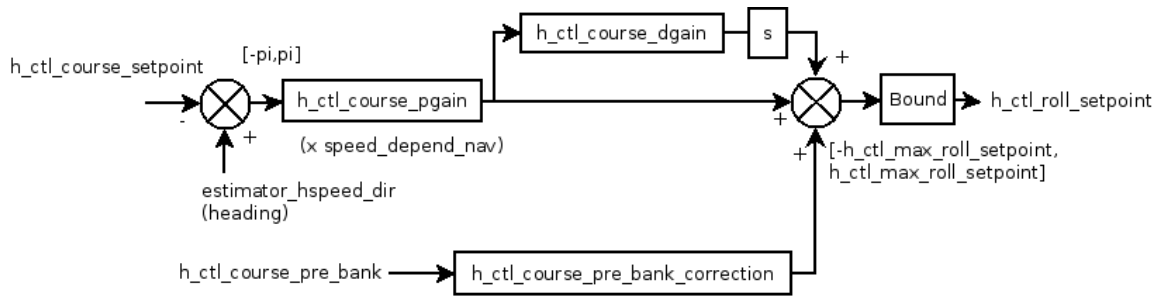
Figure 3.4: Course control, the outer horizontal control loop. [56]

rangefinder, but this was deemed unnecessary for the purpose of this work. One of the benefits of using the Paparazzi system is that many survey patterns have been created by other users and are available to be modified to suit the specific needs of each mission. Many aspects of the mission can be automated, including navigation scripts that run when certain positional or sensory conditions are met. This greatly expands the utility of the platform, allowing it to be adapted to the required mission profile.

3.2.5 Ground Station

The Paparazzi system includes a ground station with Google Maps integration that allows all aspects of the flight to be monitored and controlled in realtime during the mission. An image of the GCS interface is shown in Figure 3.5. In addition to monitoring the status of the aircraft, changes in settings can be communicated to the autopilot throughout the flight. This includes waypoint changes, flight plan progression, and control loop gain tuning. Although not used in this project, the ground station is also capable of flying multiple paparazzi UAVs simultaneously. The GCS software also includes a flight simulator which allows all flight plans to be tested prior to field deployment.

Since payload data processing is done post-flight, there is no need for a dedicated payload ground station. Payload triggering is done through the autopilot ground station or in the autopilot flight plan. All ground station software can be run on Linux and Mac computers. This testing used the

29
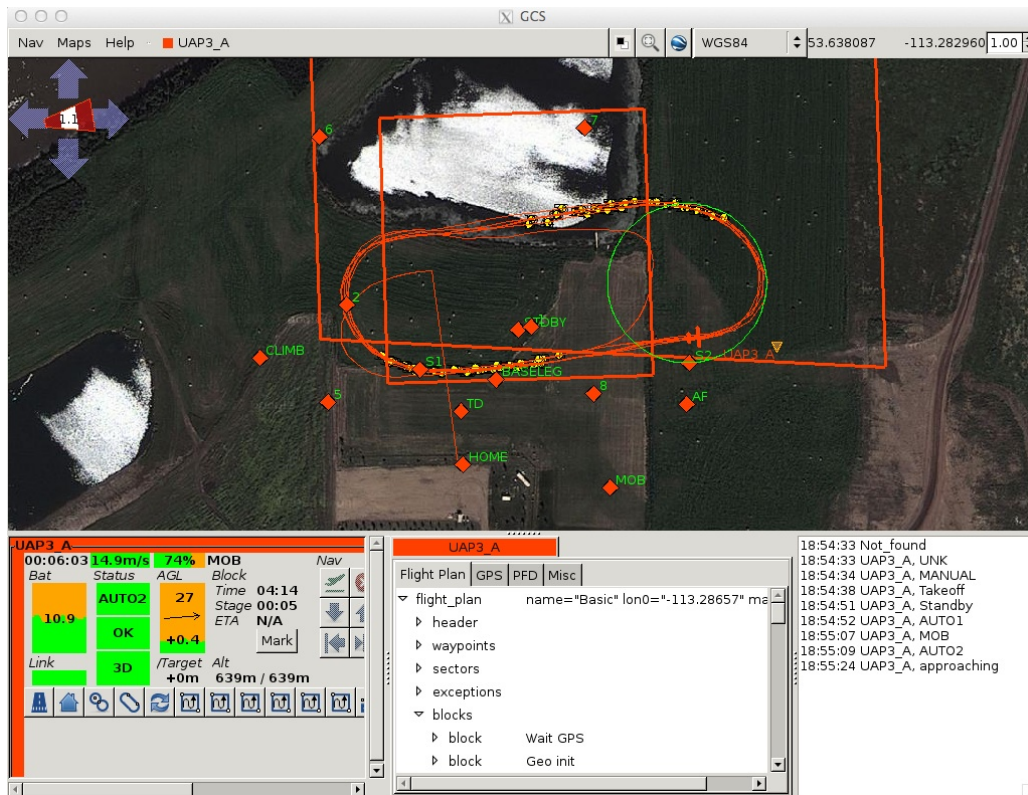
Figure 3.5: Screenshot of the GCS during a test flight at the Edmonton Bremner field.

software at `https://github.com/scdwyer/paparazzi/tree/uasgroup-v5.0` (based on Paparazzi release v5.0) running on OS X Snow Leopard.

3.2.6 Communications

There are two communications channels on all UAPs, a bidirectional data link on an XBee Pro S2 900 MHz radio modem, and Spektrum DX8 RC safety control with 2.4 GHz transmitter. The radio modem is used for communication with the autopilot and carries all telemetry to the GCS while allowing for in-flight commands and changes to be sent to the aircraft. This is required to monitor the state and position of the system and is invaluable for control loop tuning and mission execution. The RC transmitter allows for remote piloting when the system is within visual range of

the GCS. This is important during testing and for manual override in case of an emergency during short-distance flights. For the purposes of this testing, all flights were done within visual line of sight so that remote piloting was always an option.

Failsafes

All UAP are equipped with several failsafes and a full contingency plan was prepared for each flight location as required and outlined in the SFOC (Appendix D). At all times the UAP was kept within visual range of the safety pilot, who could take manual control at any time with the RC transmitter. The autopilot and RC receiver both have failsafe modes which puts the UAP into a set recovery pattern in the event of signal loss or interference. The failsafe events and actions are detailed in Table 3.4. An autopilot failure is considered catastrophic as the aircraft can no longer

Table 3.4: Failsafe reaction to UAP system failures or events

Event	Failsafe Action
Telemetry link loss	UAP returns to GPS home point above runway
RC link loss	UAP returns to home point
Soft flight bound crossed	UAP returns to home point
Hard flight bound crossed	Engine killed and low energy descent initiated
Autopilot failure	Control surfaces move to failsafe positions
GPS failure	Engine killed and low energy decent initiated
Catastrophic battery level	Engine killed and low energy decent initiated

be flown safely, so failsafe positions are set on all control surfaces. These positions (throttle off, slight rudder and opposite aileron deflection) put the aircraft into a shallow descending turn which should bring it to the ground safely in as small a radius as possible. A low energy descent can be initiated in failure cases where the autopilot is functioning. In this case a controlled shallow turn can be initiated about the aircraft's current position. The RC safety pilot can take control and override any of these failsafe behaviours as long as the aircraft is within RC range.

3.2.7   Data Storage and Processing

To reduce complexity of the onboard system, all data was stored onboard and processed after the flight. For this work, realtime sensor data streaming to the GCS was not required, but could be implemented on these systems when needed. A microcontroller (SparkFun Logomatic) with custom firmware was used to log flight telemetry and spectrometer data; and imagery was stored on the camera memory card. A sniffer line from the autopilot to the Logomatic allows it to record all messages sent from the autopilot, and the spectrometer is connected directly to a Logomatic UART port for data transfer and control. The spectrometer is triggered directly by the autopilot using a GPIO that can be toggled from the ground station or a flight plan block. Since the GoPro Hero2 does not have remote control, the video and telemetry is synchronized by sending a DTMF tone to the camera audio stream simultaneously with the spectrometer triggering. The tone is sent by an Arduino Pro Mini microcontroller that listens on the spectrometer trigger line outputs to the camera on one channel of the microphone jack. This tone is later used to extract images from the video that correspond to spectrometer samples. Telemetry is stored in the paparazzi binary format and uses the paparazzi tool *sd2log* to convert this into text and xml files that are parsed by python scripts. The spectrometer data is stored in a custom binary format that wraps the Ocean Optics format so that it can be saved in series with the telemetry on the Logomatic. The imagery is stored on the camera in H.264 mp4 files from which images are extracted. Custom python scripts were written for post processing data once it was offloaded from the aircraft.

The Logomatic was also equipped with a sample trigger button and stop log button. At the end of each flight the logger must be stopped to properly end and close the file. Data loss may occur if the logger is not stopped. The manual sample button can be used in testing, but all field samples should be triggered using the ground station so that they appear in the telemetry log and can be matched during post-processing. This procedure is outlined in the checklists in Appendix C.2 The spectrometer integration time was manually set on the Logomatic using the DIP switches. SpectraSuite was used to determine the integration time required, and the DIP switches were set in the following manner:

- P8 - Sets unit of binary number. Switch ON for microsecond, OFF for millisecond integration time.

- P7-P1 - Binary integration time, P7 MSB.

As the spectrometer records data in a raw digital number, reference measurements must be taken to convert to reflectance. This is done by taking 3 dark current and 3 white reference samples pre-flight, and 3 white reference samples post-flight. As long as the illumination is reasonably consistent pre and post-flight, the white reference samples can be averaged and used with the dark current measurement to calculate reflectance. During initial testing the dark current was found to be consistent during use, so post-flight measurements were not taken in the field.

To prepare the spectra, corresponding images, and orthophoto mosaic for viewing the steps are:

1. Download the .TLM from the logger and the .MP4 from the camera into a folder.

2. Run *postProcess.py* with the .TLM and .MP4 files. This will perform all the post processing steps and output folders with all of the spectra and their corresponding images, and an xml file containing photo filenames and GPS/IMU data. Other intermediate files will also be generated to speed subsequent runs and can be used for debugging. Detail on *postProcess.py* follows.

3. In *PhotoScan*, go to Tools → Run Script and select *photoScanLoad.py*. Select the images folder and .xml file that were generated in step 2. This loads all of the photos and GPS/IMU data into *PhotoScan*.

4. Follow *PhotoScan* workflow to Align Photos, Build Geometry, and Export Orthophoto as a .kmz to view in *Google Earth*. After the photo alignment some images may be obviously mis-aligned. No method to correct this was found, but more accurate orthophotos were obtained by simply deactivating the mis-aligned photos for the next processing steps. Fewer mis-alignments occurred when the photos were taken in exposure strips as recommended in the PhotoScan documentation.

5. Use *spectraPlotterGUI.py* to view spectra and reflectance curves. This software plots spectra and when given the white and dark reference files will also plot reflectance. Multiple spectra files can be selected and averaged to allow larger datasets to be displayed on a single plot.

postProcess.py is a wrapper script that calls the following functions to process flight data:

- *ooLogReader.py* with --cleanfile to generate *.TLM* file with spectrometer data removed. This is required as the spectrometer binary data can contain bytes that paparazzi *sd2log* interprets as telemetry messages, which causes an unexpected messages error. The spectrometer data is removed by scanning the file for the start and end bytes written around the spectrometer data by the Logomatic when the data is saved.

- Paparazzi tool *sd2log* on clean *.TLM* file to produce *.data* and *.log* files. This tool comes in the paparazzi installation and converts the telemetry messages from the logged binary to text format.

- *ooLogReader.py* with files from *sd2log* to extract spectra with telemetry data and create summary file from original *.TLM*. This tool was written for this project and converts the spectrometer binary data to text format that can be easily read and displayed by other applications. These spectra can be converted to reflectance using the dark and light calibrations that are procedurally taken at the beginning and end of each flight.

- *ooLogReader.matchLogs* to synchronize spectra and telemetry by matching timestamps.

- *specImage.py* to extract images from video timestamped with dtmf tones. This custom script scans the video file and extracts images using ffmpeg when a DTMF tone is present. These images can later be matched with the spectrometer readings.

- *ooLogReader.createSpectraFiles* to save each spectrometer reading to its own file with a header of metadata.

- *ooLogReader.createSummary* to write a summary file containing a list of all spectra, where the sample was taken, and statistics on the synchronization of log, telemetry, and video timing.

- *psxml.py* to save a summary of all images and telemetry data in a xml file that can be read by *PhotoScan* and is used to import the images and telemetry.

The *postProcess.py* script places all exported and intermediate files in the folder containing the input files. All the spectra and corresponding images collected are saved into *spectra* and *image* folders. Matching image and spectra files have the same base filename to easily view the image where each spectra was acquired. Spectra are saved in a text format with details about the acquisition in a header and the wavelength and digital number pairs following. This data can be easily viewed with the *spectraPlotterGUI.py* software custom written for this project, or using other data processing methods. See Appendix A.4 for details on file formats. The scripts and other supporting documentation can be found in an svn repository hosted in the laboratory. Archival copies are available through Dr. Lipsett.

3.2.8   Regulatory Compliance

In Canada, an SFOC is required to fly an unmanned aircraft for non-recreational purposes. All flights conducted for this study were done under a valid SFOC. The purpose of the SFOC is to ensure that all UAV flights are done safely with minimal risk to the operators and the general public who may be in the area. A risk assessment and full contingency plan to follow in the event of any failures must be presented to convince the Transport Canada officials that the planned operations can be conducted safely. As the UAPs used in this study share many similarities with hobby aircraft, the flying field rules and regulations of the Model Aircraft Association of Canada (MAAC) are also followed and all safety pilots are required to be MAAC members with sufficient RC flying experience. The major risk with a UAV is the potential to cause damage or injury in the event of a crash landing. To mitigate this risk, these flights were conducted within the visual range of an experienced safety pilot who could take control of the aircraft at any time. Although important, the consequences of a UAV crash can actually be lower when compared to a full size aircraft conducting the same work. This is because a UAV can have a much lower mass, speed and altitude than a manned aircraft, which greatly reduces the significance of a crash. There is also

no onboard human operator exposed to risk. The failsafes built into the autopilot are designed to bring the aircraft safely to the ground in the event of failures, as discussed in 3.2.6. In the event of a runaway UAV, the SFOC contains contingency procedures for each flying location. These include all the required emergency contacts and what information to provide them. Two trained ground crew members with an active cellular telephone are required for all missions to ensure this protocol can be followed and flights completed safely. For more detail, see Appendix D for a copy of the most recently issued SFOC.

3.3   Georectification

To be useful, all data collected must be linked to a physical location on the ground. This will be defined as the transformation of image coordinates to ground coordinates in a real-world system, such as latitude/longitude or Universal Transverse Mercator (UTM). If the location and orientation of the aircraft is known to a high level of accuracy and the sensor geometry is well defined, then it is possible to project the sensor field of view to a ground location. This direct projection has some significant challenges, including:

- Determining the aircraft location and orientation accurately enough to stitch images together and determine the target location within GPS accuracy. Small errors in orientation translate into large projection errors with altitude.

- Terrain variations must also be known to project the field of view onto the correct surface.

- Remote sensing typically uses large and expensive metric (or modified) cameras which have fiducial marks on the sensor [78], or are highly repeatable and have been calibrated. This allows for the direct measurement of subjects in the image and high rectification accuracy, but is not possible in the small size and low cost of this study.

These constraints meant that other methods had to be used in this work. Imagery collected from the aircraft can actually aid in the georectification process in addition to being a data product and

providing context for other sensor measurements. Several methods have been used in the past for georectifying remote sensing imagery. In this work the general concepts of ground control points and aerial triangulation will be considered.

3.3.1 Ground Control Points

In this process known ground locations are matched their corresponding points in an image and a polynomial fit is performed. While it can produce excellent results, there are a number of drawbacks. It requires prior knowledge of points that can be identified in each image; for a linear fit a minimum of 3 points is required, but for the best accuracy in a LandSat study a minimum of 25 points was required [48]. Matching of the Ground Control Points (GCP) is a manual process which must be performed on each image collected. When large areas are covered, this becomes a long and tedious task which would likely outweigh the benefits of deploying a UAS in the first place. The GCP must also be obtained from a previous or dedicated survey of the flight area which may be too expensive or impractical. Therefore, the goal is to avoid the need for GCP in the rectification process and only use GCP to assess rectification accuracy. For this reason solutions requiring GCP were not considered in this work.

3.3.2 Aerial Triangulation

Aerial triangulation is the process of matching key points between overlapping images to triangulate the position of the camera for each exposure. The process uses the estimated position and orientation of the exposure point from the GPS and IMU as a starting point and improves this estimate through triangulation calculations. The typical aerial triangulation workflow involves: [64]

- Preparation - selecting a number of well distributed points on each image such that the same point appears on as many adjacent images as possible
- Point Transfer - all points are marked on all photographs

- Point Mensuration - all points are precisely measured

- Block Adjustment - algorithm to align images with each other and the ground.

As there is significant overlap required between images, varying terrain is captured from multiple viewpoints allowing for the generation of a digital elevation model (DEM) in addition to orthogonal mosaics. A major advantage of this method is that computer algorithms have been developed that can effectively find these key points between images. This means that imagery and DEM can be generated with little to no human interaction in the workflow. Since this process requires matching points between images, this does place some restrictions on its use. The scene must not be completely homogenous so that these points can be found by the matching algorithms. A freshly snow covered landscape is an example of a natural scene where this method fails.

Early in the system development a test flight was conducted to evaluate the feasibility of georectification from a UAS without a metric camera system. To be successful, aerial imagery would need to be stitched into an orthophoto and rectified to at least 10 m accuracy from known GCPs. A series of passes was flown with the GoPro2 CMOS video camera mounted on UAP-1. The autopilot

Figure 3.6: Sample image extracted from GoPro2 video taken onboard UAP-1.

was used to log both GPS and IMU data. After separating the video into individual frames, the autopilot log file was synchronized with the images, although there was some unquantified error in the synchronization. To reduce error and ensure all images were below the horizon, they were filtered to only include images taken with roll less than $10°$. A sample of these images is shown in Figure 3.6. After reviewing available software (full list is presented in Appendix A.2), the imagery, GPS, and IMU data was entered into the most promising programs to evaluate their feasibility for this application:

- **ERDAS LPS** – allows for rectification with GCP, aerial triangulation and bundle block adjustment with automatic generation of tie points between images. Extensive testing was conducted with GPS/IMU data, but the aerial triangulation algorithm failed and the software was not able to produce any results. After contacting technical support and supplying data, ERDAS indicated that the data was too inaccurate to correct and their software algorithm would not be able to converge and produce results. This is because LPS is designed to work with remote sensing metric cameras and was not able to handle the variability and unknowns of low cost consumer cameras and MEMS IMUs.

- **BAE SOCET SET/SOCET GXP** – performs photogrammetric bundleblock adjustment with self calibration using GPS, IMU and ground measurements. The functionality of SOCET SET is currently being transferred to SOCET GXP. SOCET SET is currently available on campus, and a demo was obtained for SOCET GXP version 3.2. Both were evaluated by running the sample data set through the software and again it was found that the software could not converge the bundleblock adjustment, likely due to errors present in the data. The video analysis feature in SOCET GXP was found to be incompatible with the H.264 MP4 files created by the video camera.

- **Agisoft PhotoScan** – photo stitching software with capability for GPS input of photographs. This software has been used extensively for Kite Aerial Photography in archeology applications [77, 76]. It uses automatically generated tie points between images to reconstruct the scene with elevation, and has the ability to export Google Earth compatible files. Verhoeven found

PhotoScan to be accurate to 0.137 m horizontal and 0.310 m vertical at a 95% confidence level [77] using the Federal Geographic Data Committee National Standard for Spatial Data Accuracy [23]. During this initial testing with the GoPro and manual synchronization of autopilot log data, the generated imagery found to be accurate to ≤10 m. PhotoScan is closed source software, but some detail on its design was found in the AgiSoft forum:

> PhotoScan uses least squares adjustment. During adjustment the reconstructed scene data including model geometry and camera positions is transformed so that the RMS error between estimated and measured camera positions is minimized. The transformation used is a 7 parameter similarity transform (translation + rotation + scaling). [58]

And from another forum post:

> Here is a more detailed explanation of individual processing steps:
>
> 1. Feature matching across the photos. At the first stage PhotoScan detects points in the source photos which are stable under viewpoint and lighting variations and generates a descriptor for each point based on its local neighborhood. These descriptors are used later to detect correspondences across the photos. This is similar to the well known SIFT approach, but uses different algorithms for a little bit higher alignment quality.
>
> 2. Solving for camera intrinsic and extrinsic orientation parameters. PhotoScan uses a greedy algorithm to find approximate camera locations and refines them later using a bundle-adjustment algorithm. This should have many things in common with Bundler, although we didn't compare our algorithm with Bundler thoroughly.
>
> 3. Dense surface reconstruction. At this step several processing algorithms are available. Exact, Smooth and Height-field methods are based on pair-wise depth map computation, while Fast method utilizes a multi-view approach.

4. Texture mapping. At this stage PhotoScan parametrizes a surface possibly cutting it in smaller pieces, and then blends source photos to form a texture atlas.

Many of the PhotoScan algorithms are based in part on previously published papers, but are implemented from scratch and are thoroughly optimized for faster processing speeds. It is worth noting that we have favored algorithms with higher accuracy output over faster approaches with less accurate output. [67]

Based on these results and the results by Verhoeven, PhotoScan was chosen for use in this project. The initial data was not collected in exposure strips (as recommended by AgiSoft), so chunks containing various numbers of photos were run through PhotoScan. To perform the alignment, each image and its corresponding position and orientation information was loaded into PhotoScan and the default processing workflow was followed. It was found that chunks of approximately 100 photos produced alignment between photos with the least amount of error. After aligning these chunks, reasonable quality orthophotos were produced, as seen in Figure 3.7. The positional accuracy of the mosaic was approximately 6–8 m. Note the visibility of the 2 ft square concrete sidewalk blocks in the image. The presence of straight lines shows that the stitching algorithm is working very effectively to align all 100 images with each other. This result is within the desired 10 m accuracy and provided the confidence in the image processing procedure required to move forward with the project. Agisoft PhotoScan Professional 0.8.5 was used for georectification and orthophoto generation in this work, and it will run on Linux, Windows, and OS X.
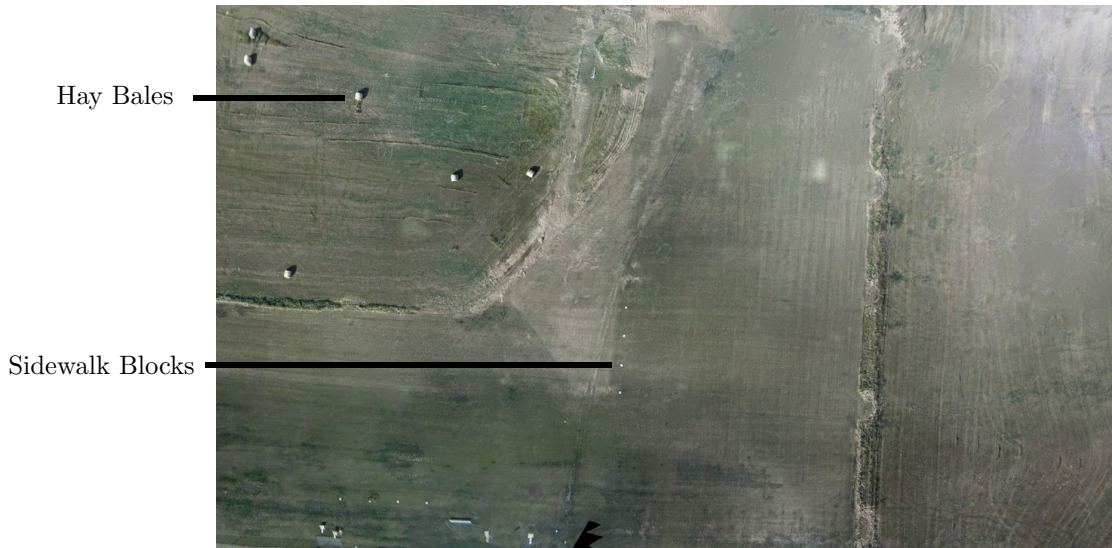
Figure 3.7: First orthophoto generated with 100 frames extracted from GoPro2 onboard video. This is a low resolution image for inclusion in this document.

3.4 Experimental Plan

One of the most challenging aspects with any time-varying measurements is accounting for the time constant of different sensors. Depending on the groundspeed and altitude of the aircraft, this can be a significant challenge that may prevent the use of certain sensors and may make accurate data collection difficult. Two previous experiments with airborne point spectrometers have required integration times of 300 ms [66] and 400 ms [28], which at a flight speed of 54 km/h causes measurements to be averaged over a 4.5–6 m strip on the ground. This would make it difficult to collect data over any specific ground target. Sensor technology has improved significantly in recent years; and one of the main unknowns in conducting this test is the integration time that will be required to achieve a signal to noise ratio high enough to detect target reflectance signatures. For some applications a smaller spot measurement may be needed and a faster sensor or rotary-wing aircraft (with no minimum speed) may be required. As the desired applications for this work include pipeline monitoring, a long-range aircraft would be required in an industrial application, and so the test procedure for this work uses fixed-wing aircraft, which have a minimum (stall) speed.

3.4.1 Goal

The goal of this testing was to determine the accuracy and usefulness of the system. This was measured in two key aspects, geolocation and spectral detection accuracy.

3.4.2 Variables

Controlled: standoff distance, sensor mount, aircraft orientation during exposure runs, ground speed, frame rate, integration time, sample rate, date and time of flight, ambient conditions (solar irradiation, temperature, windspeed, humidity, barometric pressure, target composition if variable).

Manipulated: Target composition (SIL-4 sand contaminated with increasing concentrations of paint) and location (at least 5 locations distributed over approximately 8 acres at Bremner field). These trials are detailed in Table 3.5.

Responding: Spectral measurements and georectified imagery

Ambient conditions could not be directly controlled, but flight days and times were selected during fair weather to minimize changes. Flight duration was short (< 20 min)[28] and ambient conditions measured pre and post flight. Conditions included: solar irradiation, temperature, windspeed, humidity, barometric pressure, target composition if variable (eg. water content). As in [28, 35], atmospheric correction was not required due to the low altitude of the flights (< 800 ft). The exact aircraft location and orientation during trials could not be controlled but was be recorded to determine the flight path accuracy. This was also not as important as the location of the ground targets which were known accurately to assess geolocation performance of the system. Flight operations were carried out in day/VFR conditions meeting the following weather criteria:

- average wind velocity no greater than 15 kts (17 mph, 28 km/h)

- no precipitation

- minimum visibility of 3 miles

- minimum ceiling of 1000 ft AGL or better (for flights up to 500 ft AGL)

- minimum ceiling of 1500 ft AGL or better (for flights up to 800 ft AGL)

This was primarily required to meet Transport Canada regulations, but was also necessary to achieve consistent flights over multiple days.

Table 3.5: Aerial experimental trials planned

Trial	Target Composition	Target Location
1	Bare Tarp	Point 1
2	Bare Tarp	Point 2
3	Bare Tarp	Point 3
4	Bare Tarp	Point 4
5	Dry Sand	Point 5
6	Trace Sand/Paint Mix	Point 5
7	Saturated Sand/Paint Mix	Point 5

Trace and saturated sand/paint mix was determined by volume. Points 1-5 were distributed around the approximately 8 acres of runway at the Bremner flying field. A minimum of 5 aerial samples of each target was be required to complete testing.

3.4.3   Measurement Method

Flights were conducted when ambient conditions were predicted to be stable for the duration of the flight (15 min). This may include sunny and overcast conditions depending on local weather during testing. To assess georectification accuracy, a bare tarp target was overflown and imaged in five known locations. The location determined by the UAS was compared to the known location from an RTK-GPS survey to determine accuracy. In all testing woven polyethylene 15' x 20' tarps were used.

To assess spectral accuracy, a ground target was prepared in a known location. This target consisted of a tarp, dry sand, and sand contaminated with a pigmented fluid. The tarp was laid out flat and staked to the ground at the corners. Dry SIL-4 sand was spread over the tarp by hand to a depth of 5 mm, or enough so that the colour of the tarp could not be seen through the sand. Green acrylic

paint (ASTM D-4236) was mixed in a 1:10 ratio with water, applied to the sand with a Flo-Master 2 gallon sprayer and allowed to penetrate the interstitial space in the sand to simulate an industrial spill. The trace targets were prepared with two passes of the sprayer, which is approximately 64 mL/m^2 of the paint mixture. The saturated targets were prepared by spraying approximately 800 mL/m^2 of the paint mixture. Each target was overflown and imaged at least five times per target to provide repeats of trials.

To determine the integration time required in the field, the spectrometer was unplugged from the aircraft and attached to a computer running SpectraSuite with a USB cable. The spectralon panel was then observed with SpectraSuite, and an appropriate integration time found to ensure the spectrometer does not saturate. This integration time was then set on the Logomatic using the DIP switches. All spectral measurements were converted to reflectance by taking 3 measurements of a white reference spectralon panel before and after each flight. Dark current in the spectrometer was found to be consistent, so measurements were only taken at the beginning of each flight. Further testing is required to characterize the dark current repeatability across the spectrometer's operating temperature range. The pre and post-flight samples are triggered from the ground station so that they also appear in the telemetry log and can be properly post-processed. After the post-flight samples are taken the stop button on the Logomatic must be pressed to finalize and close the log file.

3.4.4 Sensors Used

The earth observation sensors used are a GoPro Hero2 CMOS video camera and Ocean Optics USB2000+ NIR point spectrometer. Frames from the video camera are used to develop a map of the survey area and provide context for the spectrometer measurements. Care must be taken to ensure the alignment and calibration of the sensor package is sufficient to give confidence in the geolocation of spectrometer data. This was done by calibrating the field of view of the sensors while they rigidly mounted together. The spectrometer was calibrated in the lab against a Field Spec Pro spectrometer. The aircraft is equipped with the paparazzi Lisa/M v2.0 autopilot which

has an internal IMU and is using a Ublox LEA-6H GPS receiver to allow for georectification of imagery and spectra. A small weather meter was used to record ambient ground conditions during the flights.

3.5 Summary

A UAS system was designed and assembled in-house to test the ability of a low cost system for remote sensing of vegetation, surface moisture, and hydrocarbons. Visible images and spectra will be obtained with a GoPro camera and Ocean Optics VIS/NIR spectrometer on a hobby aircraft airframe to keep costs low while testing the feasibility of this system architecture. The paparazzi autopilot paired with a Logomatic board make up the onboard avionics and data logging, while a laptop computer running paparazzi and PhotoScan comprise the ground station.

System commissioning and testing was done in stages to qualify each module of the system before it was integrated completely. Module testing was done in laboratory facilities at the University of Alberta, and flight testing occurred at the Edmonton Radio Control Society Bremner field. Full testing results follow in Chapter 4.

Chapter 4

Results and Discussion

A series of tests were conducted on each aspect of the system to ensure it was functioning as expected and required. This testing progress was modular, starting with each component and subsystem before moving to the assembled system. Both laboratory and flight testing were required, and this chapter contains the results of the following tests:

- Sensor calibration - spectrometer and camera

- System integration

- Flight testing

4.1   Lab Testing

Before conducting any field or airborne testing, several lab tests were done to ensure the equipment was functioning properly and to determine the steps required to integrate the sensors into the airborne system. For the spectrometer, testing involved detailing the serial interface, evaluating different fibre optics lens (fore-optics) options, and verifying spectra readings in the lab. The camera had to be integrated into the system with timestamping and its field of view calibrated against the

spectrometer field of view. Finally, a full systems test was conducted prior to moving to flight testing.

4.1.1 Spectrometer Testing and Verification

Feasibility Tests

The USB2000+ serial communications protocol is well documented in data sheets from Ocean Optics [51]. Both USB and RS232 protocols are available to access all spectrometer features and collected data. RS232 communication is preferred due to the lower onboard system requirements, but the slower data transfer rate may cause problems. Lab testing was done to assess the feasibility of offloading spectra over RS232 in an acceptable amount of time. As the measurements need to be taken from a moving airborne platform, a sampling rate of 1 Hz was deemed to be the lowest acceptable rate.

A simple test was done with the spectrometer controlled over RS232 from a computer with the Saleae logic16 analyzer attached to measure timing. Since the USB2000+ was not initially available for testing, some testing was done with a USB4000 demo unit before proceeding with the purchase. This showed that data transfer for one spectrum from the USB4000 at 115200 baud took 0.6375 s in binary format and 2.13 s in ASCII, so all communications must be in binary to meet the time requirement. To collect a spectrum at 100 ms integration time took 0.229 s (overhead of 129 ms, mostly data transfer time). The timing was recorded for several samples and is shown in Figure 4.1. This data was collected with the USB4000 communicating with a computer over RS232. The spectrometer was triggered over RS232, and the time elapsed from the trigger to the start and end of the transmitted spectra is shown. Since the total time remained under one second, this shows that for an integration time of 100 ms and under the spectrometer should be able to sample at 1 Hz. There was significant jitter in these measurements, and although the cause is not known the Ocean Optics distributor indicated that timing on the USB4000 is not as reliable as the USB2000+. Test results from the USB2000+ shown below confirm that its timing is much more consistent, so this
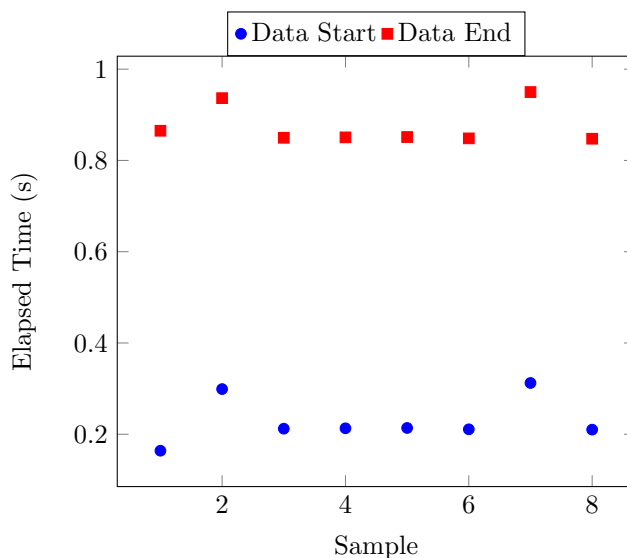
Figure 4.1: USB4000 timing over RS232. Serial trigger, 115200 baud rate, 100 ms integration time.

was not a concern in further testing.

These tests were repeated with the SparkFun Logomatic board with custom firmware to communicate with the spectrometer. There was some concern regarding the lengthy time required to write data to the SD card. After testing it was shown that a sampling rate of 1 Hz could be achieved, so it was not necessary to introduce the added complexity of a single board computer for high speed USB host capability. To increase sampling rate in the future, this would be the first upgrade to consider, as it would also allow interfacing with more advanced cameras. Figure 4.2 shows timing results from testing of the USB2000+ with the autopilot and Logomatic. It clearly shows that the time elapsed from autopilot trigger to the start of data transfer is very consistently 68 ms. This is crucial to characterizing the timing of the spectrometer in relation to other sensors, which would be difficult if it was not consistent. The variation in the time elapsed to the end of data transfer reflects the nature of the filesystem that stores data onto the SD card, and also indicates the time required to conduct a complete spectrometer sample cycle. All end times are below 0.5 seconds, indicating this setup is able to perform 2 Hz sampling.

During initial flight testing it was found to be difficult to sample the spectrometer directly over a
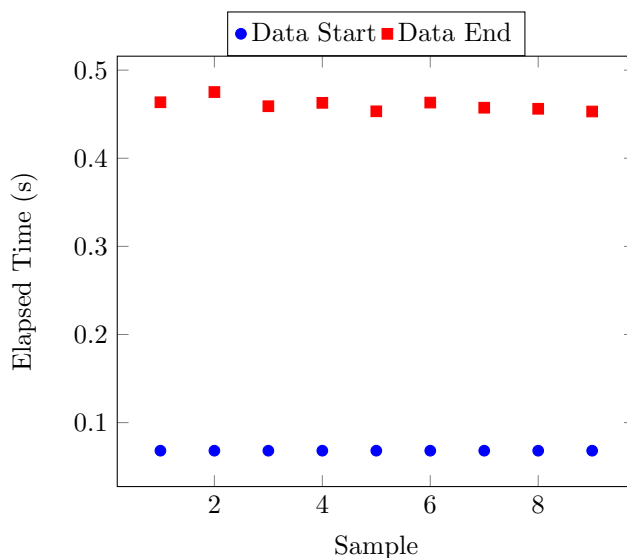
Figure 4.2: USB2000+ timing over RS232 at 1 Hz sample rate. Autopilot trigger, 115200 baud rate, 10 ms integration time.

15x20 foot tarp at a 2 Hz sample rate. In order to increase the sampling rate without drastically changing the system, the spectrometer was reconfigured to return only every other pixel in the wavelength range from 400 - 1000 nm. Since the low and high range of the spectrometer is largely noise, this resulted in a 4 Hz sampling rate without reducing useful information or physical modification of the system. Figure 4.3 shows the timing results of this modified setup. An additional benefit of this modification is evident in the consistent 0.22 s time required to finish a sampling cycle, giving added confidence that the logger will be able to handle a 4 Hz sample rate. Upgrading to a USB host device would also increase the sampling rate as the limiting factor is the data transfer rate over RS-232. This was not done as a USB device would require writing a USB driver and would increase the size and complexity of the system. It should also be noted that the integration time shown in Figure 4.3 to achieve the 4 Hz rate was lowered to 2 ms. It was found in outdoor testing of the spectrometer that a low integration time was required to avoid sensor saturation, and a 2 ms integration time was mostly commonly used during the field testing described in Section 4.2.

With confidence that the sampling system was performing satisfactorily, some feasibility testing
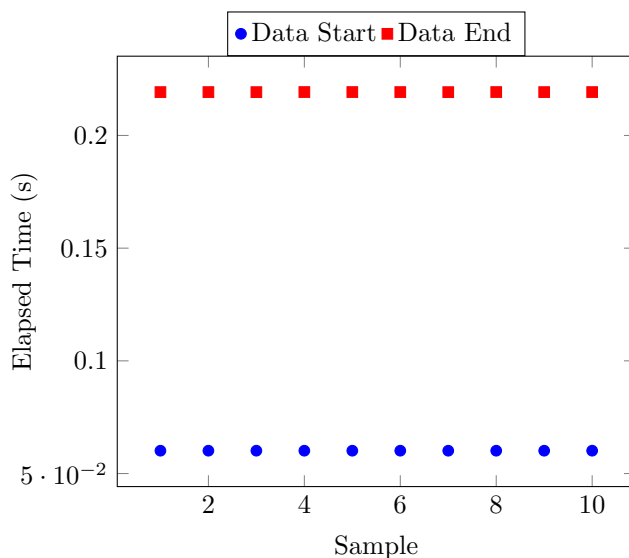
Figure 4.3: USB2000+ timing over RS232 at 4 Hz sample rate. Autopilot trigger, 115200 baud rate, 2 ms integration time.

was done to estimate integration time. Using the Ocean Optics USB4000 (25 um slit, grating of 600 lines/mm set to 350-1000 nm) and 74-UV lens (5 mm diameter and 10 mm focal length), a series of locations around the University of Alberta campus were measured from ground level. Although this test was basic, integration times less than 100 ms from ground level and second story were achieved, as shown in Figure 4.4. There was no noticeable difference in signal strength when the standoff distance was changed from 1 to 10 m. Of interest is the oxygen absorption band that can be seen at 760 nm. When corrected to reflectance, atmospheric effects like this will be accounted for. Amplitudes in the figure cannot be directly compared as the linearity of the sensor over different integration times is not known and the measurements were taken over a period of time where the solar illumination may have changed. This still gave a relative measurement and provided confidence to proceed with fore-optic testing in preparation for integration into the UAS.

51
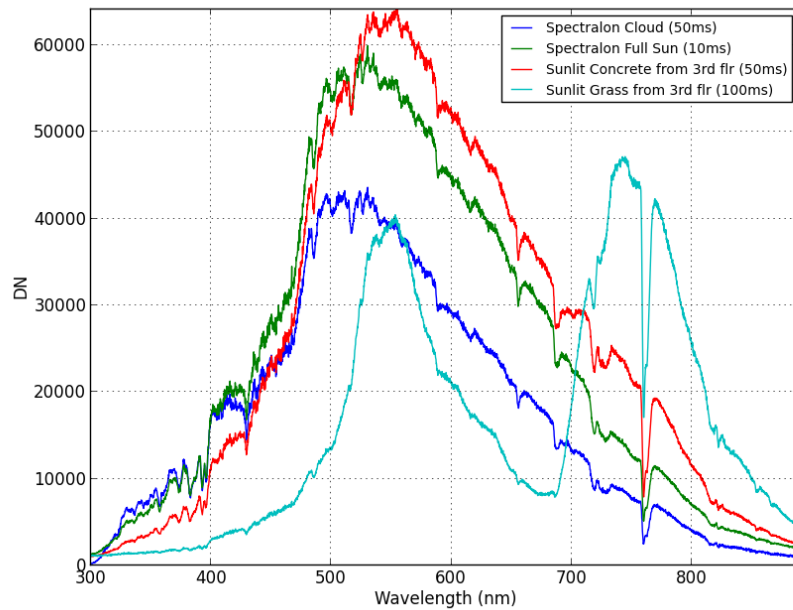
Figure 4.4: Initial integration time testing with the USB4000.

Fore-optic Testing

To speed development and keep cost low, off-the-shelf fore-optics from Ocean Optics were chosen for testing. The 84-UV-25, 74-DA, and GER-KIT are shown in Figure 4.5. A test rig, shown in Figure 4.6, was constructed to hold each lens over a bench-top target and an ASD FieldSpec Pro was used for verification.

To compare the signal strength through each fore-optic, the spectrum of a spectralon panel, red notebook and tray of Sil 4 sand were taken using each lens. Although the standoff distance was only 30 cm in this test, it was conducted under controlled lab conditions so any differences in signal strength can be associated to the lens. Since airborne application requires a large standoff, signal strength will be given the highest priority in the final fore optic selection. Spot size is also important to limit the ground area that is averaged with each measurement. As shown in Figure 4.7, the highest signal strength was achieved with the 74-DA lens.
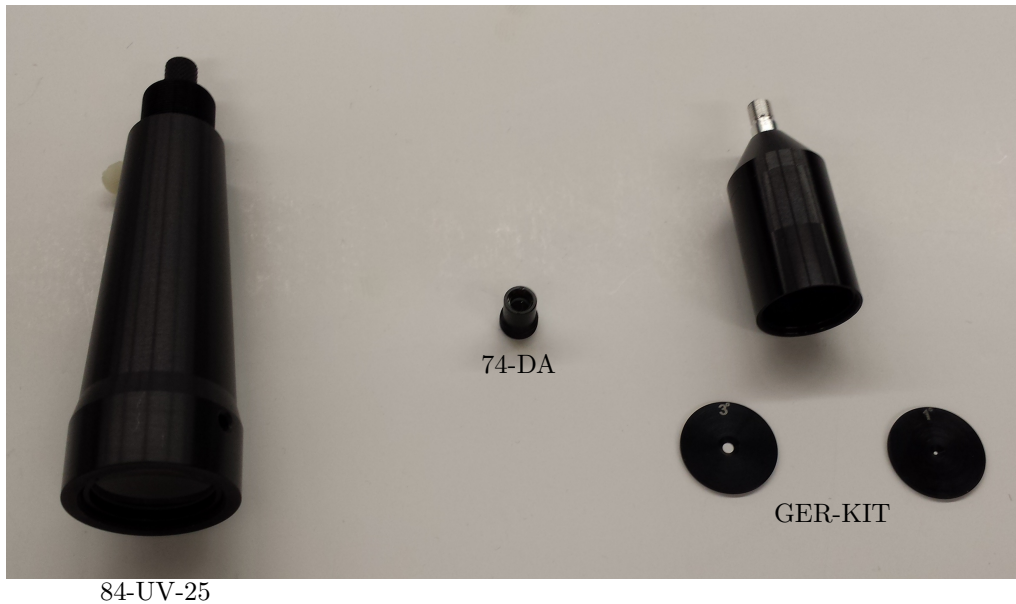
Figure 4.5: Ocean Optics fore optic lenses tested

It should also be noted that the 84-UV-25 lens does not directly attach to the spectrometer and requires a length of fibre optic cable to connect. In this testing a 1 m fibre was used which will further attenuate the signal and could explain its lower signal. Details on this cable are included in Appendix A.3. Further testing could be done with an 84-UV-25 modified for direct attachment.

Instead of a lens, the GER-KIT is a Gershun tube supplied with disks of varying aperture to provide a set field of view. The signal strength through the GER-KIT was too low at fields of view below $8°$ to use in further testing – at $1°$ a 5 second integration time was required to reach half scale on the spectrometer. The $8°$ disk gave signal strength close to that of the 74-DA, but the large increase in spot size was deemed to be unacceptable. At 100 m standoff the GER-KIT would have a spot size of 14 m compared to the 4 m of the 74-DA. Since these both attach directly to the spectrometer, it would be simple to substitute a wider angle GER-KIT disk if absolutely necessary to get a stronger signal for airborne measurements. The relationship between standoff distance and spot size is shown in Table 4.1 for the 84-UV-25, 74-DA and GER-KIT. Since flight altitude above ground level
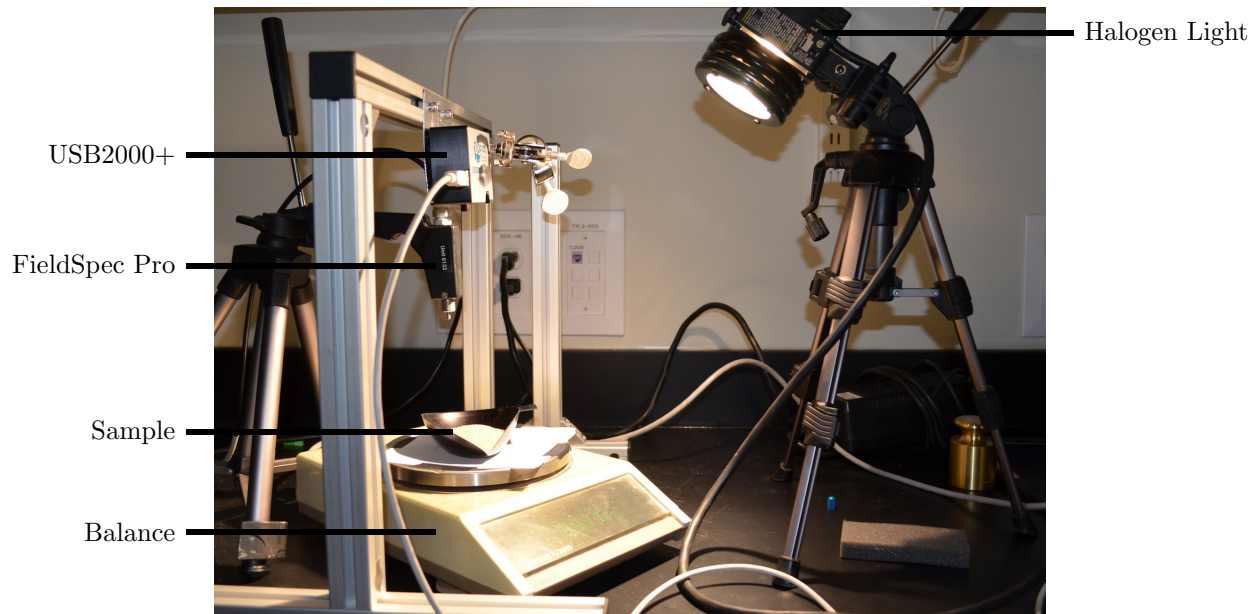
Figure 4.6: Lab setup for spectrometer testing and verification

will not exceed 100 m during testing, a maximum 4 m spot diameter is deemed acceptable. This is comparable to the 3 x 16 m spot size used by Groeneveld [28], which is approximately half a Landsat TM pixel. The spot size for the 74-DA at a 30 cm standoff was estimated during testing to be 1.3 cm, which corresponds closely to the calculated value of 1.52 cm.

Further testing was done to compare reflectance values calculated for the 74-DA and 84-UV-25 against measurements taken with the ASD FieldSpec Pro as reference. These results are shown in Figures 4.8 and 4.9. All results here show good agreement with the ASD measurement, aside from the region from approximately 500-700 nm where the USB2000+ departs significantly from the ASD spectrum. This anomaly is present for all targets measured and with both the 74-DA and 84-UV-25 lenses, which suggests that it is internal to the USB2000+ spectrometer itself. It is much more pronounced with the 74-DA lens, but this could simply be because the signal transmitted through the 74-DA is stronger and so the feature is exaggerated. In 4.1.2, further testing with sand and clay targets is described and this anomaly is further analyzed as it must be characterized to
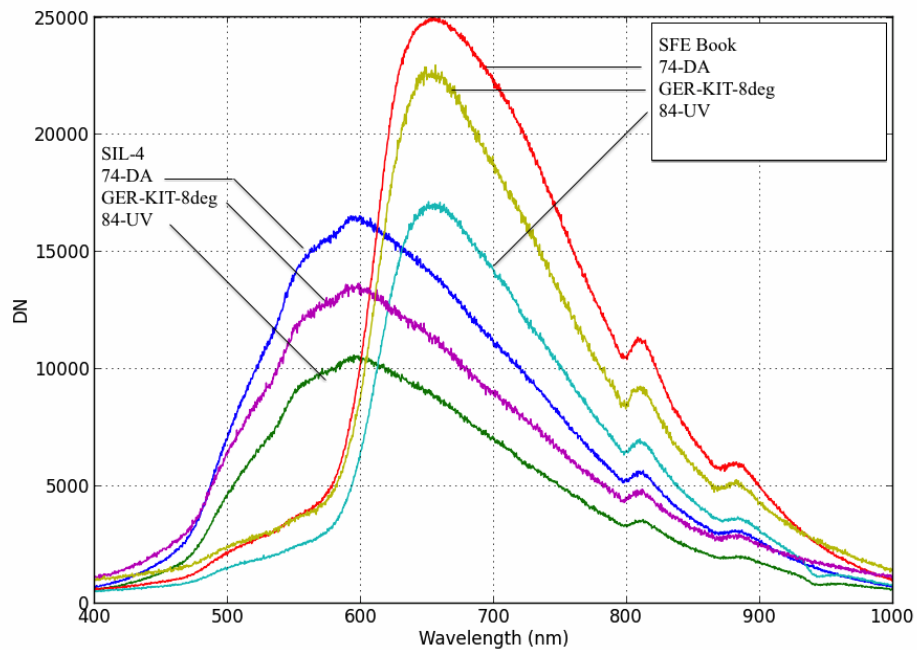
Figure 4.7: Raw spectrometer readings minus dark current to compare signal strength through various fore-optic setups

make accurate measurements. This is also a good example of the limitations and variability that must be accounted for in lower cost instruments.

During this process the procedure for post processing the spectral data was also verified as it uses custom software written in python. The USB2000+ only outputs the raw digital number spectrum and the reflectance calculations are done in the Ocean Optics software. To test the custom software, its output was compared against the reflectance output by the Ocean Optics software and was found to match. In all cases, the reflectance was calculated by taking a dark current measurement with the spectrometer input covered and a white current measurement of a spectralon panel.
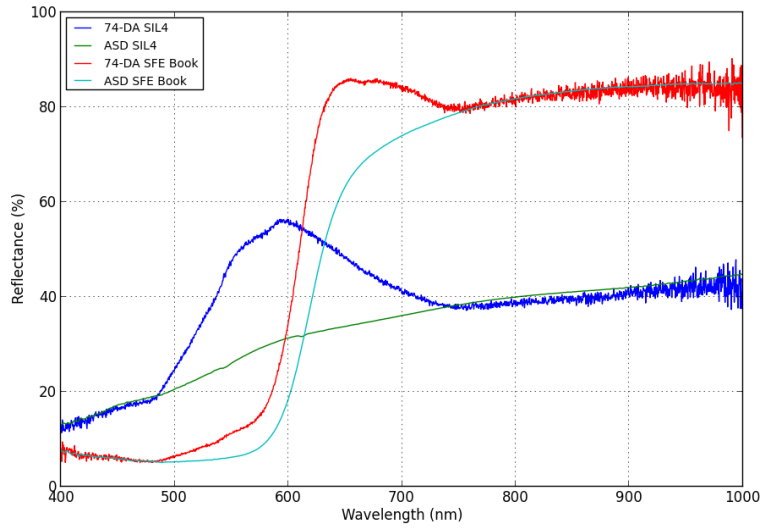
Figure 4.8: 74-DA spectra compared against ASD
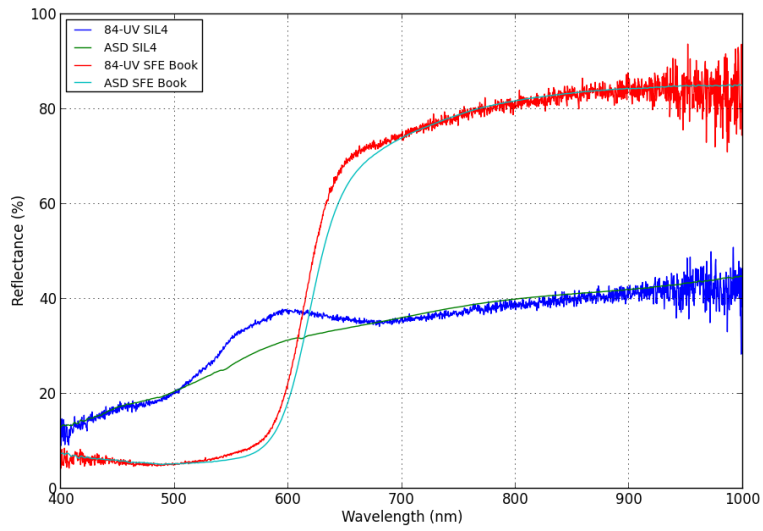
Figure 4.9: 84-UV-25 spectra compared against ASD

56

Table 4.1: Calculated spot size for Ocean Optics fore-optics with various standoff distance. All entries in meters.

Standoff	84-UV-25	74-DA	GER-KIT 8deg
10	$6 \cdot 10^{-2}$	0.4	1.4
20	0.1	0.8	2.8
30	0.14	1.2	4.2
40	0.18	1.6	5.59
60	0.26	2.4	8.39
80	0.34	3.2	11.19
100	0.42	4	13.99

Summary

First, the spectrometer serial communications speed was tested to ensure an acceptable sampling rate could be obtained. After testing, a rate of 4 Hz was achieved. As the integration time at large standoff distances was unknown, some simple outdoor testing showed that integration times under 100 ms are achievable outdoors, which corresponds to a 1.4 m strip at 50 km/h. Laboratory fore-optic testing showed that the 74-DA lens gave the highest signal strength while not exceeding a 4 m spot size at 100 m standoff. When comparing spectral measurements to the FieldSpec Pro reference measurement, the measurements agreed except for the region from 500-700 nm where the USB2000+ measured significantly higher reflectance.

These results showed that the system would be able to collect spectra at a rate and standoff distance similar to in-flight conditions. While there were limitations with the spectral accuracy of the system, it was deemed to be performing well enough to collect useful information and gave confidence to proceed with the study.

4.1.2 Prepared Soil Sample Testing

The USB2000+ was tested against the ASD FieldSpec to check its response when measuring a variety of known targets. A full description and test procedure is listed in Appendix A.1. Samples of sand, clay, and sand-clay mixture were prepared to make targets containing varying concentrations

of water and canola oil. Canola oil was used as an environmentally friendly analogue to petroleum with the goal of eventually using this system for hydrocarbon leak detection. The reflectance spectra was then measured in the lab with the ASD and Ocean Optics spectrometers, as shown in Figure 4.6, and the results compared for consistency. Large spectral features and practical sample ratios were also identified that could be used in the field for airborne testing.

The sand used was SIL-4 [69] from Sil Industrial Minerals, the kaolin was EPK Kaolin, CAS #1332-58-7, and the bentonite was a bulk Haliburton sample. To ensure the samples did not contain water prior to testing, they were dried according to ASTM D2216 [7]. These results, shown in Table 4.2, indicate that the bulk samples received contained very little water, especially in the case of silica sand which had only a 0.04% mass change. This indicates that it can be used for future trials without oven drying. Bentonite had the largest mass change, but this is still small compared to the 90-150% by weight of water that was added during testing.

Table 4.2: Results of oven drying lab test samples

Sample	Tray Number	Change in Mass (%)			
		1st hour	2nd hour	3rd hour	4th hour
Kaolin	1	0.92	0.08	-	-
	2	0.94	0.03	-	-
Bentonite	3	2.48	2.18	2.35	1.49
	4	3.47	2.52	1.69	1.25
Silicia Sand	5	0.04	-	-	-
	6	0.04	-	-	-

Lab testing was done to compare the readings of the low-cost USB2000+ against the FieldSpec as a reference standard. Aside from verifying the functionality of the USB2000+, the various sand and clay targets were evaluated for ease of preparation and ability to differentiate with the USB2000+ in preparation for airborne field trials.

Objective: Establish a baseline by measuring known samples with the Ocean Optics (OO) airborne setup and comparing against the Analytical Spectral Devices FieldSpec (ASD), determine the sensitivity of the spectrometer and the feasibility of using it to detect various concentrations of water and oil.

Manipulated: Target composition, water content and oil content.

Responding: Spectral readings from OO and ASD.

Controlled: Lighting, viewing angle, ambient conditions, target size (edge effects).

The results of this testing are summarized here, while the full results can be found in Appendix A.1. A total of 31 samples of sand and clay were prepared and measured. Three locations on the surface of each sample were measured with each spectrometer to test for variation across the sample. As the 74-DA lens was found to give the highest signal to noise ratio in preliminary testing, most trials used this lens. All plots included here are from the 74-DA data. Ten samples were also measured with the 84-UV-25 lens for comparison.

Figure 4.10 shows the spectra of dry sand, bentonite, and kaolin. The same area of increased sensitivity from 500-700 nm in the USB2000+ can be seen as in the initial lab testing. The cause is unknown, but it occurs with consistency so it can be corrected for. There is also a discrepancy between the ASD and Ocean Optics measurements for the kaolin sample. This was a trend for all the kaolin samples, so it seems that the Ocean Optics spectrometer had difficulty with the kaolin reflectance signature, and is likely a sensor limitation for identifying this soil type.

An important aspect of this testing was to determine whether the different samples could be differentiated with the limited range USB2000+ spectrometer. Its detection capability in lab testing dictated the design of experiments that could be run in the field. As expected, Figure 4.11 shows the clear differentiation of oily sand from wet and dry sand with the ASD FieldSpec in the 1000-2000 nm range. In the 400-1000 nm range covered by the Ocean Optics spectrometer, the features are less pronounced but there is still a significant difference in slope between the dry and mixed samples that should be detectable. As this is a feasibility study, an extended range spectrometer is not available to integrate into the airborne test platform. The differentiation of dry from wet samples will still prove the concept, as only the addition of a different spectrometer would be required to improve capability, while the remainder of the procedure remains the same. Figure 4.12 shows the 400-1000 nm region of Figure 4.11 with the Ocean Optics data overlaid. It shows that the same
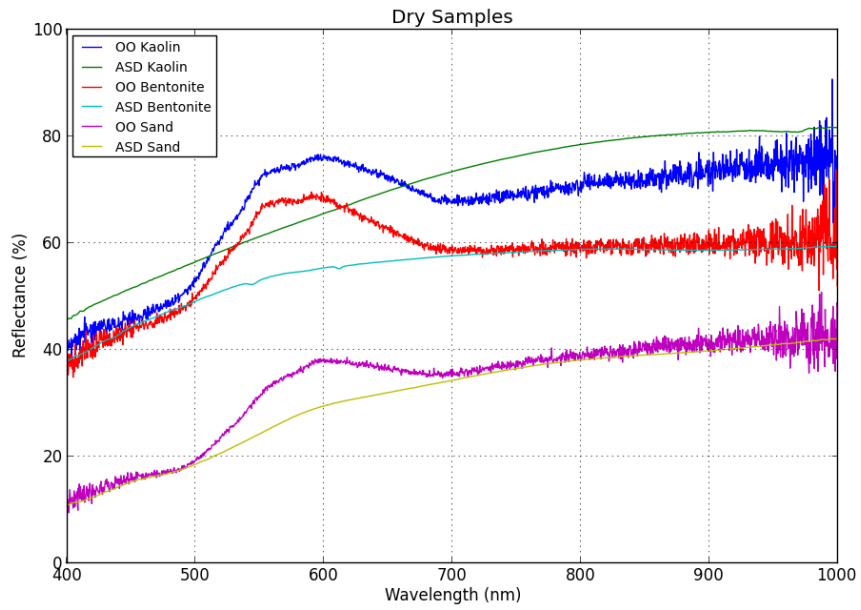
Figure 4.10: Dry prepared samples measured with ASD and OO spectrometers.
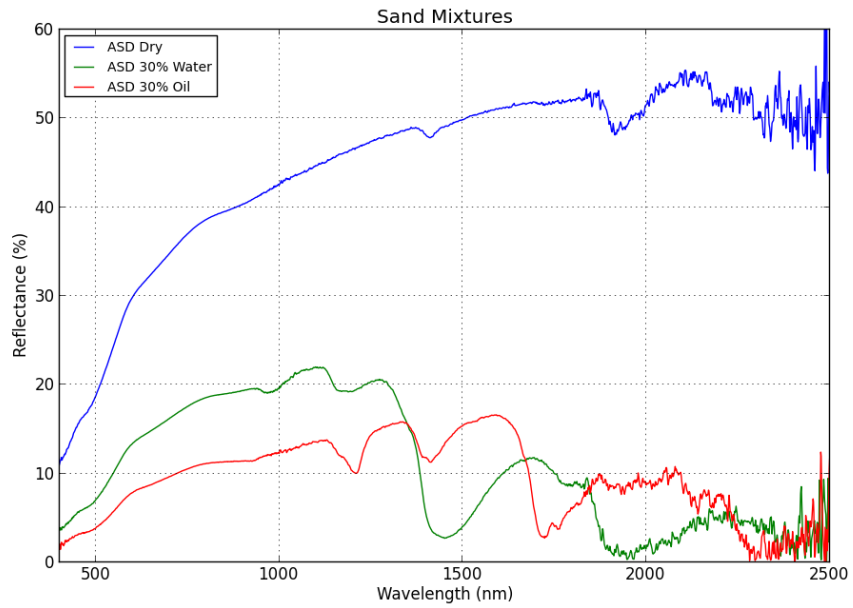
Figure 4.11: Mixtures of sand and water or oil over full range of ASD spectrometer.

slope variation is visible in the USB2000+ data, which suggests that it will also be detectable from airborne measurements.
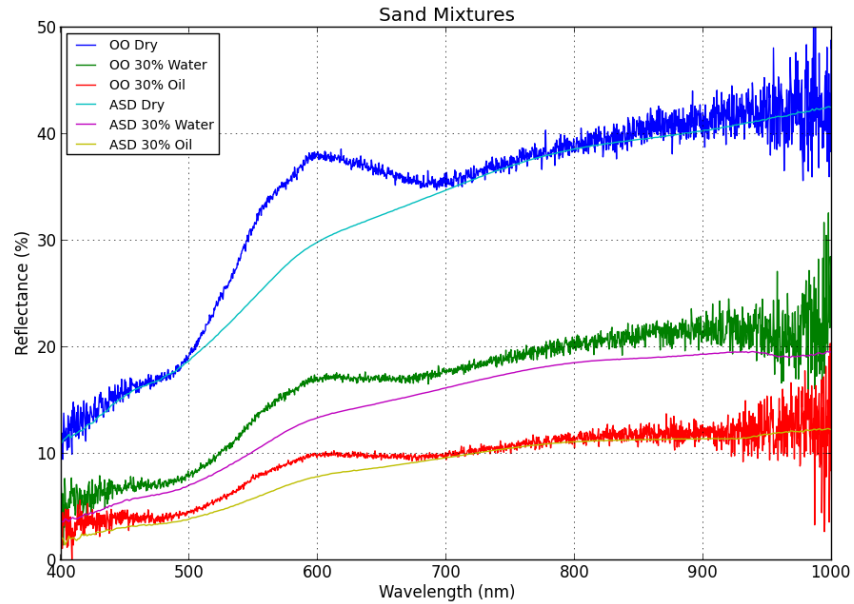
Figure 4.12: Mixtures of sand and water or oil over range of OO spectrometer.

Since kaolin was not reliably measured by the USB2000+, it will not be used in further testing. The bentonite and kaolin were much more difficult to mix with water and oil, which would make it very time consuming to prepare large scale samples for field testing. In all mixtures the sand was easy to prepare samples with and gave consistent results with the Ocean Optics spectrometer. The bulk sand samples were also very dry when received and will not require drying before testing. For these reasons sand will be used for large scale field testing with the spectrometer airborne.

Since the difference between oil and water is very small in the Ocean Optics data, it is not expected to be detectable in airborne data. Therefore it is suggested that field testing involve dry and wet sand as an experimental analogue to clean and oil contaminated soil. As it has already been shown that oily and wet sand can be easily identified with the ASD, the purpose of field testing is to determine if a point spectrometer can be used to detect ground characteristics from a low cost

UAS. Simply using wet and dry sand will provide a realistic target with sufficient contrast that poses no environmental hazards. If water evaporation becomes a challenge, canola oil will be used as there are no evaporation concerns and it will not cause any environmental contamination.

4.1.3   Sensor Geometric Calibration

With the completion of spectrometer data verification, the final remaining test of the USB2000+ was the field of view definition within the visible camera frame. As the mount was designed to rigidly fix the camera and spectrometer to a removable sensor tray, the sensor package can be calibrated independently from the aircraft and even moved between aircraft without need for recalibration. The calibration setup shown in Figure 4.13 was used for the sensor package field of view (FOV), and the test used the following procedure:
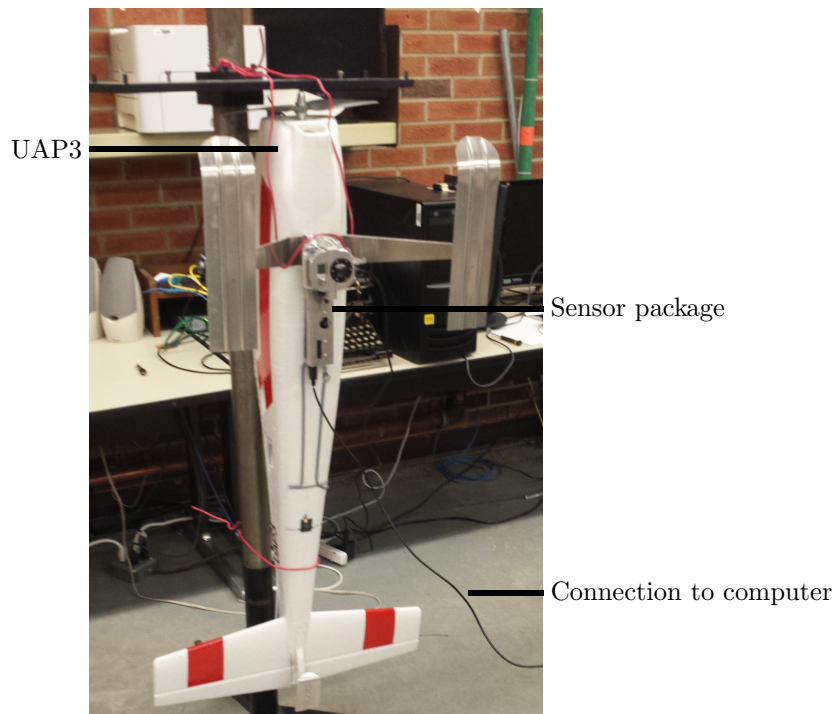
Figure 4.13: Sensor field of view calibration setup

Objective: Bound the location of the field of view of the point spectrometer within the frame of the camera.

Manipulated: Distance from sensor package.

Responding: Change in spectrum when calibration panel is detected.

Controlled: Lighting, sensor mount, viewing angle, ambient conditions, calibration panel.

Materials: Brightly coloured calibration panel much larger than the expected spectrometer spot size, measuring tape, UAP sensor package, sensor mount stand, computer with SpectraSuite, USB A-B cable, SD card and reader for GoPro.

1. Mount the sensor package with the lens axes perpendicular to the ground. The mount must be secured from movement for the duration of the calibration. Ensure there is a clear line of sight from the sensor for the entire distance to calibrated over.

2. Connect the spectrometer to a computer running *SpectraSuite* to display a live spectrum view. *SpectraSuite* will show the spectrum by default - ensure the integration time is set so that the background spectrum and panel spectrum can be clearly seen. Ensure the live spectrum can be seen for the duration of the test.

3. Determine the standoff distances to collect calibration data at. Measure and mark each distance along the ground from the sensor package.

4. Start video recording on the GoPro.

5. Move to the first calibration distance and position the panel so its surface is facing the lenses but is out of frame.

6. Move the panel in front of the spectrometer to approximately find its FOV. Watch for change in the live spectrum to determine the location and note the change in the spectrum so it can be recognized in step 8.

7. Slowly bring the panel into the FOV of the spectrometer from the bottom.

8. The live spectrum view will change when the panel reaches the edge of the spectrometer FOV. Indicate when this happens with a sound or motion that will be recorded by the GoPro.

9. Repeat steps 7 - 8 from the top and both sides.

10. Repeat steps 7 - 9 for each desired distance from the sensor.

11. Post process the video to determine the location of the spectrometer FOV at each distance. This requires playing the video back and recording the location of the edge of the coloured panel when it is indicated to be at the edge of the spectrometer field of view. The location of the FOV will then be bounded at the top, bottom and sides, and can be measured in pixels on the image.

The calibration was done with standoff distances from 1-10 m. An example of a composite image from the 3 m distance is shown in Figure 4.14. The calibration results are summarized in Figure
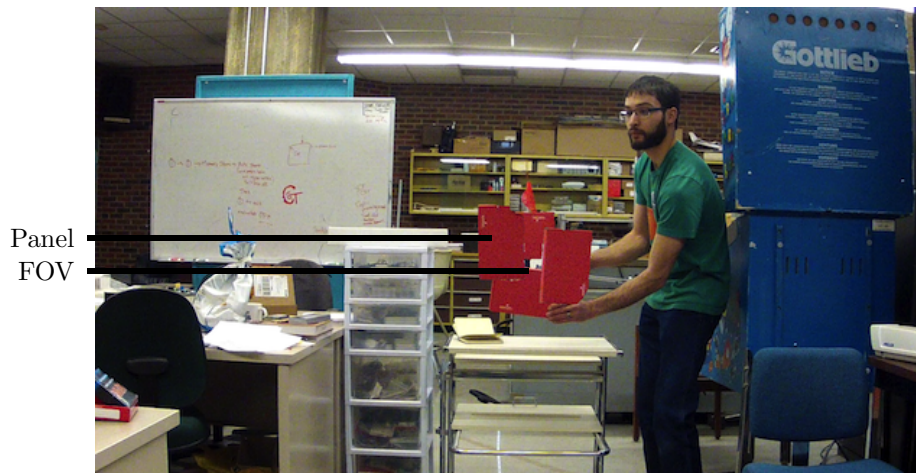
Figure 4.14: FOV calibration from a 3 m standoff distance.

4.15, which shows the measured location of the spectrometer spot in the GoPro image at each distance. These calibration results show that the spectrometer spot is near the centre of the image frame. The X-axis location is constant over the tested range, but there is some discrepancy on the Y-axis at short standoff distances. This is likely due to the large barrel distortions present in the
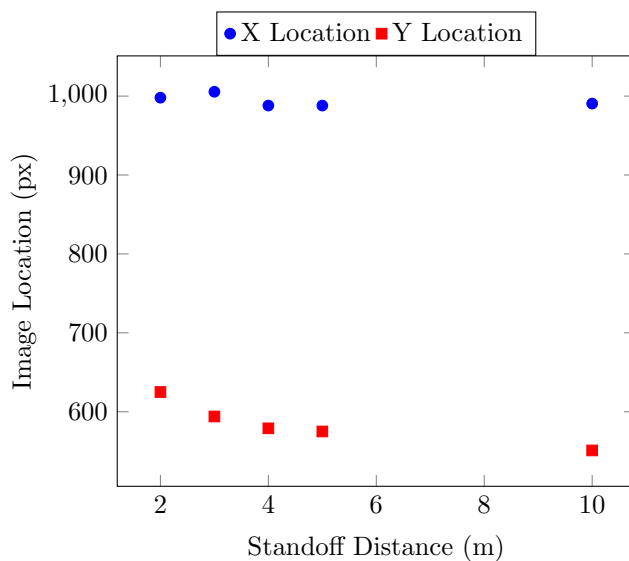
Figure 4.15: Location of spectrometer FOV in image frame.

GoPro and parallax on the test target, which are particularly pronounced at close distance. At larger distances the spectrometer point location remained stable. This calibration will allow the spectral data to be matched to a specific location on an image which is essential to give context to the data.

Camera calibration of the GoPro was also performed to characterize its lens distortion which should improve image rectification accuracy. The Camera Calibration Toolbox for Matlab [9] and was used to perform the camera calibration. This software uses images taken of known calibration targets to measure any distortion from the expected pattern. The software can then compute the image transformation required to correct the distortion, which forms the basis for the camera distortion model. Examples of the calibration images are shown in Figure 4.16. Note that Figure 4.16b only shows the calibration target in one position, but during calibration multiple images are used with the target in several positions to cover the entire frame. To perform the calibration, images showing the target in all areas of the camera frame were loaded into the software along with details of the target geometry. Details on the calibration procedure can be found in the software documentation [9].
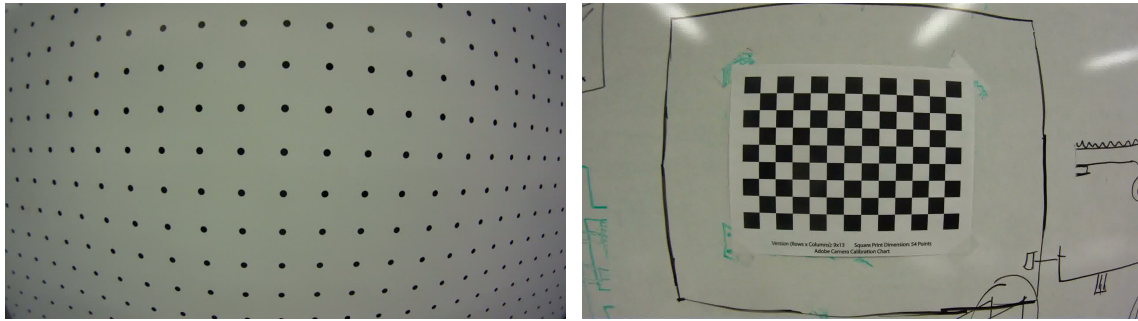
(a) DaVis calibration target   (b) Matlab calibration target

Figure 4.16: Examples of uncorrected images of calibration targets showing the high level of distortion in the GoPro

The Matlab results showing the high levels of distortion are shown in Figure 4.17. Note the simi-

Pixel error	= [0.5394, 0.4035]	
Focal Length	= (1217.02, 1218.8)	+/- [10.94, 10.91]
Principal Point	= (980.237, 518.517)	+/- [5.707, 5.803]
Skew	= 0	+/- 0
Radial coefficients	= (-0.2815, 0.07312, 0)	+/- [0.003019, 0.002034, 0]
Tangential coefficients	= (-0.0005175, -0.001535)	+/- [0.0003894, 0.000406]
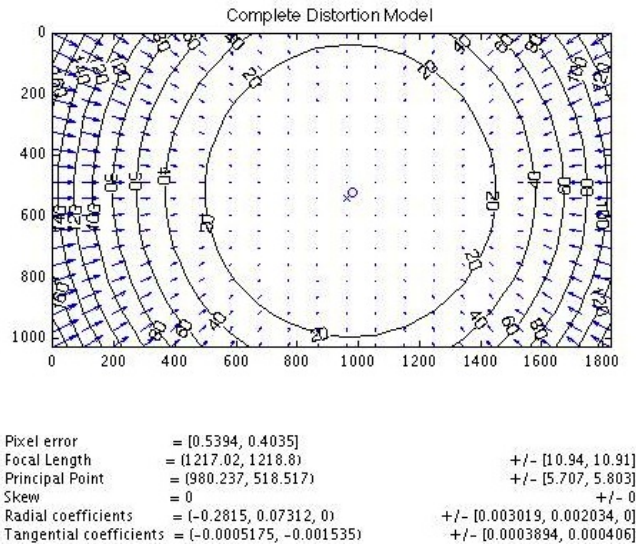
Figure 4.17: Complete distortion model for GoPro camera [9].

larity of the modelled distortion pattern in Figure 4.17 with the raw image in Figure 4.16a, giving

confidence in the calculated model. During subsequent testing, it was found that the PhotoScan

software did not require the inclusion of a camera model to produce accurately rectified images, so

these camera models were not used and further effort was not spent verifying their accuracy.

66

4.2 Field Testing

Several field trials were carried out at the Edmonton Radio Control Society's (ERCS) Bremner field and the University of Alberta EMEND forest research site near Peace River. Some preliminary flights were done with UAP1, but all full system tests were done with UAP3. Since these aircraft use different propulsion types, this also allowed the performance of internal combustion and electric drives to be compared. Flight tests of UAP3 were conducted in both summer and winter conditions to assess the year-round performance of the system. As colder temperatures negatively impact battery performance, flight times were shorter in the winter at around 15 minutes. In addition, the USB2000+ spectrometer is only rated to $-10°$C, which is the limiting factor of this system for winter operation. Some flights were conducted below this temperature, and it was found that the spectrometer functioned intermittently. The optical path of the camera and spectrometer during field testing is shown in Figure 4.18.

Figure 4.18: Optical path of spectrometer and camera

4.2.1 ERCS

All initial airframe and sensor flight testing was conducted at the ERCS field. First, each airframe was flight tested under remote pilot control to ensure it performed well and had favourable flight characteristics. After the integration of the autopilot and its sensors, further flights were performed to test the system functionality and tune autopilot gains as necessary. This is a lengthy process as the autopilot consists of nested PID control loops which must be tuned. Full details of the control loop structure is shown in Appendix C.4. A tuning process was developed to decouple most of the control loops by Stephen Dwyer. Full details on this process is provided in Appendix C.3.

The integration of the autopilot into UAP1 was significantly more difficult due to its internal combustion engine. Large vibrations were transmitted to the airframe from the engine causing the autopilot IMU to drift. Before the system could be flown, a vibration isolation system for the IMU was designed and tested to prevent this sensor error. Ideally a vibration isolation engine mount would be used in conjunction with an internal combustion engine to prevent transmission to the airframe, but limitations of budget and time prevented the purchase or design of a high performance mount. More information on the vibration isolation process can be found in [81]. Although the range of UAP3 is approximately 25 km compared to 100 km for UAP1, the autopilot integration was simple and only required rubber foam to damp vibrations from the electric motor.

Image Rectification

The imaging system was tested once the aircraft was found to be performing satisfactorily. This involved several flights to collect raw imagery and corresponding position data. To assess the geolocation accuracy of any generated imagery and spectrometer data, a full site survey with the Trimble R8 Base/Rover and TSC2 Survey Controller RTK-GPS was conducted. This allowed the location of the base point and landmarks around the field to be determined to centimetre accuracy. The base point was surveyed with a scale factor of 0.99994918, with an average horizontal and vertical precision of 5.9 mm and 8.6 mm, respectively. All subsequent survey points were collected

with a precision of at least 1 cm with respect to the base point. This is sufficient accuracy as the UAS imaging system was not expected to achieve better than 5 m accuracy. Future test targets can also be placed directly with measurements relative to the surveyed base point, greatly speeding and improving the test process.

These imaging test flights were done with both UAP1 and UAP3 to look at the effect of propulsion type on the imagery. As vibration levels were much higher on UAP1 due to the internal combustion engine, the images had more distortions. This did not prevent accurate stitching of the images and good results were achieved with both platforms. An example mosaic obtained from UAP1 imagery is shown in Figure 4.19. This is comparable to imagery obtained from the UAP3 platform, which is

Figure 4.19: Bremner mosaic from UAP1 imagery. This is a reduced resolution image for inclusion in this document. Note the visibility of two foot square sidewalk blocks.

shown in Figure 4.20. Even with the lens distortion of the GoPro camera, stitching and rectification produced imagery over the test area clearly showing 2 ft sidewalk blocks. A minimum geolocation accuracy of 3 m was measured by comparing the location of targets around the field with locations surveyed with the RTK-GPS system. This was taken from flights using both UAP1 and UAP3, as
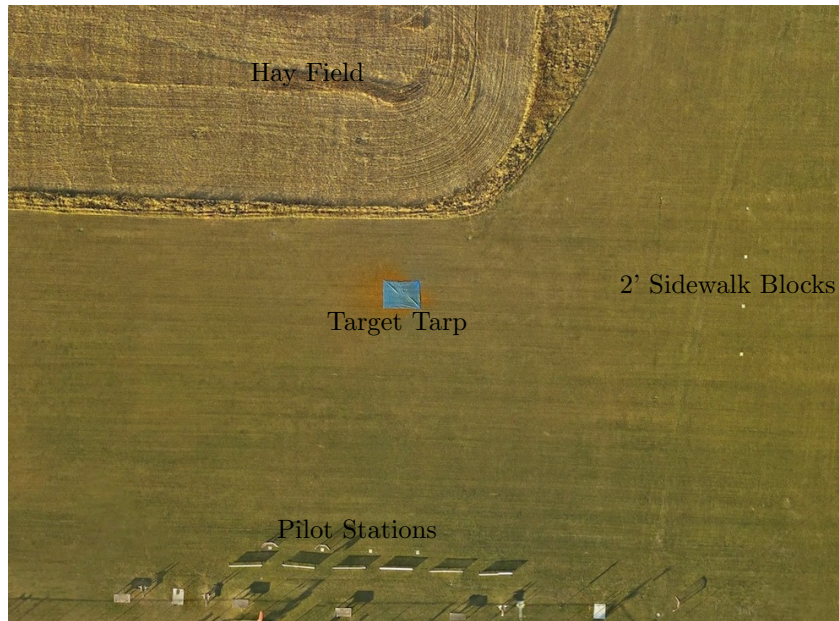
Figure 4.20: Bremner mosaic from UAP3 imagery. This is a reduced resolution image for inclusion in this document. Note the visibility of two foot square sidewalk blocks.

shown in Table 4.3. Note that survey data was not available for the EMEND location, so GCPs were collected with a handheld GPS receiver which would have introduced significant error of at least 5 m. Even with this error the image and GCP locations agree within the goal accuracy of 10 m. Image accuracy was calculated using the final mosaic image output, so errors due to tie points falling in the high distortion areas at the edge of the GoPro frame were not measured.

Table 4.3: Image Geolocation Accuracy

Flight/Aircraft	Targets	Measured Points	Average Offset (m)	Offset Heading (deg)
13-10-29 F2/UAP3	41	89	2.99 ± 1.90	229 ± 42
13-10-29 F4/UAP3	44	92	2.29 ± 1.14	207 ± 98
11-09-22 F1/UAP1	6	18	2.13 ± 0.79	280 ± 31
EMEND/UAP3	7	7	7.0 ± 1.1	-

The image accuracy is significantly better than the 10 m average accuracy of the onboard GPS receiver, which highlights the advantage of the aerial triangulation process used in PhotoScan.

By finding matching points in multiple images, the software is able to triangulate the position of the camera and improve the position and orientation estimates from the GPS and IMU. This effectively reduces the size and cost of avionics components required since high accuracy is not required. An important limitation of this strategy is the requirement of multiple tie points between images. When the area surveyed appears largely homogenous, for example after a large snowfall, the stitching algorithm will not be able to find tie points and the image rectification will fail. If there is not enough overlap between images, this process will also fail. Approximately 20% image overlap is recommended and this produced excellent results in this testing.

The inclusion of a camera model from camera calibration results did not improve the stitching and rectification accuracy. Geolocation accuracy was between 5-7 m regardless of if the camera model was used in the workflow or not. Although this theoretically should have improved the results, it is thought to be a limitation in the PhotoScan software that is causing a conflict between the external calibration and internal process that PhotoScan performs to self-correct the imagery. It is also important to consider that PhotoScan was in an early Beta stage (0.8.5) during this project, and many features were still in development. The work of Gurtner [29] in the calibration and use of fisheye lenses on UAVs may be useful. Even without the external camera calibration parameters, PhotoScan was able to achieve these results which simplifies the data processing procedure. Since the goal of this work is to assess the feasibility of the system, 10 m image accuracy is sufficient so improvement in the imagery was not pursued.

One limitation with the current image processing procedure is the requirement for tie-points between images. For most landscapes PhotoScan automatically generates points easily, but winter testing revealed that snow covered ground appears largely homogenous to the visible camera which prevents image stitching and rectification. Spectrometer and image data can still be collected and matched in this case, but the location accuracy will be limited to the position and orientation estimate of the autopilot as there is no improvement from aerial triangulation.

These results are also limited by the small number of field tests done, and further trials are required to verify reproducibility. Possible sources of error in georectification are: GPS/IMU inaccuracy,

lens distortion, data timestamping errors, video and telemetry synchronization error, image parallax and homogeneity of the aerial scene. Further work is required to quantify these sources of error if the system accuracy is to be improved. Effort was made to reduce these errors in the system design, and the under 10 m accuracy achieved meets the goal of the project.

Spectrometer Flight Testing

Once the image processing was tested, the spectrometer was integrated into the system and tested from the air. This was done using tarps as ground targets, as they are easily discernible with both the images and spectrometer data. As the USB2000+ only records the raw digital number spectrum, calibration against a white reference and conversion to reflectance was required to display the data. This was by taking three measurements of a spectralon panel before and after each flight. Due to the short duration (15 min) of each flight, the solar illumination was assumed to be reasonably constant during the flight and the pre- and post-flight white reference measurements were averaged to calculate reflectance [28]. In flights conducted around midday, the illumination was found to be fairly stable, as shown in Figure 4.21. Measurements of a known ground target during the flight
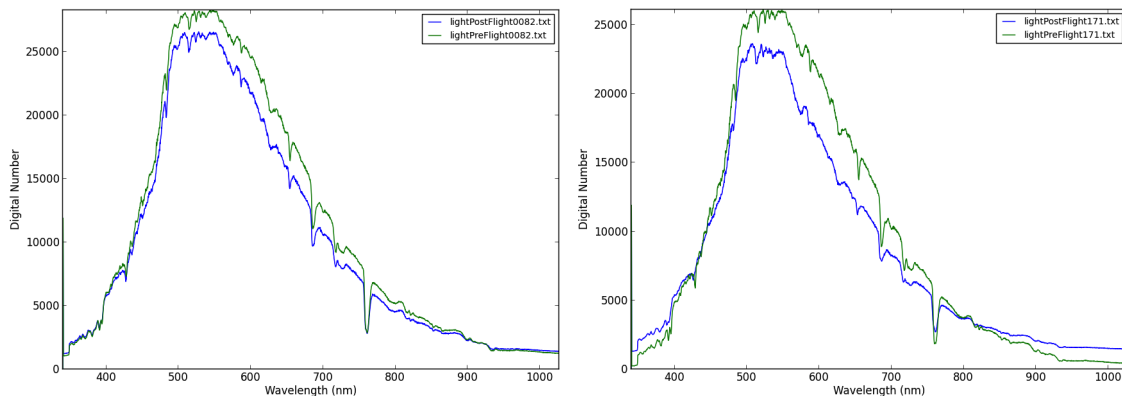
(a) Pre and post-flight illumination at EMEND site. (b) Pre and post-flight illumination at Bremner site.

Figure 4.21: Example illumination change during flight.

can also be used to correct the spectral data for inflight changes in irradiance. When longer flights are required over inaccessible terrain, an up-looking sensor can be added to the system to measure

solar irradiance directly. Since the dark current of the sensor was found to be stable, it was only measured before each flight. Custom software was written in python to post process the data and produce the plots included in this document.

A sample airborne tarp image is shown in Figure 4.22a and the corresponding spectrometer data is shown in Figure 4.22b. The image and spectral data both clearly show the presence of the tarp. This shows that the alignment of the spectrometer and camera field-of-view and electronic synchronization of the data sources is working to good effect. Any errors in alignment or calibration of the system would be evident in this testing as the tarp signature would appear in different locations. The level of contrast shown in Figure 4.22b is similar to what was achieved with the ASD in differentiating oily and watery sand (Figure 4.11). Since the tarp is readily identifiable with this airborne data, it suggests that with an extended range spectrometer the presence of oil would be similarly apparent and its detection could be automated. This means that a similar system could be outfitted with an upgraded spectrometer and tested with oily and watery targets in short order, paving the way for full scale industrial trials. With these promising results further testing was conducted with sand test targets, and the results are detailed in Section 4.2.3.

4.2.2 EMEND

A forestry case study was conducted at the University of Alberta EMEND forest research site near Peace River. Flight operations were based out of a clearing and georectified imagery was desired for the neighbouring forest where numerous instruments are deployed to monitor forest health. UAP3 was used for this testing as its small size and runway requirements are advantageous for forest deployment. The EMEND research area is approximately 4 km^2, which can be covered by UAP3 in a single flight. Since the area is remote and weather conditions were variable, four flights were conducted to ensure full coverage. The system performed well with some areas for control loop tuning identified. Some preliminary images were obtained, and a number of areas for improvement have been identified. An example image of the forest and operations area in the clearing is shown in Figure 4.23.

(a) Aerial image of tarp test target.
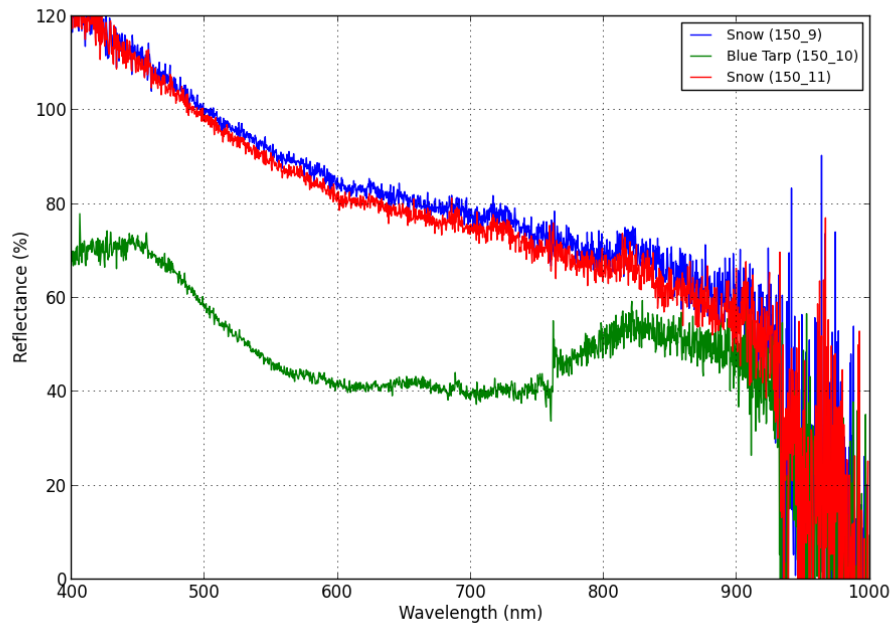
(b) Spectra corresponding area shown in Figure 4.22a. Snow spectra was taken immediately before and after the tarp along the flight line.

Figure 4.22: Corresponding image and spectrum from first flight testing over a tarp test target.

Figure 4.23: EMEND mosaic from Mentor imagery. This is a reduced resolution image for inclusion in this document.

Over the clearing, high quality imagery with approximately 7 m accuracy was obtained which is still within the target accuracy of 10 m. The ground control points at EMEND were taken with a handheld GPS receiver, so their accuracy is not well known. Due to the similarity of the clearing to the terrain at the Bremner test site, this is the expected result. Images obtained over the forest itself proved to be very challenging to align and georectify. This is due to the large amount of parallax in the images that cause inconsistencies in the tie points generated between images. For example, the sides of tree trunks are visible and appear to be in a different location in each image which makes the PhotoScan alignment algorithm fail. Several sources of error were identified from this test, along with recommendations for reduction that were implemented in subsequent testing:

Image Parallax: This restricts the number of images for which accurate tie points can be generated. Masking the images to include only the near nadir viewing angles may improve the matching, but this also decreases the overlap between images. A higher flight altitude and/or narrower field of view camera are recommended to improve the quality of data collected. It is important to note that the altitude must be determined relative to the tallest feature in the

survey area (ie. tree tops).

Image Sync: Slight misalignment of the video file and flight log will directly effect the accuracy of image geolocation. An electronic triggering device to automate the synchronization of the images and flight telemetry was not included in the system at the time. This has been implemented since the first EMEND test flights and has allowed the image processing procedure to be mostly automated.

Image Quality: The resolution of images obtained was not high enough to discern the location of forest monitoring nodes. Flying at a higher altitude to reduce image parallax will further reduce resolution, suggesting that a higher resolution camera is required to visually locate node position.

This EMEND site also provided a valuable opportunity to test field deployment procedures since it is a remote location. The preparation of checklists and operations procedures ensured everything went smoothly resulting in successful imagery and spectrometer data collection over the site. These can be found in Appendix C.2.

4.2.3   Ground Targets

Final system testing involved the preparation of large ground targets consisting of dry and paint saturated sand as an analogue to clean and oily sand. This test is intended to simulate a hydrocarbon seepage leak in such a manner that it could be detected with the sensor suite on UAP-3. To prepare the paint samples, green acrylic paint (ASTM D-4236) was mixed in a 1:10 ratio with water and applied to the sand with a Flo-Master 2 gallon sprayer (see full details in Section 3.4.3). As shown in lab testing, the USB2000+ is not sensitive enough to differentiate oily and wet sand, so testing with wet and dry sand was used to prove the concept. These targets were laid out on tarps placed at known locations to verify the geolocation accuracy in addition to spectral measurements. A ground view of the target is shown in Figure 4.24, and an aerial shot of the targets is shown in Figure 4.25. Tarps were laid flat and staked to the ground at the corners, and enough sand was spread over

76

Figure 4.24: Ground view of field prepared sand target.
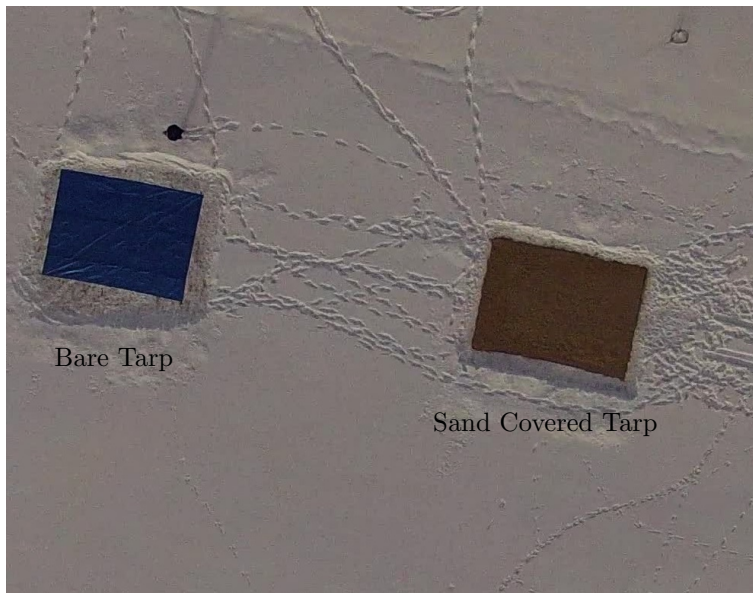
Figure 4.25: Aerial image of sand test target.

the tarp to prevent the blue colour of the tarp from being seen. Approximately twenty 50 lb bags of Sil-4 sand were used to cover the entire surface of the tarp. The position, height, and speed of each acquisition was recorded to allow for the calculation of spectrometer spot size. Spectrometer integration time remained constant during each flight to ensure that all spectra recorded could be directly compared, and a white reference spectrum was recorded before and after each flight. The painted sand target was prepared in the field as discussed in 3.4.3 and is shown in Figure 4.26.
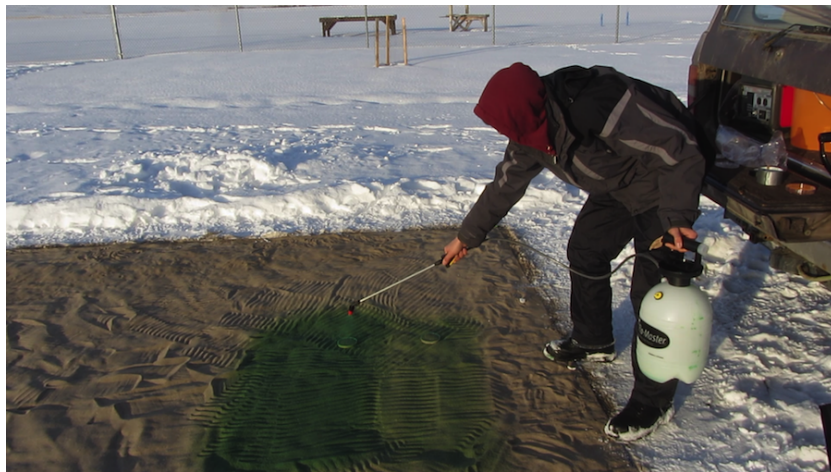
Figure 4.26: Painting sand target in the field.

During initial flight testing with bare tarp targets it was found to be difficult to align the spectrometer field of view over the tarp at a 2 Hz sampling rate. This drove the software rework to allow 4 Hz sampling, as discussed in 4.1.1, which greatly improved the chances of hitting the tarp. Unfortunately, equipment failure during field testing meant that the original experimental procedure for sand target testing could not be followed. Snow entered the Logomatic board during landing on a test flight which caused a failure of a crucial input pin, disabling the data logging system on the aircraft. Without the ability to log flight and spectrometer data on the aircraft, testing continued with the prepared sand targets and ground station based data logging. This required holding the aircraft by hand above the target and running the spectrometer via USB from a laptop computer,
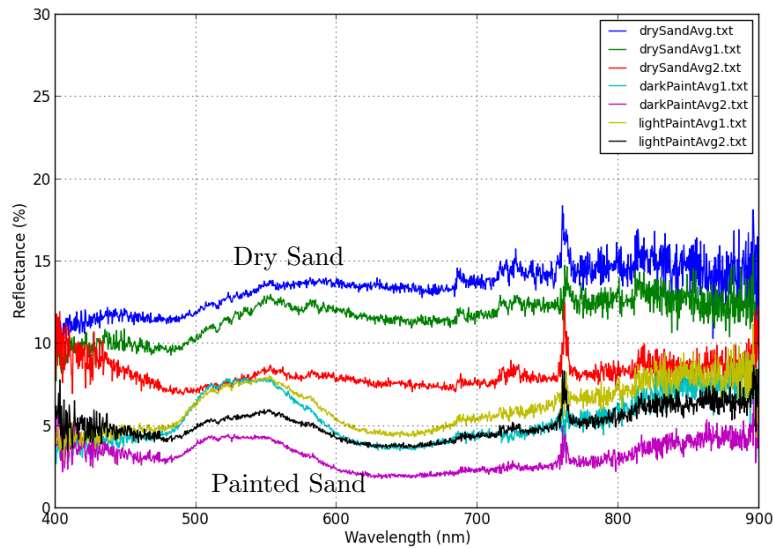
Figure 4.27: Summary of spectra from field sand testing

which limited testing to a standoff distance of 3-4 ft. Although this is not ideal, earlier airborne testing (Figure 4.22) showed that the system is capable of making airborne spectral measurements, so it was more important to collect measurements of the sand targets in the field than to do it from the air. Figure 4.27 shows a summary of the spectra obtained during this test. Each line on the plot is an average of three separate, unaveraged measurements as they would have been obtained on the aircraft. The numeral suffix on each filename indicates which experiment repeat the data is from. The difference between the painted and unpainted targets can be clearly seen, but the light and dark areas cannot be differentiated. This is largely to do with the geometry of the test setup. The 3 ft standoff distance makes the spectrometer spot size approximately 4 cm, which is much smaller than the planned 2 m spot size from 50 m standoff. This small spot size caused local variations in the application of the paint and the geometry of the sand to influence the results. Small bumps in the sand cast shadows which appear large at this small spot size which greatly affect the calculated reflectance. At the anticipated standoff distance of approximately 50 m the spot size is 2 m, and at this scale the small surface variations would have much less impact making the measurement a

79
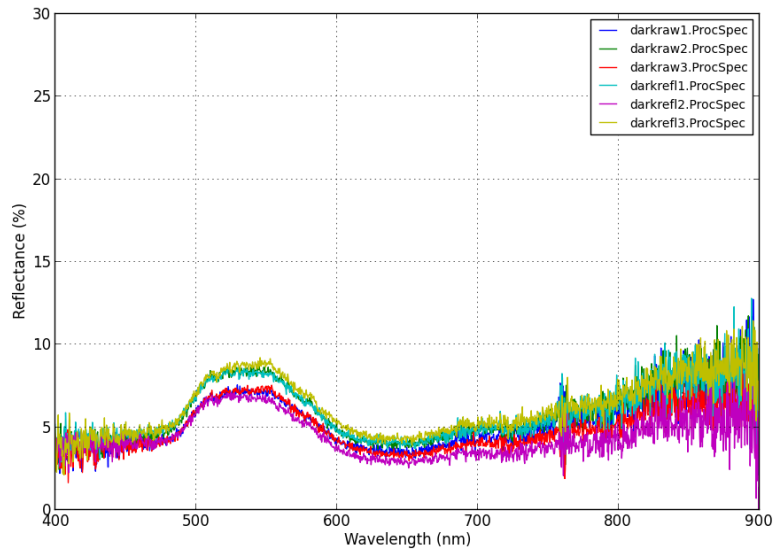
Figure 4.28: Individual spectra of the dark target from repeat one.

better average of the entire target.

The affect of local geometry on the reflectance can be seen in Figure 4.28, which shows all the individual samples that make up the darkPaint1 average. Each spectra has the same shape but is translated up or down relative to the others, indicating that the illumination was not constant for each sample. Since the spectrometer was calibrated with a white reference before each sample, this illumination change can be attributed to surface variations which cast shadows near the scale of the 4 cm spot size. This suggests that better results may actually be obtained from the 50 m in-flight standoff distance in the original design.

4.3 Discussion

4.3.1 Overall Performance

The development and testing of these UAS have shown the potential for small and inexpensive airborne sensors to monitor important industrial and environmental assets. Despite the low $6000 cost of the entire UAP3 system, it was able to produce high quality results with minimal user input. The aircraft is able to stably and reliably fly under automatic control to survey pre-programmed areas of interest. Aerial maps and corresponding spectra were produced using very low cost and readily accessible tools, which accomplished the main goal of this work. Even with the limitations of the GoPro camera and USB2000+ spectrometer, this data would be very useful for environmental monitoring. Since each component of the system was chosen primarily to reduce cost, the limitations of the current system can be addressed with upgrades to individual components as required. For short duration missions, simply using an extended range spectrometer and higher resolution camera would greatly improve utility of the collected data. As this work has shown that inexpensive point spectrometers can be effectively used in airborne applications they were not originally designed for, the cost of the spectrometer can be kept low. A higher quality camera would produce more detailed aerial imagery, but for many applications the ground image resolution of 3 cm that can be easily obtained with the GoPro is sufficient, and its low cost, light weight, and ease of use makes it an attractive option. In cases where the surrounding landscape is flat, higher resolution can also be obtained by flying at a lower altitude. For some applications like pipeline monitoring, long duration flights are required and the UAP systems developed for this project are not capable of meeting this need. Several commercial airframes and UAV service providers that are capable of extended duration flights are already available, and the current sensory package could easily be integrated into them.

4.3.2 Error Analysis

The results of initial image geolocation accuracy testing are shown in Table 4.3. This shows that all tested imagery was within experimental error and the largest expected error is less than 5 m. The direction of the error varied enough between test points and flights that no direction can be confidently associated with the error. Further analysis of the imagery spatial error was conducted using the National Standard for Spatial Data Accuracy [23]. Using this standard UAP3 flights 2 and 4 shown in Table 4.3 were tested to 6.11 m horizontal accuracy at 95% confidence interval and 4.42 m horizontal accuracy at 95% confidence interval, respectively. This is valid assuming that systematic errors have been eliminated as much as possible and errors are normally distributed and independent in the east and north component. The vertical accuracy of the system was untested. Since high accuracy ground survey points were only available at the Bremner test field, further flights should be conducted in various locations to confirm the error is not heavily dependent on the flight location. An estimation of the sources of error present in the system is included in Appendix B. Further work is required to quantify the error contributions.

As expected, spectra from the $3000 Ocean Optics USB2000+ spectrometer had some discrepancies compared to spectra from the $30,000 ASD FieldSpec. Although not as accurate and more noisy (Figure 4.12), the USB2000+ measurements were repeatable, indicating that at least some inaccuracy can be corrected. Reflectance data collected with the USB2000+ during the sand field trials are shown in Figure 4.29. While some spectra, particularly in Figure 4.29a, show some deviation from one another, the majority of measurements agree very closely. Most of this deviation is likely causes by local surface geometry causing illumination variation near the scale of the sensor, which was only 4 cm in these handheld tests. The shape of each spectrum is largely the same and remains consistent between trials, indicating the repeatability of the testing. There is also a large difference between the painted samples and the dry sand spectra in Figure 4.29e, showing that the spectrometer was functioning and is easily able to detect the presence of the paint.
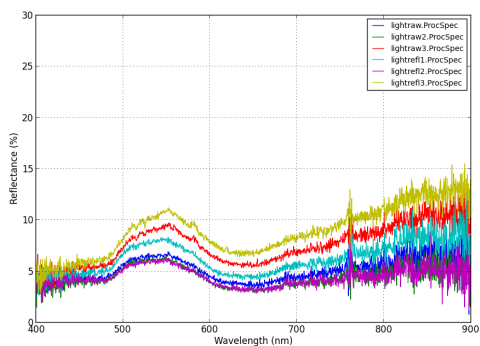
(a) Light paint spectra, trial 1
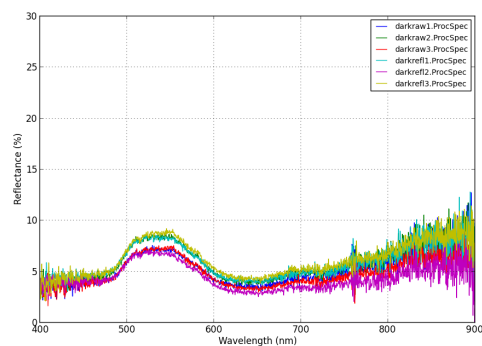
(b) Dark paint spectra, trial 1
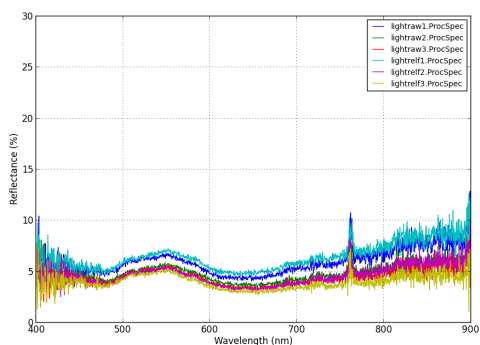
(c) Light paint spectra, trial 2
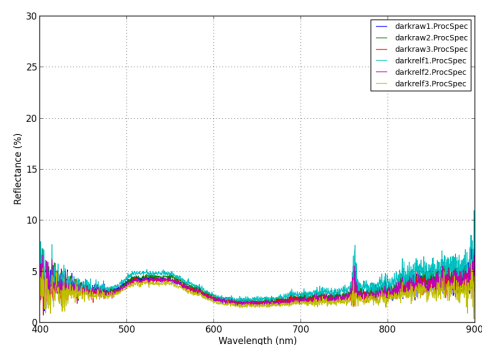
(d) Dark paint spectra, trial 2
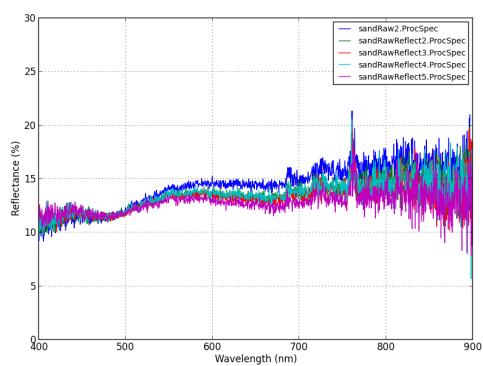
(e) Dry sand control spectra

Figure 4.29: Measurements taken during painted sand field trials

4.3.3 Potential Future Field Implementation

With the feasibility of this approach shown, there are several steps still required before industrial deployment of this technology. Since flying time was limited during this work to a total of approximately 8 hours, more testing and study is required to assess and improve the reliability of this type of system. Repeats of the field trials also need to be done to verify the reproducibility of the results presented here. As an industrial deployment would often be conducted over valuable assets or members of the public, the reliability of the system would have to be proven. It is also important to note that the small size and mass of these systems result in minimal damage in the event of a critical failure, which reduces the reliability requirement due to lowered consequence. This evaluation would be done as part of a full risk assessment that is required to meet SFOC regulations in Canada. Currently regulatory approval is handled on an individual case basis by Transport Canada, which can result in deployment delays. Additionally, SFOCs are issued by regional offices which causes requirement inconsistencies in different parts of the country, further complicating the industry. New regulation is in development that will ease the process for UAV operation which will soon become common practice.

A more robust airframe and sensor package is also required, as the current system is not able to operate in precipitation or temperatures below $-10°$C (USB2000+ limitation). This environmental limitation of the current system is the root cause of the failures during field testing that prevented airborne measurements, which highlights the need for ruggedization. For some missions, such as pipeline monitoring, a long range aircraft would be required which is outside the capability of the vehicles used in this work, but there are several commercially available UAVs and UAV service providers that are capable of such missions. A more difficult requirement for long range missions is meeting regulatory requirements as most current UAV operations are conducted within line of sight or in segregated airspace and the regulations for beyond line of sight UAS operations are not yet well defined. Finally, a full economic study of UAV use will be required to ensure the commercial viability of this type of system. The economics should be compelling, as the cost of an entire small-scale UAS is typically less than the cost of a single full scale manned survey mission,

which for corridors mapped to centimetre accuracy can cost \$7,800 per mile [43]. Manned surveys have the advantage of a proven history and have crew members on board who can monitor mission progress and take action if equipment malfunctions occur.

Chapter 5

Conclusions and Future Work

A series of tests were conducted on a custom built UAS to assess the feasibility of using a low-cost airborne system for environmental monitoring applications. This included testing during development and field case studies over forest and farm terrain with prepared ground targets. Although the entire system was built for less than \$6000, it performed well and produced useful results. Autonomous missions were achieved that collected spectral data and imagery of a defined survey area. The only manual control was by the RC pilot during takeoff and landing; all other aspects of the flight were controlled by the Paparazzi autopilot based on the preflight mission plan created by the GCS operator.

5.1   Performance Assessment

The system was able to produce maps with better than 5 m spatial accuracy, despite the 10 m nominal accuracy of the GPS receiver. This was possible due to the aerial triangulation that was performed on the collected imagery by the *PhotoScan* image processing software. There was also no need for camera calibration or the camera model in the post processing workflow, which makes the process widely applicable to different systems and drastically reduces the cost and setup time

of the system.

The USB2000+ spectrometer performed well integrated into the UAS, and was able to differentiate between bare, sand, and painted sand targets. Unfortunately a pin failure on the data logging board prevented airborne testing of sand and painted targets. Ground testing showed the system can differentiate between dry and painted sand, and airborne measurements of a bare tarp showed that the system can take measurements while flying. These results gave confidence that the system can effectively collect ground spectra from the air. Since the system design is modular, it is also expected that components can be easily upgraded to create a system sensitive to features outside the visible wavelengths.

Once the system had been upgraded for 4 Hz spectrometer sampling, collecting spectra over the 15' x 20' target became feasible. At lower sampling rates the chances of the aircraft being directly over the target when the spectrometer was sampled were too low to be confident of getting a sample during a 10 minute flight. While it was possible to get a target tarp sample, further development of flight planning is required to reduce the trial and error that is currently required in setting waypoint locations. The survey flight plan performed well in collecting map imagery over the flight area, and a similar routine could be developed for sampling over a small target. While this kind of survey would be useful for future research use, it is not required for most monitoring applications where distributed sampling over a large area is desired. The current system works well for a typical surveying application.

Through the development and testing of the current system, the objectives laid out at the beginning of the project were accomplished. The feasibility of a small scale, low cost UAS for environmental monitoring was demonstrated, and the design methodology to create such a system was provided. This resulted in an affordable procedure for collecting airborne remote sensing data. As this was a feasibility study, there are gaps between the current system and the requirements of an industrial version, which are discussed next.

5.2 Future Work

Having demonstrated the feasibility and utility of an inexpensive UAS, there are many areas of development to improve performance of the system. The overall system architecture was effective, so these are generally component upgrades to expand system capability, including:

- a higher resolution camera with less distortion for higher quality imagery;

- an extended range spectrometer for hydrocarbon detection at 1730 nm;

- and a ruggedized airframe for all weather flights and winter operation.

These items would take the current system from a laboratory research platform to a fully integrated commercial package that could be used for industrial surveying. Each item would require dedicated laboratory research and testing prior to deployment, and some component upgrades will cause a cascading series of upgrades. For example, an imaging or spectrometer upgrade would likely require an upgrade of the onboard data logging system, and all of this may then require a larger airframe to get airborne. Long range testing would also be required in preparation for pipeline surveying and other mission types that require covering a large area of land.

5.2.1 Imaging System

The GoPro camera system used in this work was rudimentary and better results could undoubtably be obtained with a higher quality camera. Since the techniques developed during this study worked well using the GoPro, they should transfer easily to higher quality sensors. Of particular interest is quantifying the improvement in resolution and accuracy of the generated mosaic obtainable with a better camera. More study is also required to determine the gains that can be made with a fully calibrated camera model in the workflow. The PhotoScan software is also under active development and is currently still in beta release, so there will also be improvements in future PhotoScan releases that should be used in future system revisions.

Further calibration of the imaging system at standoff distances similar to flying height is recom-

mended to confirm that the trend from the FOV calibration at up to 10 m holds at long distances. It was found that including a camera model into the PhotoScan georectification procedure did not improve accuracy. More testing is required to determine the cause of this and the procedure for achieving the most accurate imagery. The synchronization of the GoPro imagery should also be tested in the lab to quantify its accuracy. This can be done by running the sampling system with an LED in the field of view so that the offset between LED trigger and DTMF tone extraction can be measured.

5.2.2 Extended Range Spectrometer

To detect the presence of hydrocarbons, a spectrometer sensitive to wavelengths around 1730 nm and 2310 nm is required [35]. Detection of other substances would be possible with an appropriately selected spectrometer. For example, the Ocean Optics NIRQuest256 measures from 900-2500 nm, weighs 1.2 kg and costs around $23,000. This spectrometer should be capable of hydrocarbon detection since it operates in the same wavelength range as the ASD FieldSpec Pro used as a reference standard in this work. This particular instrument would require a larger airframe to handle its larger mass, but the same system architecture used in this work would be applicable. Integrating an extended range spectrometer would require following the same steps taken in this work to test and integrate the USB2000+, from bench testing with a known reference to full scale field tests with prepared targets.

5.2.3 Ruggedized Airframe

The Mentor aircraft used in this work is a small hobby aircraft that is not sealed to the weather. While useful for development, an all-weather year-round system is required to move beyond a feasibility study. In addition, most industrial applications would require much longer than the current 15 minute flight duration to survey areas of interest. There are many commercially available airframes and even UAS service providers which would be the preferred route to achieve these goals.

Development of a custom airframe would be an independent research project that would not be required to meet the needs of this system.

5.2.4 Software Development

Further software development would allow for the integration of spectral data and mosaic imagery in a user friendly interface. Currently the spectra files and corresponding image files are saved with the same base name to allow them to be matched. In a commercial deployment, a GUI would be required that can show the location of spectral acquisitions as an overlay on the stitched map and have a combined interface to view spectra plots. All the data required to implement a system like this is already available, and it would greatly improve ease of use. This would be needed before the system was commercialized, otherwise the data processing procedure would require too much manual file matching and keystrokes to be viable.

The current data post-processing workflow is not quite fully automated. While scripts have been written to extract all of the flight data and images, there is still one manual step involved during the offloading of flight data from the aircraft and one during import of this data into *PhotoScan*. With the current system offloading aircraft data is likely to remain manual as this data is saved directly onto SD cards and there is no high bandwidth datalink between the aircraft and ground station. Adding a link capable of full data transfer would require a major system redesign. The manual step during import into *PhotoScan* could be easily automated as *PhotoScan* contains a Python API with access to all required functions. In order to automate this step, further testing is required to determine the processing settings in *PhotoScan* that produce the best results for the data set types generated by the UAP system.

To make the system accessible to more users, fully autonomous takeoff and landing can be accomplished with some additional flight testing and control loop tuning. The Paparazzi system is already capable of takeoff and landing as demonstrated on other aircraft, but testing is required to tune control loops and settings on UAP3 before it is attempted with this system.

5.3   Summary

The objective of this work was to demonstrate the feasibility of a small UAS for environmental monitoring and provide a design methodology for affordably obtaining aerial remote sensing data. To do this, two UAVs were custom built using hobby aircraft and off the shelf sensors and electronics. The aircraft were outfitted with a low cost earth observation payload consisting of a video camera and point spectrometer. A combination of commercial software and custom scripts were used to process data collected from the UAS. For a total system cost of $6000, UAP3 was able to generate maps of the test site with 3 cm resolution and horizontal accuracy of 4.42 m, along with spectrometer data for each photo along the flight path. The key specifications achieved are shown in Table 5.1, and a full cost breakdown is shown in Appendix C.1. This shows the high capability that can

Table 5.1: Key specifications for the final UAS

	UAP-3
Total Cost (CAD)	6000
Image Resolution (cm)	3
Image Accuracy (m)	4.42
Spectral Range (nm)	400-1000
Spectral Resolution (nm)	0.75
Spot Size @ 80m AGL	3.2m
Airframe	Multiplex Mentor
Propulsion	Electric
Fuel	Lithium polymer batteries
Wingspan (m)	1.7
Length (m)	1.2
Max Speed (km/h)	90
Payload Capacity (kg)	2
Max Takeoff Weight (kg)	2.7
Max Endurance (min)	20

be achieved at a very affordable rate. The modularity of the system will also allow sensors to be exchanged for higher performance models, which will expand the functionality of the system without requiring a new procedure.

Future laboratory work could quantify the gains achievable with various sensor upgrades, which

would be required prior to an industrial deployment of this system. Several upgrades to the aircraft and further testing would also be required to meet most commercial requirements. The current work is an important step in developing UAS for commercial work, and contributed a working procedure for collecting imagery and spectra data with low cost equipment. Methods developed during this project can be applied to monitoring applications such as tailings pong stability and hydrocarbon leak detection, where they would help to improve the performance and reduce the cost of monitoring.

This study successfully demonstrated that low cost UAS can be built to effectively gather remote sensing data. The system flew autonomously and was able to collect spectral measurements and generate high resolution maps with under 5 m horizontal accuracy. Methods developed can be applied to industrial monitoring applications, and suggestions have been made to extend the study to include instruments capable of detecting surface hydrocarbons and moisture content. Altogether, the procedures and techniques developed in this work can be used to bring down the entry costs of remote sensing and enhance the capabilities of researchers and copororations.

Appendix A

Experimental Procedures

A.1 Lab Spectrometer Verification

A.1.1 Test Plan

Lab testing was done to compare the readings of the low-cost USB2000+ against the FieldSpec as a reference standard. Aside from verifying the functionality of the USB2000+, the various sand and clay targets were evaluated for ease of preparation and ability to differentiate with the USB2000+ in preparation for airborne field trials.

Objective: Establish a baseline by measuring known samples with the Ocean Optics (OO) airborne setup and comparing against the Analytical Spectral Devices FieldSpec (ASD)

Manipulated: Target composition, water content and oil content

Responding: Spectral readings from OO and ASD

Controlled: Lighting, viewing angle, ambient conditions, target size (edge effects)

Equipment: Listed below:

- ASD FieldSpec

- Ocean Optics USB2000+ VIS-NIR-ES

- computer with ASD and OO software

- traceable sand and clay samples

- water

- canola oil

- weigh scale

- oven

- petri dishes for samples

- 50W halogen Lowel Pro-light

- mount stand, tripod

- ASD 25° fiber tip

- OO 84-UV-25 lens

- 74-DA lens

- fiber optic patch cable

- weather meter

- air tight sample bags

- Spectralon panel

- graduated cylinder, beakers, spatula

Table A.1: Lab verification trials with traceable sand and clay samples[30]. Silica sand is fully saturated at $\sim 30\%$ water - testing will not proceed beyond full saturation to avoid surface pooling

Additive	Content By Weight	Sand	Clay	50% Sand/Clay	Soil
	0%	A0	B0	C0	D0
Water	10%	Aw10	Bw10	Cw10	Dw10
	20%	Aw20	Bw20	Cw20	Dw20
	30%	Aw30	Bw30	Cw30	Dw30
	40%	Aw40	Bw40	Cw40	Dw40
Canola Oil	10%	Ac10	Bc10	Cc10	Dc10
	20%	Ac20	Bc20	Cc20	Dc20
	30%	Ac30	Bc30	Cc30	Dc30
	40%	Ac40	Bc40	Cc40	Dc40

Water content is determined by (ASTM D2216)[7]:

$$w(\%) = \frac{M_{cms} - M_{cds}}{M_{cds} - M_c} * 100 = \frac{M_{water}}{M_{specimin}} * 100 \tag{A.1a}$$

$$M_{water} = \frac{w(\%) * M_{soil}}{100} \tag{A.1b}$$

The same equation will be used to determine oil content by weight.

Spot Size

For comparison, at $1m$ stand off distance the 84-UV-25 lens has a spot size of $26.5mm$ and a $1°$ field of view has a spot size of $17.5mm$

Table A.2: Calculated spot size for various field of view and standoff distance

Standoff (cm)	FFOV (degrees)									
	1	2	3	6	8	10	14	16	20	25
10	0.17	0.35	0.52	1.05	1.4	1.75	2.46	2.81	3.53	4.43
20	0.35	0.7	1.05	2.1	2.8	3.5	4.91	5.62	7.05	8.87
30	0.52	1.05	1.57	3.14	4.2	5.25	7.37	8.43	10.58	13.3
40	0.7	1.4	2.09	4.19	5.59	7	9.82	11.24	14.11	17.74
60	1.05	2.09	3.14	6.29	8.39	10.5	14.73	16.86	21.16	26.6
80	1.4	2.79	4.19	8.39	11.19	14	19.65	22.49	28.21	35.47
100	1.75	3.49	5.24	10.48	13.99	17.5	24.56	28.11	35.27	44.34

Table A.3: Calculated spot size for Ocean Optics lenses with various standoff distance

Standoff (m)	84-UV-25 (m)	74-DA (m)	Standoff (cm)	84-UV-25 (cm)	74-DA (cm)
10	$6 \cdot 10^{-2}$	0.4	10	2.29	0.72
20	0.1	0.8	20	2.33	1.12
30	0.14	1.2	30	2.37	1.52
40	0.18	1.6	40	2.41	1.92
60	0.26	2.4	60	2.49	2.72
80	0.34	3.2	80	2.57	3.52
100	0.42	4	100	2.65	4.32

From Ocean Optics:

$$D_{spot} = 2 \cdot d_s \tan \theta_{div} + D_{ca} \tag{A.2a}$$

$$\theta_{div} = \arctan \frac{(D_{core}/1000)}{2f_l} \tag{A.2b}$$

Where:

D_{spot} = spot diameter in mm

d_s = standoff distance in mm

θ_{div} = divergence angle

D_{ca} = clear aperature in mm

D_{core} = fiber core size in μm

f_l = focal length in mm

A.1.2   Procedure

1. Dry sand, clay and soil as per ASTM D2216 [7]. Record initial water content for reference.

2. Setup measurement equipment - verify operation, field of view, viewing angle, ambient conditions are constant (log throughout testing with Kestrel 4500)

   - Set ASD to average 25 samples for each reading

   - For ASD, 'Optimize' instrument after any change in geometry

   - Fix measurement lenses at nadir with illumination at 45°

   - Mark location of sample tray at center of field of view

   - Focus light for even illumination across sample

   - Turn off all other light sources

3. Allow 30 minutes for ASD to warm up before commencing measurements

4. Calibrate instruments by recording dark current and white reference (Spectralon panel) using:

   - ASD

   - OO with SpectraSuite (84-UV-25 & 74-DA)

   Repeat calibration every 15 minutes during testing

5. Record spectra of water and canola oil with ASD and OO for reference

6. Prepare sample:

(a) Measure X grams of material (enough to ensure $\geq 5mm$ depth throughout container)

(b) Add additive until desired mass content is achieved (A.1b)

(c) Mix thoroughly until sample appears homogeneous

(d) Shake sample to level surface - ensure $5mm$ depth throughout petri dish

7. Place sample at center of instrument field of view

8. Record spectra of 3 spots on surface using:

   - ASD

   - OO with SpectraSuite (84-UV-25 & 74-DA)

9. Seal sample in petri dish, label and store to check for stratification over time

10. Repeat steps 6 - 9 for all samples listed in Table A.1. Recalibrate with Spectralon panel every 15 minutes during testing.

A.1.3 Results

The sand used was SIL-4 [69] from Sil Industrial Minerals. The kaolin was EPK Kaolin, CAS #1332-58-7. To ensure the samples did not contain water prior to testing, they were dried according to ASTM D2216 [7]. These results, shown in Table A.4, indicate that the bulk sample received contained very little water, especially in the case of silica sand.

Table A.4: Results of oven drying lab test samples

| Sample | Tray Number | Change in Mass (%) | | | |
		1st hour	2nd hour	3rd hour	4th hour
Kaolin	1	0.92	0.08	-	-
	2	0.94	0.03	-	-
Bentonite	3	2.48	2.18	2.35	1.49
	4	3.47	2.52	1.69	1.25
Silicia Sand	5	0.04	-	-	-
	6	0.04	-	-	-

Table A.5 summarizes the lab trials that were conducted to determine the sensitivity of the spectrometer, and the feasibility of using to detect various concentration of water and oil. Trials were done with silica sand, bentonite and kaolin mixed with varying amounts of water or canola oil. As the 74-DA lens was found to give the highest signal to noise ratio in preliminary testing, it most trials used this lens. Ten samples were also measured with the 84-UV-25 lens for comparison.

Table A.5: Results of spectrometer lab testing with 74-DA lens

Sample	By Weight	ASD Filename	Additional Note
A0	0.0	003-005	None
Aw10	10.8	006-008	None
Aw20	19.7	009-011	None
Aw30	23.3	012-014	Saturated at 30%, pooling water removed
Ac10	9.9	015-018	None
Ac20	19.4	019-021	None
Ac30	13.6	022-024	Saturated at 30%, pooling oil removed
B0	0.0	025-027	None
Bc30	29.1	028-030	4mm depth
Bw90	91.9	031-034	4mm depth
Bw120	120.0	038-040	None
Bw150	152.9	041-043	Almost saturated
Bc120	117.7	044-046	Way too saturated!
Bc60	63.7	047-049	Looks saturated
Bc45	45.7	050-053	almost saturated
K0	0.0	054-056	None
Kw50	50.3	057-062	2mm depth as lowest point, Kw90 saturated!
Kw60	59.5	063-065	almost saturated, 5mm depth
Kw70	70.8	066-068	almost saturated, 4-6mm depth
Kc45	45.3	069-071	None
Kc60	62.6	072-074	Lowest point is 3mm depth
Kc75	76.0	075-077	About saturated
Bc35	35.3	103-105	3mm depth
Bc40	40.2	106-108	about saturated

Sample	Weight A	Weight B	By Weight	ASD Filename	Additional Note
A/B0	49.5	50.5	0.0	078-080	None
A/Bw70	50.2	49.8	70.7	081-083	None
A/Bw85	50.2	49.8	85.3	084-086	None
A/Bw120	50.4	49.6	120.7	087-089	Almost saturated
A/Bc30	49.8	50.2	30.6	090-092	Pretty saturated
A/Bc20	50.3	49.7	19.9	093-095	None
A/Bc15	50.0	50.0	15.1	096-098	4mm depth

A.2   Image Processing Software Reviewed

- ILWIS - opensource GIS software, allows for GCP georeferencing only.

- ENVI - allows for GCP rectification. Ortho module required for inputting pos/orient of sensors.

- OSSIM - opensource GIS package. Supports rectification with RPC for sensor model and position. Stuck on getting elevation to read properly.

- Orfeo Toolbox - open software development toolbox for making GIS software. Supports rectification, but again only with RPC (capable of generating RPC from GCP). Does not currently support bundleblock adjustment.

- AirPhoto - Part of the Bonn Archaeological Software Package, can be used to create orthophotos from aerial imagery. Shareware, accuracy not as high as commercial packages. Only has support for GCP based rectification.

- EnzoMosaic - Commercial software designed for rectification of UAV imagery. Uses GPS location, aerial triangulation, bundleblock adjustment and optional orientation input to generate orthophotos. Received evaluation software. Testing pending.

- BAE SOCET SET - photogrammetric bundleblock adjustment with self calibration. Integrates GPS, IMU and ground measurements. Available in EAS (outdated version). Dongle being retrieved from former postdoc. Software evaluation in progress. Functionality being transferred to SOCET GXP.

- Noobeed - Interactive Geomatic Object Oriented Language. Shareware, crashed when run on XP (32 and 64 bit). Email for support bounced.

- MATCH-AT, inpho (a trimble company). Contacted for website login, which was granted. Request for evaluation software pending.

- ERDAS LPS - allows for rectification with GCP, aerial triangulation and bundle block adjust-

ment. Auto generates tie points between images. Initial trials have been unsuccessful with only GPS/IMU data. Next step are with some GCP to aid in aerial triangulation. Extensive testing with GoPro imagery and GPS/IMU data (low accuracy data due to sync of video with sensors). Was never able to get aerial triangulation to converge. Orthophoto with fixed orientation produced large errors in lat/long ($60°$ $120°$). Technical support contacted, data sent and initially looked over. Response pending. Told our data was too inaccurate to correct.

- PhotoScan - photo stitching software with capability for GPS input of photographs. Used extensively for Kite Aerial Photography in GIS applications. Primarily uses tie points between images to reconstruct scene including elevation. Allows for exporting DEM. Unable to test accuracy without purchase. Conference paper being published that compares LiDAR with PhotoScan for archeological surveys. [77, 76] Found PhotoScan to be accurate to $10cm$ in height (positional accuracy not tested). During initial testing with GoPro and poor sync of autopilot log data, found to be accurate to $\leq$10m.

  From AgiSoft forum: PhotoScan uses least squares adjustment. During adjustment the reconstructed scene data including model geometry and camera positions is transformed so that the RMS error between estimated and measured camera positions is minimized. The transformation used is a 7 parameter similarity transform (translation + rotation + scaling).

- Bundler - open source from washington university. Used by Dandois [14] for kite remote sensing of vegetation structure (forest canopy height). Obtained good height results ($3 - 4m$ error), but used manual GCP identification for georectification.

A.3 Fibre-optic Cable Specification

A.4 File Formats

A.4.1 Data Logger File Format

The onboard data from the spectrometer and autopilot is saved to the SD card in a custom binary format. Autopilot telemetry is saved in the custom Paparazzi format and is extracted using the Paparazzi provided tools.

The paparazzi message format is:

```
A PPRZ_STX (0x99)

B LENGTH (A->E)

C PPRZ_DATA

    0 SENDER_ID

    1 MSG_ID

    2 MSG_PAYLOAD

    . DATA (messages.xml)

D PPRZ_CHECKSUM_A (sum[B->C])

E PPRZ_CHECKSUM_B (sum[ck_a])
```

The spectrometer message format is:

```
A OO_STX (0x9898)

B TIMESTAMP (uint_32)

C STX (0xFFFF)

   0 dataSize (uint_16)

   1 numScans (uint_16)

   2 intTime (uint_16)

   3 fpgaBase1 (uint_16)

   4 fpgaBase2 (uint_16)

   5 pixelMode (uint_16)

      pixelMode = 3:

         pixelStart (uint_16)

         pixelEnd (uint_16)

         pixelEveryN (uint_16)

      pixelMode = 1:

         pixelEveryN (uint_16)

   . data

D ETX (0xFFFD)

E OO_CHECKSUM (data)
```

Appendix B

Sources of Error

Table B.1 identifies the sources of error present in the system in approximate descending order of contribution. Further testing is required to quantify the sources of error and determine areas for improvement.

Table B.1: Estimation of error contributions

Source of Error	Estimated Contribution
IMU measurement	orientation measurement, <5 deg
GPS receiver	location reported by receiver, 10 m
tie point errors when stitching images	misaligned images, georectification errors and lost data
data synchronization	linking data from autopilot, camera, and spectrometer, causing errors in rectification
camera resolution, focus, distortion	image location of objects, stitching errors during processing
spectrometer spot size	ground area spectrum is averaged over, 2 m
pixel motion blur	georectification errors, ground target error
pointing accuracy	sensor misalignment not accounted for in calibration, georectification errors
spectrometer integration time	spectral measurement averaged over an elongated ground strip, <1 m
environmental effects - optic fouling, cold weather	misaligned images, lost imagery and spectral data
solar illumination variation	errors in conversion to reflectance, can be checked with pre and post-flight measurements

Appendix C

UAP Reference Material

C.1 UAP-3 BOM

This section contains details on the components used to build UAP-3. The BOM can be found in Table C.1, and all items are pictured in Figures C.2-C.6.

Note 1: While most stranded 26 AWG - 28 AWG wire will work, the best choice is Teflon insulated. Ideally, all colours as shown in the wiring diagram given in Figure C.1 would be available, but to reduce cost, fewer may be used. For example, red may be used for power, black for ground, and white or another colour for signal lines. If fewer colours are used, it is a good idea to label the wires, for example with small pieces of coloured heat shrink distributed along the wire.

Note 2: The autopilot and battery mount plates can be made of a variety of materials including acrylic, aircraft plywood, polycarbonate or other similar plastics.
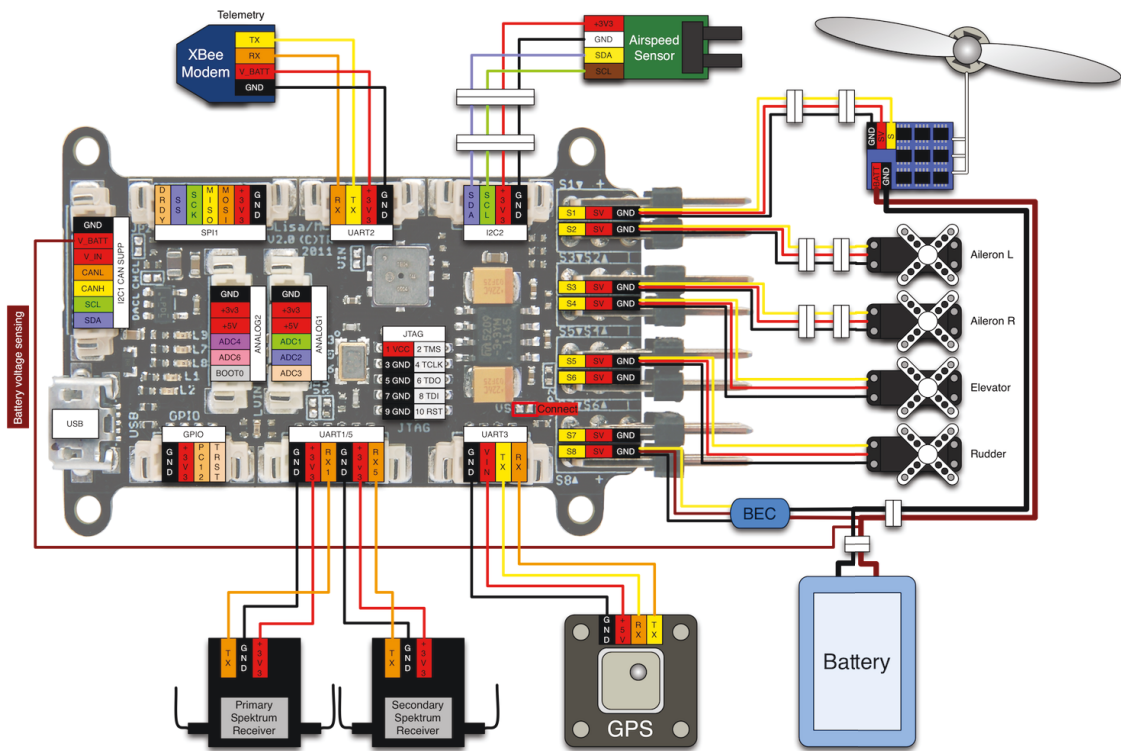
Figure C.1: UAP-3 basic wiring diagram, modified by Stephen Dwyer [55]

Figure C.2: UAP-3 standard RC component layout, image by Stephen Dwyer
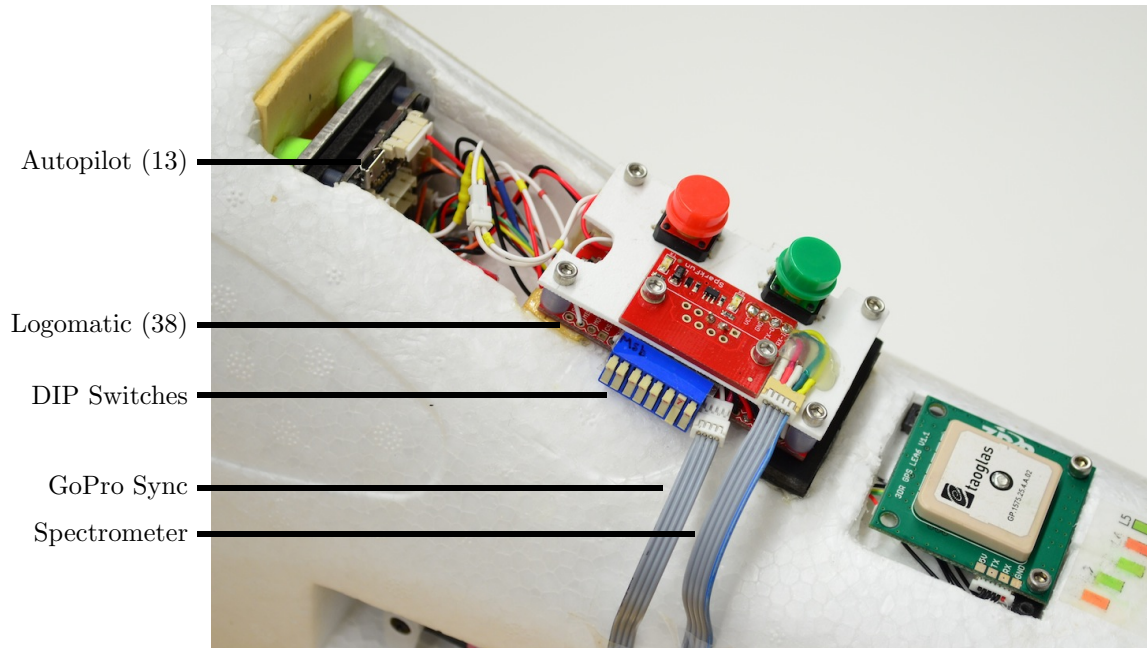
Figure C.3: Top view of UAP-3 showing autopilot (Item 13) and logomatic (Item 38)
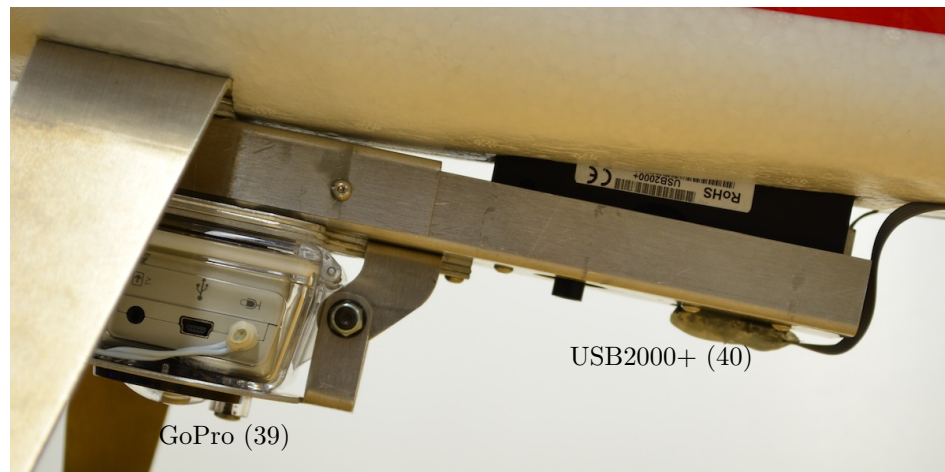
Figure C.4: UAP-3 sensor package side view showing GoPro (Item 39) and USB2000+ (Item 40)
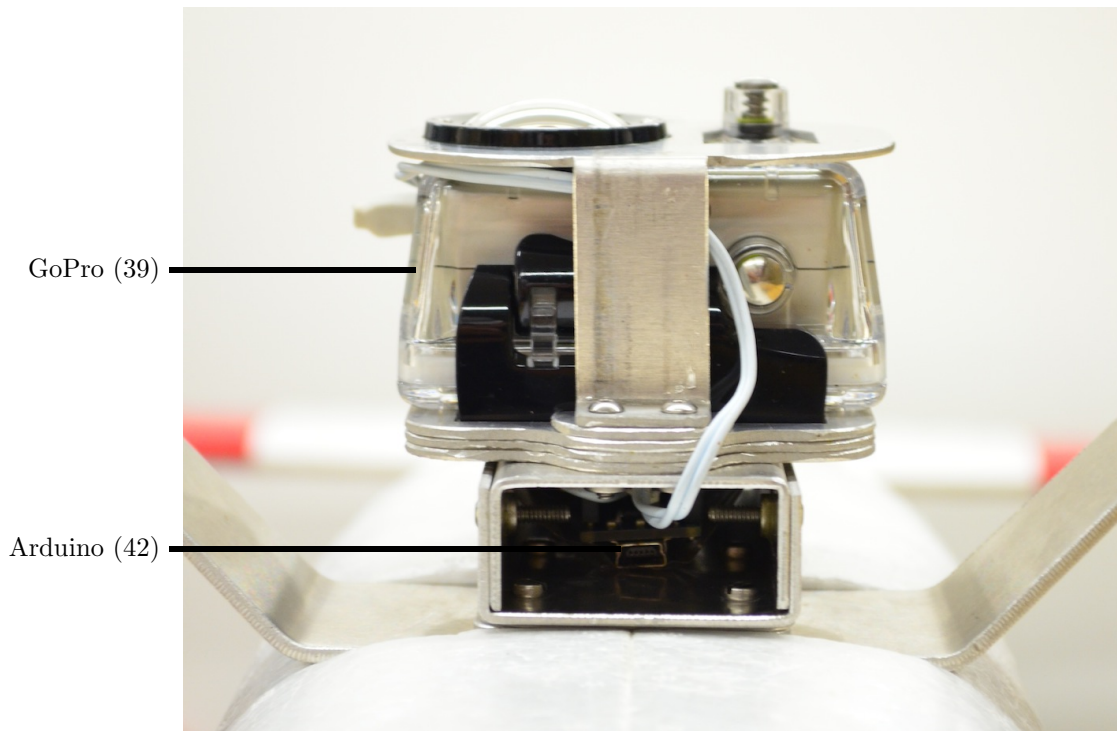
GoPro (39)

Arduino (42)

Figure C.5: UAP-3 sensor package front view showing GoPro (Item 39) and Arduino image sync board (Item 42)

Figure C.6: UAP-3 sensor package removed showing GoPro (Item 39) and USB2000+ (Item 40)

Table C.1: UAP-3 Bill of Materials

Item	Name	Qty.	Manufacturer	Mfg. Part Number	Cost
1	Mentor Electric Kit	1	Multiplex USA	M214228	140
2	Mentor/Magister Power Pack	1	Multiplex USA	M993228	148
3	3S 2200mAh LiPo Battery	4	Team Great Hobbies	TGHL22003C35	80
4	11x5.5E Propeller	2	APC	LP11055E	12
5	HS-322HD Servos	2	Hitec RCD USA	33322S	40
6	HS-81 Servos	2	Hitec RCD USA	31081S	50
7	Servo Extension 12in	4	Team Great Hobbies	TGHXSE12	16
8	HD Servo Extension 12in	1	Maxx Products Intl	3430	5
9	Ultratrim True Red Covering	1	Hanger 9	HANU83500	10
10	DX8 R/C Transmitter	1	Spektrum	SPM8800	315
11	DSM2 Remote Receiver	2	Spektrum	SPM9545	80
12	Remote Receiver Extension 36in	1	Spektrum	SPM9014	9
13	Lisa/M v2.0 Autopilot w/ Aspirin	1	Transition Robotics		230
14	GPS13 GPS Receiver	1	PPZUAV	ppzgps13nogp	120
15	XBee-PRO S2 Radio - Wire	1	Digi International	XBP24-Z7WIT-004	40
16	XBee-PRO S2 Radio - RPSMA	1	Digi International	XBP24-Z7SIT-004	40
17	XBee Breakout Board	1	Sparkfun	BOB-08276	3
18	XBee Header	2	Sparkfun	PRT-08272	2
19	XBee Explorer USB Board	1	Sparkfun	WRL-08687	25
20	2.4GHz Dipole Antenna	1	Sparkfun	WRL-00145	8
21	Airspeed Microsensor V3	1	Eagle Tree Systems	AIRSPEED-V3	45
22	Air Coupling Straight 1/16in	2	Robart		5
23	Silicon Tubing Small 3ft	1			5
24	CC BEC 10A	1	Castle Creations	010-0004-00	24
25	26 or 28 AWG Wire 10ft	1	See Note 1	See Note 1	10
26	Ultra Deans Male Connector	4	W. S. Deans	1302	8
27	Ultra Deans Female Connector	2	W. S. Deans	1301	4
28	Picoblade Connector 4pin	4	Molex	51021-0400	4
29	Picoblade Connector 6pin	2	Molex	51021-0600	2
30	Picoblade Connector 7pin	1	Molex	51021-0700	1
31	Picoblade Female Crimp	75	Molex	500798000	20
32	M2 x 12mm SHCS	4			
33	M3 x 6mm SHCS	2			
34	Latex Foam Rubber Sheet 1/4in	1	DU-BRO	513	5
35	Autopilot Mount plates	1	See Note 2	See Note 2	
36	Battery Tray Lite Ply 1/8in	1	See Note 2	See Note 2	
37	Transmitter Case	1	Spektrum	SPM6701	63
38	Logomatic	1	Sparkfun	WIG-10216	60
39	GoPro Hero2	1	GoPro		300
40	USB2000+ Spectrometer preconfigured 330-1000nm	1	Ocean Optics	VIS-NIR-ES	3200
41	Spectralon Panel	1	Labsphere		800
42	Arduino Nano	1			40
				Total:	5969

C.2 UAP-3 Checklists

Preflight Checklist 1

Environment
- ☐ Weather Conditions
- ☐ Flight Path Clear
- ☐ Spectators Secure

Aircraft
- ☐ R/C Bound with Failsafe
- ☐ Battery Check
- ☐ CG Check
- ☐ Verify Mechanical Integrity

Cable Connections
- ☐ Left Aileron
- ☐ Right Aileron
- ☐ Airspeed Sensor
- ☐ Speed Control
- ☐ Battery
- ☐ Spectrometer to Logger
- ☐ Tone Generator to Logger
- ☐ Logger to Autopilot (x2)
- ☐ Logger switched ON

Preflight Checklist 2

Command & Control
- ○ R/C
  - ☐ Control Check
  - ☐ Range Check
- ○ Ground Station
  - ☐ Telemetry
  - ☐ Personnel Comms
- ☐ Mission Plan Reviewed

Payload
- ☐ Spectrometer Calibration
  - ☐ Integration Time Set
  - ☐ Dark Reference
  - ☐ Light Reference
- ☐ GoPro Video Started

Final Checks
- ☐ R/C Control
- ☐ Full Throttle Available
- ☐ Flight Path Clear
- ☐ Takeoff Block Enabled

Field Kit Checklist 1

Critical Tools
- ○ Hex Keys
    - ☐ Metric
    - ☐ Imperial
- ☐ Screwdrivers
- ☐ Gloves
- ☐ Fire Extinguisher
- ☐ First Aid Kit

Critical Hardware
- ☐ Wings
- ☐ Spar
- ☐ Wing Bolts
- ☐ Pitot Tube
- ☐ Hatch Cover
- ☐ Antennas

Field Kit Checklist 2

UAS Equipment
- ☐ R/C Transmitter
    - ☐ Bind Plugs
    - ☐ Manual
    - ☐ Frequency Tag
- ☐ Watt/Voltmeter
- ☐ Battery Charger & Supply
- ☐ Servo Programmer
- ☐ Generator/Battery
    - ☐ Extension Cord
    - ☐ Power Bar
    - ☐ Fuel
- ☐ Radio Modem
    - ☐ Power Supply
    - ☐ USB Adapter/Cable
    - ☐ Tripod
- ☐ GCS Computer & Power
- ☐ GCS Router & Power
- ☐ Cellphones
    - ☐ Chargers
    - ☐ Headphones and Mics
- ☐ Binoculars
- ☐ Sunglasses

Field Kit Checklist 3

Additional Equipment
- ☐ Vehicle Heater (Winter)
- ☐ Transmitter Glove (Winter)
- ☐ Weather Meter & Tripod
- ☐ Camera Equipment

Payload
- ☐ GoPro
  - ☐ SD Card
  - ☐ Mini USB Cable
- ☐ Spectrometer
  - ☐ Lens & Lens Cap
  - ☐ Calibration Target
  - ☐ USB Cable
  - ☐ Logger
  - ☐ Micro SD Card & Reader
  - ☐ Computer & Software
- ☐ Ground Targets

Documentation
- ☐ SFOC document
- ☐ Checklists
- ☐ Weather Report
- ☐ Notebooks & Pencils/Pens
- ☐ Dry Erase Marker

Field Kit Checklist 4

Tools
- ☐ Crescent Wrench
- ☐ Pliers
- ☐ Cutters
- ☐ Knife
- ☐ Tape
- ☐ Glue
- ☐ Loctite
- ☐ Velcro
- ☐ Prop Reamer
- ☐ Zip Ties
- ☐ Rubbing Alcohol
- ☐ Shop Towels
- ☐ Shovels
- ☐ Marker Stakes & Flagging Tape

Spare Parts
- ☐ Wing Bolts
- ☐ Mounting Hardware
- ☐ Control Surface Clevis
- ☐ Propeller

Post-flight Checklist

Every Flight

- ☐ Spectrometer Calibration
  - ☐ Light Reference
- ☐ Logomatic Stopped
- ☐ GoPro Stopped
- ☐ A/C Powered Down
- ☐ R/C Transmitter Off
- ☐ Batteries Removed
- ☐ Verify Mechanical Integrity
- ☐ Complete Flight Report

Final Flight

- ☐ Airframe Disassembled
- ☐ Payload Stowed
- ☐ Equipment Packed
- ☐ Area Clean

Pre-Deployment Checklist

- ○ Batteries Charged
  - ☐ Transmitter
  - ☐ Flight
- ☐ Flight Plan Complete
- ☐ Field Kit Checklist Complete
- ☐ Weather Conditions Verified
- ☐ Weather Report Obtained

Vehicle Packing Checklist

- ☐ UAS Airframe
- ☐ R/C Transmitter
- ☐ Toolkit
- ☐ Equipment Box
- ☐ Battery and Cable Box
- ☐ GCS Computers/Packs
- ☐ Generator
- ☐ Jerry Can
- ☐ Ground Targets

Field Site Setup Checklist

- ☐ Setup GCS Power
  - ☐ Generator
  - ☐ Extension Cord & Powerbar
- ☐ Setup Vehicle Heater (Winter)
- ☐ Setup Weather Meter & Start Logging
- ☐ Setup GCS Radio Modem and USB Cable
- ☐ Setup GCS Router
- ☐ Setup Ground Targets and Cameras As Necessary
- ☐ Setup GCS Computer
- ☐ Unpack and assemble UAS
  - ☐ *Preflight Checklist 1*
- ☐ Setup and Test GCS Personnel Comms
- ☐ Start GCS Software and Boot UAS
  - ☐ *Preflight Checklist 2*

C.3 UAP Tuning Procedure

Developed by and included with the permission of Stephen Dwyer.

<!DOCTYPE flight_plan SYSTEM "../flight_plan.dtd">
<!--

This fightplan is designed to aid in tuning **default** *control loops on a fixed wing aircraft. It should work in both simulation and for real flights, provided the main information is changed and waypoints are adapted to a suitable location for your airspace. The airspeed tuning may not work correctly in simulation CHECK THIS !!!!!!!!!!!!!!!!!.*

This flightplan is designed to be used in the first parts of the tuning process, and does NOT contain a landing block. It is likely extensive use of manual and auto1 modes are required. Ensure you are comfortable with manual flight, stall recovery, spin recovery, power−on landings, deadstick landings etc. Also ensure you do not fly beyond R/C range.

Since it is likely the aircraft is not tuned, do NOT rely on any stabilization or navigation features. For example, the STANDBY block may not work properly if the control loops are unstable. In addition, the flightplan blocks used to tune loops will not bring the aircraft back and will often let the aircraft continue on a straight course indefinitely. They may also allow unlimited climbs or descents.

*This flightplan was inspired by versatile.*__xml__*. For further information about flightplans, visit:*
http://paparazzi.enac.fr/wiki/Flight_Plans

When obtaining values, sometimes they can be gleaned from standard GCS display widgets, but better is to use the realtime plotter and the average functionality or visually estimate from the plotter.

You will probably need at least two people (one pilot, one GCS operator ; a spotter and/or data recorder may help as well).

It is expected the airframe file contain most __default__ *parameters. In addition, this tuning assumes some flags are NOT set, in particular AGR_CLIMB and STRONG_WIND.*

Most controllers for the aircraft are PID controllers with variations. Most common, there is no D term and sometimes no I term. Some controllers implement ramping, feed−forward, etc. A good review of PID control loops and tuning methodology is available on Wikipedia:
http://en.wikipedia.org/wiki/PID_controller

After preliminary tuning, fine tuning will undoubtedly help your aircraft perform better. The Flight Benchmark module is useful for this process:
http://paparazzi.enac.fr/wiki/FlightBenchmark

See http://paparazzi.enac.fr/wiki/Tuning first for more information and to get started.

Tuning Procedure:

1. Try some manual flights , adjust trim mechanically and in the airframe file for nominal aircraft cruise speed. Make sure the GPS, datalink and others sensors are in correct working order. During the flight(s), record the following information:

a. V_CTL_AUTO_THROTTLE_(NOMINAL|MIN|MAX)_CRUISE_THROTTLE and

V_CTL_AUTO_THROTTLE_(LOITER|DASH)_TRIM

> *−Fly straight and level at the nominal cruise, where the aircraft is trimmed properly, and write down the throttle setting and airspeed (if available from an airspeed sensor) or groundspeed. Ground speed will be affected by wind, but try to make a good guess by flying in different directions. Adjust any trims mechanically and/or in airframe file if this hasn't been done.*

> −Fly straight and level at a low speed, but still comfortably above stall (i.e. the lowest speed you would want the aircraft to loiter at), then trim the aircraft in pitch (up) to maintain altitude. Write down the throttle setting, speed and the trim of the pitch (look at COMMANDS:values[0]) .

> −Same as before , but at the highest speed the aircraft can maintain level flight forward (without climbing) and the highest speed you would like the aircraft to travel. Trim the aircraft in pitch (down) to maintain constant altitude. Write down the throttle setting , speed and pitch trim as before .

b. INS_(ROLL|PITCH)_NEUTRAL_DEFAULT (or IR_∗)

- Fly straight and level at nominal cruise throttle after mechanical trims have been set and write down the pitch and roll readings.

c. AUTO1_MAX_(ROLL|PITCH) and H_CTL_(ROLL|PITCH)_(MAX|MIN)_SETPOINT
- Fly the aircraft through a series of banked turns (same altitude) with an aggressiveness you are comfortable with, and you feel the aircraft can handle. More aggressive means faster autopilot response. Write down the average maximum roll values (will need to visually check).
- Fly the aircraft through a series of short and longer climbs and descents, primarily using the elevator to induce pitch changes (as opposed to throttle). Write down the maximum corrective and climb/descent pitches observed.
- NOTE: If your radio is not producing $1000us - 2000us$ pulses over the full stick range (i.e. maximum throw usually, full rates) then it is likely your radio will never make the auto1 setpoints reach their maximum value. Either adjust radio settings, airframe file and radio file to ensure full range, or increase the maximum auto1 pitch and roll to account for this. Otherwise, you may have trouble maintaining sufficient control authority in auto1.

d. DEFAULT_CIRCLE_RADIUS and HOME_RADIUS
- Fly the aircraft continuous in circles. Try to find a comfortable diameter that isn't *difficult to maintain, but is small enough the aircraft doesn*'t fly far away during circles. Lean towards a larger diameter. Check approximate diameter by plotting NAVIGATION:pos_x and NAVIGATION:pos_y and looking at the amplitude of the sinusoids generated

123

during the circles.

e. FAILSAFE_(DEFAULT_THROTTLE|DEFAULT_ROLL|DEFAULT_PITCH)

  – Fly the aircraft in a gentle circle slowly with a slow (<1m/s) descent. Write down the pitch, roll and throttle. You should not have to correct pitch, roll or throttle very much during this action. In the event of the failsafe mode kicking in, and you want your aircraft to survive, envision the aircraft descending in this manner to the ground. Feel free to adjust to a different pattern if required (full dive for quick kill or straight and level descent if you have an extremely large flight region).

f. ALTITUDE_MAX_CLIMB and AGR_(CLIMB|DESCENT)_(THROTTLE|PITCH)

  – Fly the aircraft at a constant average climb rate both up and down, and write down the average climb rate. Be sure the same value is comfortable for both climbs and descents

  – Fly the aircraft at a constant aggressive climb rate, both up and down, and write down the pitch and throttle settings for both up and down. The aggressive climbs and descents may have different settings, depending on what looks reasonable.

After flying and trimming the aircraft, and recording the various parameters for the trimmed aircraft, land and update the airframe file. Use judgement when supplying values to the airframe file. For the INS_(ROLL|PITCH)_NEUTRAL_DEFAULT, put the negative of the recorded value in the airframe file.

2. Use auto1 to do the pitch/roll stabilization loop tuning. (In simulation, try it with the block Sim Pitch Roll Tuning)

124

WARNING: The Sim Pitch Roll Tuning block will undoubtedly cause a runaway aircraft with no altitude control if used and left on. Best if only used in simulation, and use auto1 in real flight testing.

a. Fly to a safe altitude and start a pass at cruise throttle in front of the pilot.

b. Switch to auto1 and immediately check if you can turn (roll) left AND right, and if you can pitch up and down. Be prepared to immediately take back manual control if something goes wrong (i.e. sudden dive or roll). If the response is extremely sluggish, you may need to increase gains (try double) or the max pitch/roll in auto1 may need to be increased.

c. Fly at cruise and adjust ROLL_ATTITUDE_GAIN (or ROLL_PGAIN). Increase the gain (more negative) if the response is sluggish, and decrease the gain if the aircraft oscillates in roll. The goal is to get the aircraft to have fast response without oscillating. It may help to use the realtime plotter and plot ATTITUDE:phi and DESIRED:roll together. If the aircraft is behaving, attempt some aggressive (i.e. step) setpoint changes and watch the response on the realtime plot. Also, you may try adjusting the ROLL_RATE_GAIN. Try varying the speed to ensure the control is reasonable over the aircraft's speed range.

d. Do the same as above for the pitch (PITCH_PGAIN, ATTITUDE:theta, DESIRED:pitch, PITCH_IGAIN, PITCH_DGAIN).

e. If the aircraft seems to drift a bit in roll or pitch, you may need to adjust the *_(ROLL|PITCH)_NEUTRAL_DEFAULT; check the attitude readout when the elevator and aileron are neutral. If changing the throttle seems to induce a bit of roll, you can try adjusting AILERON_OF_THROTTLE, but this is best fixed mechanically with engine

mounting.

f. It is ideal if the aircraft does not climb or descend as a result of rolling the aircraft. In addition, the "bank and yank" method of heading control in Paparazzi requires up elevator in addition to roll to properly turn. Normally in flight, when an aircraft banks the nose will fall off (sink) without any additional pitch input. Even when maintaining level flight in pitch (i.e. pitch setpoint of 0), under the same velocity, the effective lifting area/vector of the aircraft is reduced, likely resulting in a descent. To counter this, the pitch control loop uses the ELEVATOR_OF_ROLL gain to increase the pitch setpoint (thereby increasing angle of attack and thus lift). In auto1, hold a constant bank (experiment with different magnitudes) and observe the aircraft and data from ESTIMATOR:z_dot and DESIRED:climb. Adjust the ELEVATOR_OF_ROLL until climb is zero in banked turns.

After completing this, your aircraft should be able to stabilize itself. However, higher level control loops may still be unstable, so don't count on the autopilot bringing your plane back yet.

NOTE: Settings (like gains), when changed during a flight, are not automatically saved. Either write down the changed settings and gains before shutting down your system and type them into the airframe file manually, or use the Save Settings button in the Settings pane of the Notebook in the GCS. Before using the Save Settings feature, be sure to review the warnings on the wiki: http://paparazzi.enac.fr/wiki/GCS#Settings

In tuning the remainder of the control loops, the goal is to slowly move upwards in the hiearchy of control enabling different control loops as you go while attempting to decouple any untuned control loops. To do this, various flight modes will be used.

3. Tune the auto throttle climb loop

a. Fly to a safe altitude some distance away on a course such that the aircraft will fly by the pilot/GCS.

b. Activate the block Level Auto Throttle Tuning and switch to auto2 (optionally, use block Variable Auto Throttle Tuning, where climb is initialized to zero and adjustable in the GCS notebook settings with nav_climb).

c. Observe the aircraft and data from ESTIMATOR:z_dot and DESIRED:climb . The aircraft should remain wings level and near constant pitch, with the climb rate remaining at zero. If oscillations in climb rate , aircraft pitch, or throttle setting occur, reduce gains. There are a significant number of gains in the auto throttle control loop, and several may need to be adjusted. You may also experiment adjusting the cruise, dash and loiter values if previous tests aren' t providing sufficient performance. If slower oscillations or climb rate is drifting from zero, consider increasing the gains for crisper response without causing oscillations. The relevant gains are: V_CTL_AUTO_THROTTLE_(P|I|D)GAIN (for climb rate feedback), V_CTL_AUTO_THROTTLE_CLIMB_THROTTLE_INCREMENT (for climb rate feedforward), and V_CTL_AUTO_THROTTLE_PITCH_OF_VZ_PGAIN (for pitch loop feedforward from climb).

d. Activate the blocks Ascent Auto Throttle Tuning and Descent Auto Throttle Tuning and repeat C realizing the climb rate should be a

minimum or maximum as set with V_CTL_ALTITUDE_MAX_CLIMB (optionally ,
change the nav_climb value with the notebook settings instead).

e. *Try changing between Loiter , Cruise and Dash throttle settings*
corresponding to V_CTL_AUTO_THROTTLE_(NOMINAL|MIN|MAX)
_CRUISE_THROTTLE and ensure climb remains stable . Adjust gains if
required as in C.

f. *Ensure the aircraft is switched to manual control as it passes and*
gets further away from the pilot , at the pilot's discretion . Turn
and line up for another pass , and switch to auto2 . The previous
block should still be active .

g. To help with tuning , a climb rate other than that specified in the
current block could be induced by the pilot just prior to switching
to auto2 to check various climb rate setpoint step changes . This
also helps if one is nervous about allowing the autopilot to command
a steep descent . One can descend manually and then switch to auto2
when the Level Auto Throttle Tuning block is active , which will
cause the autopilot to stop the aircraft descending .

4. Tune the auto pitch climb loop

a. Fly to a safe altitude some distance away on a course such that the
aircraft will fly by the pilot/GCS.

b. Activate the block Level Auto Pitch Tuning and switch to auto2 (
optionally , use block Variable Auto Pitch Tuning , where climb is
initialized to zero and adjustable in the GCS notebook settings with
nav_climb).

c. Observe the aircraft and data from ESTIMATOR:z_dot and DESIRED:climb
. The aircraft should remain wings level , with the climb rate
remaining at zero . If fast oscillations in climb rate occur , reduce

128

gains. Consider increasing gains until just before the onset of oscillations. The relevant gains are: V_CTL_AUTO_PITCH_(P|I)GAIN (for climb rate feedback loop).

d. Activate the blocks Ascent Auto Pitch Tuning and Descent Auto Pitch Tuning and repeat C realizing the climb rate should be a minimum or maximum as set with V_CTL_ALTITUDE_MAX_CLIMB (optionally, change the nav_climb value with the notebook settings instead).

e. Try changing between Loiter, Cruise and Dash throttle settings corresponding to V_CTL_AUTO_THROTTLE_(NOMINAL|MIN|MAX) _CRUISE_THROTTLE and ensure climb remains stable. Adjust gains if required as in C.

f. Ensure the aircraft is switched to manual control as it passes and gets further away from the pilot, at the pilot's discretion. Turn and line up for another pass, and switch to auto2. The previous block should still be active.

g. To help with tuning, a climb rate other than that specified in the current block could be induced by the pilot just prior to switching to auto2 to check various climb rate setpoint step changes. This also helps if one is nervous about allowing the autopilot to command a steep descent. One can descend manually and then switch to auto2 when the Level Auto Throttle Tuning block is active, which will cause the autopilot to stop the aircraft descending. If the aircraft does not seem to stabilize at the desired climb rate while in Loiter or Dash throttle modes (i.e always climbs or descends with a 0.0 climb setpoint), chances are the settings for V_CTL_AUTO_THROTTLE_(LOITER|DASH)_TRIM are set incorrectly.

The climb loop(s) should now be sufficiently tuned, unless one wishes to use the airspeed loops. If you plan to use airspeed, please tune the airspeed loop, which replaces the traditional Auto Throttle control loop.

5. Tune the altitude loop

a. Fly to a safe altitude some distance away on a course such that the aircraft will fly by the pilot/GCS.

b. Activate the block Altitude Tuning and switch to auto2.

c. Observe the aircraft and data from ESTIMATOR:z and DESIRED:altitude. The aircraft should remain wings level, with a constant altitude equal to the altitude which the aircraft was at when the Altitude Tuning block was activated. If oscillations occur in altitude, reduce the ALTITUDE_PGAIN. If the aircraft very slowly drifts or doesn't reach altitude, increase gain until just before oscillations begin.

d. You can adjust the altitude setpoint in the notebook using the altitude slider under flight params. Check response to step changes in altitude setpoints and adjust gain as required.

e. Try changing between Loiter, Cruise and Dash throttle settings corresponding to V_CTL_AUTO_THROTTLE_(NOMINAL|MIN|MAX) _CRUISE_THROTTLE and ensure climb remains stable. Adjust gains if required as in C.

f. Ensure the aircraft switched to manual control as it passes and gets further away from the pilot, at the pilot's discretion. Turn and line up for another pass, and switch to auto2. The previous block should still be active.

Now, all of the vertical loops should be tuned decently. Finally, the course loop can be tuned.

6. Tune the course loop

a. Fly to a safe altitude on a course you wish the aircraft to attempt to follow. A good suggestion would be away from the pilot perpendicular to the flight line.

b. While flying this course, but being near the pilot/GCS, activate the block Course Tuning then switch to auto2. This will use the aircrafts current course at the moment of activating the Course Tuning block. Note that no altitude control will be enabled, only a fixed throttle setting.

c. When the aircraft starts getting far away (but before it leaves piloting range!) return to manual control and complete a pattern that will bring the aircraft across the front of the pilot/GCS approximately parallel to the flight line (i.e. perpendicular to the course setpoint). When the aircraft is approaching the pilot/GCS, switch back to auto2. The aircraft will attempt to match the desired heading.

d. When switching to auto2, observe the behaviour of the aircraft and ATTITUDE:psi and DESIRED:course. It should turn to the desired course, but may change altitude (probably descend) depending on the aircraft's performance and the nominal cruise throttle setting. If the aircraft overshoots the course and oscillates back and forth, reduce the COURSE_PGAIN in settings and/or adjust the COURSE_DGAIN. If the aircraft is sluggish in meeting the desired course or doesn*'t quite reach the proper course, increase the gain. If the aircraft tends to lose altitude during the course correction, try increasing*

ELEVATOR_OF_ROLL (for climbs, reduce the gain).

e. Repeat C as necessary to tune the loop for crisp response without oscillations. Preferably, begin the course changes from both directions. Also, one can induce setpoint changes under auto2 continuously by adjusting nav_course in the settings.

f. Experiment with Loiter and Dash throttle settings.

g. Try out the advance course tuning loops: these will fly the aircraft around a rectangle, either clockwise or counter−clockwise. The CCW loop should be engaged while the aircraft is flying approximately along the vector between waypoint 2 and waypoint 1, towards waypoint 1. The CW loop should be engaged while the aircraft is flying the opposite direction to this. Note that this mode uses an hmode of "route" between waypoints, meaning the aircraft will attempt to track a line between the waypoints, not just go directly towards the next waypoint.

The primary control loops should now be decently tuned!

7. Try activating STANDBY

a. Now that the control loops have been tuned, activate the Standby block. The aircraft should have no trouble joining and maintaining orbit around the waypoint. If there are oscillations across many parameters, you may need to tune (or detune) some loops more closely. This will undoubtedly take some practice and time. One gain to look at is ELEVATOR_OF_ROLL. Experience has shown trying to maintain a circular loiter can be helped by adjusting this gain. In addition, increasing the radius of the circle may help as well.

132

Other things to consider:

This tuning only considers the base number of parameters. For many loops, PI, PD or full PID controllers (sometimes with feedforward and biases) are available. In addition, various flags and extra features introduce further parameters to adjust. For example, AGR_CLIMB modifies the altitude loop, the auto throttle loop and the course loop. The COURSE_SLEW_INCREMENT flag and value limits the change rate of the course setpoint, which may help with the course loop tuning or under extreme course setpoint changes. The COURSE_PRE_BANK_CORRECTION value adjusts a bias used if the aircraft is navigating a circle to tune the best bank angle when circling. The Flight Benchmark module may help in fine−tuning.

In addition, these loops were tuned with an effort to isolate loops (especially untuned ones) during tuning. Under normal navigation, there may be some interaction between these loops. This can be addressed with some gain and parameter fine−tuning. A good example is if the aircraft significantly loses altitude when banked, for example during a course correction. This may cause some oscillation between altitude and course loops.

Take a look at other airframe files for examples of other available parameters. For better understanding of control loops and how some of the flags add features and affect loops, the best method is to look at the code.

8. Tune the airspeed loop

The altitude loop has a couple different cascaded loops. Thus a number of state variables need to be watched. Climb is controlled by the pitch, as in the auto pitch loop (PI controller). As the pitch/climb will affect airspeed, this is compensated for in the airspeed loops. The airspeed and ground speed setpoints can be used in two ways. First, never set the airspeed setpoint below a safe low speed, i.e. above stall speed.

Case 1: Airspeed setpoint greater than groundspeed setpoint:
  − controller attempts to maintain constant airspeed
  − if groundspeed falls below its setpoint, minimum groundspeed control takes precedence
  − this results in a higher airspeed to avoid aircraft being unable to fly upwind in high winds

Case 2: Groundspeed setpoint greater than airspeed setpoint:
  − controller attempts to maintain constant groundspeed
  − if airspeed falls below its setpoint, minimum airspeed control takes precedence
  − this results in a higher airspeed to avoid aircraft stalling

The groundspeed setpoint is set from the airframe file. A PI loop on the groundspeed generates the airspeed setpoint. This is bounded low by the airspeed setpoint in the airframe file. A PI loop on the airspeed generates the desired throttle setting. To tune these loops, an attempt will be made to decouple them. First, the airspeed loop will be tuned, then the groundspeed loop, then the pitch loop.

Before tuning the airspeed loop, be sure to measure the approximate cruise airspeed and groundspeed of the aircraft and use these as setpoints for tuning (can use the same value). After tuning, set each according to the desired control style (airspeed or groundspeed). In addition, be sure to use the settings file airspeed_ctl_tuning **.xml** *.*

a. *Fly to a safe altitude some distance away on a course such that the aircraft will fly by the pilot/GCS.*

b. *Activate the block Airspeed (Airspeed) Tuning and switch to auto2.*

c. *Observe the aircraft and data from AIRSPEED:airspeed and AIRSPEED:airspeed_sp. The aircraft should remain wings level, with the airspeed constant around the setpoint. If there are oscillations or control is sluggish, adjust auto airspeed gains. You may also experiment adjusting the airspeed setpoint in settings to induce step changes.*

d. *Activate the block Airspeed (Groundspeed) Tuning and switch to auto2.*

e. *Observe the aircraft and data from GPS:speed and AIRSPEED:groundspeed_sp. The aircraft should remain wings level, with the groundspeed constant around the setpoint. If there are oscillations or control is sluggish, adjust auto groundspeed gains. You may also experiment adjusting the groundspeed setpoint in settings to induce step changes.*

f. *Activate the block Airspeed (Auto Pitch) Tuning and switch to auto2.*

g. *Observe the aircraft and data from ESTIMATOR:z_dot and DESIRED:climb. The aircraft should remain wings level, with the climb rate remaining at zero. If fast oscillations in climb rate occur, reduce*

135

gains. Consider increasing gains until just before the onset of oscillations. Adjust the nav_climb value with the notebook settings to induce step changes. The relevant gains are: V_CTL_AUTO_PITCH_(P | I)GAIN.

h. *Ensure the aircraft is switched to manual control as it passes and gets further away from the pilot, at the pilot's discretion. Turn and line up for another pass, and switch to auto2. The previous block should still be active.*

After this, the airspeed loops should be tuned.

!!!!!!!!!!!!!!!!!SHOULD THE BLOCKS AUTOMATICALLY PROTECT AGAINST ALTITUDE AND OTHER STUFF? TIMEOUTS?!!!!!!!!!!!!!!

something like 20m/s*15s = 300m away, so do a 15sec timeout on blocks?

—>
<!–– Change the root element to match your airspace ––>
<flight_plan alt="675" ground_alt="605" lat0="53.63838" lon0
="−113.28657" max_dist_from_home="1000" name="Tuning_Bremner"
security_height="25" qfu="270"> <!–– Bremner ––>

  <!–– The header section allows one to include advanced navigation
    routines and header files that allow access to variables that may
    be useful for exceptions or advanced flightplan routines dependent
    on various internal autopilot variables ––>
  <header>
#include "subsystems/navigation/nav_line.h"

```
#include "datalink.h"
  </header>
  <!-- The waypoints section must contain 1 or more waypoints. For
      tuning, setup STDBY in a location in front of the pilot at least
      DEFAULT_CIRCLE_RADIUS metres away from the flight line if
      restricted to no overflights. Setup 1 and 2 in front of and to the
      right and left of the pilot, respectively, with waypoints 4 and 3
      offset back away from the pilot further, so as to make a
      clockwise rectangle from waypoints 1-2-3-4. These are used for
      advanced course tuning and testing ovals and eights after tuning.
      Again, waypoints should be at least a radius away from the flight
      line (probably 1.5xRadius) to prevent overflights. HOME can be set
      somewhere in the vicinity of STDBY or the pilot. CLIMB is for
      takeoff (mostly for sim, should manually takeoff for tuning)-->
  <waypoints>
    <waypoint name="HOME" x="0" y="0"/>
    <waypoint name="STDBY" x="30." y="130."/>
    <waypoint name="1" x="100.1" y="100.9"/>
    <waypoint name="2" x="-100.3" y="110.1"/>
    <waypoint name="3" x="-100.3" y="225.1"/>
    <waypoint name="4" x="100.1" y="215.1"/>
    <waypoint name="CLIMB" x="-125.0" y="55.0"/>
    <waypoint name="MOB" x="0" y="50"/>
    <waypoint name="S1" x="-150.2" y="69.6"/>
    <waypoint name="S2" x="150.4" y="209.5"/>
  </waypoints>
  <!-- The sectors section allows the definiton of regions of space
      from waypoints, useful for restricting flight area with exceptions
```

```
         -->
<sectors/>
<!-- The includes section allows predefined blocks of flightplan to
     be included -->
<includes>
  <!-- <include name="SoftKillOut" procedure="sectors/
       bremner_sectors_outside.xml"/> -->
</includes>
<!-- The exceptions section allows for global error and failsafe
     handling -->
<exceptions>
  <!-- <exception cond="datalink_time > 15" deroute="Standby"/> -->
  <exception cond="And((estimator_z > ground_alt + 240),launch)"
       deroute="Standby"/>
  <!-- <exception cond="And(!InsideSoftKillOut(estimator_x,
       estimator_y),launch)" deroute="Standby"/> -->
</exceptions>
<!-- The blocks section contains each block of the flightplan, which
     actually make the aircraft do something -->
<blocks>
  <block name="Wait GPS">
    <set value="1" var="kill_throttle"/>
    <while cond="!GpsFixValid()"/>
  </block>
  <block name="Geo init">
    <while cond="LessThan(NavBlockTime(), 10)"/>
    <call fun="NavSetGroundReferenceHere()"/>
  </block>
```

```xml
<block name="Holding point">
  <!--set var="nav_mode" value="NAV_MODE_ROLL"/-->
  <set value="1" var="kill_throttle"/>
  <attitude roll="0" throttle="0" vmode="throttle"/>
</block>
<!-- need this for simulation, manual takeoff for real testing -->
<block key="t" name="Takeoff" strip_button="Takeoff (wp CLIMB)"
    strip_icon="takeoff.png" group="home">
  <exception cond="estimator_z > (ground_alt+25)" deroute="Standby
      "/>
  <set value="0" var="kill_throttle"/>
  <set value="0" var="estimator_flight_time"/>
  <go from="HOME" throttle="1.0" vmode="throttle" wp="CLIMB" pitch
      ="15"/>
</block>
<block key="<Control>a" name="Standby" strip_button="Standby"
    strip_icon="home.png" group="home">
  <circle radius="nav_radius" wp="STDBY"/>
</block>
<!-- first, tune the pitch and roll loops. This can be done using
    auto1. Here for sim demos. This block may cause a fly-away -->
<block name="Sim Pitch Roll Tuning">
  <while cond="TRUE">
    <attitude roll="0.0" pitch="0.0" vmode="throttle" throttle="
        V_CTL_AUTO_THROTTLE_NOMINAL_CRUISE_THROTTLE" until="
        stage_time>7"/>
    <attitude roll="30.0" pitch="0.0" vmode="throttle" throttle="
        V_CTL_AUTO_THROTTLE_NOMINAL_CRUISE_THROTTLE" until="
```

```
              stage_time>7"/>
      <attitude roll="0.0" pitch="0.0" vmode="throttle" throttle="
          V_CTL_AUTO_THROTTLE_NOMINAL_CRUISE_THROTTLE" until="
          stage_time>7"/>
      <attitude roll="-30.0" pitch="0.0" vmode="throttle" throttle="
          V_CTL_AUTO_THROTTLE_NOMINAL_CRUISE_THROTTLE" until="
          stage_time>7"/>
      <attitude roll="0.0" pitch="0.0" vmode="throttle" throttle="
          V_CTL_AUTO_THROTTLE_NOMINAL_CRUISE_THROTTLE" until="
          stage_time>7"/>
      <attitude roll="0.0" pitch="20.0" vmode="throttle" throttle="
          V_CTL_AUTO_THROTTLE_NOMINAL_CRUISE_THROTTLE" until="
          stage_time>7"/>
      <attitude roll="0.0" pitch="0.0" vmode="throttle" throttle="
          V_CTL_AUTO_THROTTLE_NOMINAL_CRUISE_THROTTLE" until="
          stage_time>7"/>
      <attitude roll="0.0" pitch="-20.0" vmode="throttle" throttle="
          V_CTL_AUTO_THROTTLE_NOMINAL_CRUISE_THROTTLE" until="
          stage_time>7"/>
      <attitude roll="0.0" pitch="0.0" vmode="throttle" throttle="
          V_CTL_AUTO_THROTTLE_NOMINAL_CRUISE_THROTTLE" until="
          stage_time>7"/>
    </while>
  </block>
  <!-- now tune the auto throttle climb loop -->
  <!--          lateral_mode = LATERAL_MODE_ROLL
                h_ctl_roll_setpoint = 0.0deg
                v_ctl_climb_mode = V_CTL_CLIMB_MODE_AUTO_THROTTLE
```

```
                    nav_pitch = 0.0 deg
                    v_ctl_mode = V_CTL_MODE_AUTO_CLIMB
                    v_ctl_climb_setpoint = 0.0
-->
<block name="Level Auto Throttle Tuning">
  <while cond="TRUE">
    <attitude roll="0.0" vmode="climb" climb="0.0"/>
  </while>
</block>
<block name="Ascent Auto Throttle Tuning">
  <while cond="TRUE">
    <attitude roll="0.0" vmode="climb" climb="
        V_CTL_ALTITUDE_MAX_CLIMB"/>
  </while>
</block>
<block name="Descent Auto Throttle Tuning">
  <while cond="estimator_z > (ground_alt + 25)">
    <attitude roll="0.0" vmode="climb" climb="-
        V_CTL_ALTITUDE_MAX_CLIMB"/>
  </while>
</block>
<block name="Variable Auto Throttle Tuning">
  <set var="nav_climb" value="0.0"/>
  <while cond="TRUE">
    <attitude roll="0.0" vmode="climb" climb="nav_climb"/>
  </while>
</block>
<!-- now tune the auto pitch loop -->
```

```xml
<!--           lateral_mode = LATERAL_MODE_ROLL
               h_ctl_roll_setpoint = 0.0deg
               v_ctl_climb_mode = V_CTL_CLIMB_MODE_AUTO_PITCH
               nav_throttle_setpoint = 9600*(
                   V_CTL_AUTO_THROTTLE_NOMINAL_CRUISE_THROTTLE)
               v_ctl_mode = V_CTL_MODE_AUTO_CLIMB
               v_ctl_climb_setpoint = 0.0
-->
<block name="Level Auto Pitch Tuning">
  <while cond="TRUE">
    <attitude roll="0.0" pitch="auto" throttle="
        V_CTL_AUTO_THROTTLE_NOMINAL_CRUISE_THROTTLE" vmode="climb"
        climb="0.0"/>
  </while>
</block>
<block name="Ascent Auto Pitch Tuning">
  <while cond="TRUE">
    <attitude roll="0.0" pitch="auto" throttle="
        V_CTL_AUTO_THROTTLE_NOMINAL_CRUISE_THROTTLE" vmode="climb"
        climb="V_CTL_ALTITUDE_MAX_CLIMB"/>
  </while>
</block>
<block name="Descent Auto Pitch Tuning">
  <while cond="estimator_z > (ground_alt + 25)">
    <attitude roll="0.0" pitch="auto" throttle="
        V_CTL_AUTO_THROTTLE_NOMINAL_CRUISE_THROTTLE" vmode="climb"
        climb="-V_CTL_ALTITUDE_MAX_CLIMB"/>
  </while>
```

142

```xml
</block>
<block name="Variable Auto Pitch Tuning">
  <set var="nav_climb" value="0.0"/>
  <while cond="TRUE">
    <attitude roll="0.0" pitch="auto" throttle="
        V_CTL_AUTO_THROTTLE_NOMINAL_CRUISE_THROTTLE" vmode="climb"
        climb="nav_climb"/>
  </while>
</block>
<!-- now tune the altitude loop -->
<!--        lateral_mode = LATERAL_MODE_ROLL
            h_ctl_roll_setpoint = 0.0 deg
            v_ctl_climb_mode = V_CTL_CLIMB_MODE_AUTO_THROTTLE
            nav_pitch = 0.0 deg
            v_ctl_mode = V_CTL_MODE_AUTO_ALT
            nav_altitude = flight_altitude
-->
<block name="Altitude Tuning">
  <set var="flight_altitude" value="estimator_z"/>
  <while cond="TRUE">
    <attitude roll="0.0" vmode="alt" alt="flight_altitude"/>
  </while>
</block>
<!-- now that the stabilization and altitude working, tune the
    course loop -->
<!--        lateral_mode = LATERAL_MODE_COURSE
            h_ctl_course_setpoint = nav_course
            v_ctl_climb_mode = V_CTL_CLIMB_MODE_AUTO_THROTTLE
```

```
              nav_pitch = 0.0 deg
              v_ctl_mode = V_CTL_MODE_AUTO_THROTTLE
              nav_throttle_setpoint = 9600*(
                  V_CTL_AUTO_THROTTLE_NOMINAL_CRUISE_THROTTLE)
-->
<block name="Course Tuning">
  <set var="nav_course" value="estimator_hspeed_dir"/>
  <while cond="TRUE">
    <heading course="nav_course" vmode="throttle" throttle="
        V_CTL_AUTO_THROTTLE_NOMINAL_CRUISE_THROTTLE" until="FALSE"/>
        <!--continues forever-->
  </while>
</block>
<!-- advanced course loop tuning CCW -->
<!--          NEED TO FIND OUT PARAMETERS FOR THIS
              Flys in a CCW square, starting the run on the line
                  between waypoints 2 and 1 (engage here)
-->
<block name="Course Tuning Adv CCW">
  <while cond="TRUE">
    <go from="2" wp="1" hmode="route" approaching_time="3"/>
    <go from="1" wp="4" hmode="route" approaching_time="3"/>
    <go from="4" wp="3" hmode="route" approaching_time="3"/>
    <go from="3" wp="2" hmode="route" approaching_time="3"/>
  </while>
</block>
<!-- advanced course loop tuning CW-->
<!--          NEED TO FIND OUT PARAMETERS FOR THIS
```

```
                    Flys in a CW square, starting the run on the line
                        between waypoints 1 and 2 (engage here)
-->
<block name="Course Tuning Adv CW">
  <while cond="TRUE">
    <go from="1" wp="2" hmode="route" approaching_time="3"/>
    <go from="2" wp="3" hmode="route" approaching_time="3"/>
    <go from="3" wp="4" hmode="route" approaching_time="3"/>
    <go from="4" wp="1" hmode="route" approaching_time="3"/>
  </while>
</block>
<!-- everything should be good, try some stuff -->


<!-- airspeed control loop tuning -->
<!-- be sure to use the settings file airspeed_ctl_tuning.xml -->
<!--       airspeed will take precedence as groundspeed set lower
               setting pitch pgain to zero disables the auto pitch
                   part of the airspeed loop, no climb control
-->
<!--<block name="Airspeed (Airspeed) Tuning">
  <set var="v_ctl_auto_groundspeed_setpoint" value="0.5*
      V_CTL_AUTO_AIRSPEED_SETPOINT"/>
  <set var="v_ctl_auto_airspeed_setpoint" value="
      V_CTL_AUTO_AIRSPEED_SETPOINT"/>
  <set var="v_ctl_auto_pitch_pgain" value="0.0"/>
  <while cond="TRUE">
    <attitude roll="0.0" vmode="climb" climb="0.0"/>
  </while>
```

```xml
</block> -->

<!-- groundspeed will take precedence as airspeed set lower
     setting pitch pgain to zero disables the auto pitch part of
         the airspeed loop, no climb control
-->
<!--<block name="Airspeed (Groundspeed) Tuning">
  <set var="v_ctl_auto_groundspeed_setpoint" value="
     V_CTL_AUTO_GROUNDSPEED_SETPOINT"/>
  <set var="v_ctl_auto_airspeed_setpoint" value="0.5*
     V_CTL_AUTO_GROUNDSPEED_SETPOINT"/>
  <set var="v_ctl_auto_pitch_pgain" value="0.0"/>
  <while cond="TRUE">
    <attitude roll="0.0" vmode="climb" climb="0.0"/>
  </while>
</block>-->
<!-- airspeed should be tuned now, use in addition to pitch,
     airspeed will take precedence (coupled with climb more than
     groundspeed) -->
<!--<block name="Airspeed (Auto Pitch) Tuning">
  <set var="v_ctl_auto_groundspeed_setpoint" value="0.5*
     V_CTL_AUTO_AIRSPEED_SETPOINT"/>
  <set var="v_ctl_auto_airspeed_setpoint" value="
     V_CTL_AUTO_AIRSPEED_SETPOINT"/>
  <set var="v_ctl_auto_pitch_pgain" value="V_CTL_AUTO_PITCH_PGAIN
     "/>
  <set var="nav_climb" value="0.0"/>
  <while cond="TRUE">
```

146

```xml
        <attitude roll="0.0" vmode="climb" climb="nav_climb"/>
    </while>
</block>-->


<!-- extra typical blocks for testing after tuning -->
<block key="F8" name="Figure 8 around wp 1" strip_button="Figure 8
    (wp 1-2)" strip_icon="eight.png" group="base_pattern">
    <eight center="1" radius="nav_radius" turn_around="2"/>
</block>
<block name="Oval 1-2" strip_button="Oval (wp 1-2)" strip_icon="
    oval.png" group="base_pattern">
    <oval p1="1" p2="2" radius="nav_radius"/>
</block>
<block name="Line 1-2" strip_button="Line (wp 1-2)" strip_icon="
    line.png" group="base_pattern">
    <call fun="nav_line_init()"/>
    <call fun="nav_line(WP_1, WP_2, nav_radius)"/>
</block>
<block name="MOB" strip_button="Turn around here" strip_icon="mob.
    png" group="base_pattern">
    <call fun="NavSetWaypointHere(WP_MOB)"/>
    <set value="DEFAULT_CIRCLE_RADIUS" var="nav_radius"/>
    <circle radius="nav_radius" wp="MOB"/>
</block>
<block name="Survey S1-S2" strip_button="Survey (wp S1-S2)"
    strip_icon="survey.png" group="extra_pattern">
    <survey_rectangle grid="150" wp1="S1" wp2="S2"/>
</block>
```

```
<block name="Path 1,S1,2,1,4,3,1,S2,STDBY" strip_button="Path (1,S1
    ,2,1,4,3,1,S2,STDBY)" strip_icon="path.png" group="extra_pattern
    ">
  <path wpts="1,S1,2,1,4"/>
  <path wpts="3, 1, S2" approaching_time="1" pitch="auto" throttle
      ="0.21"/>
  <deroute block="Standby"/>
</block>


</blocks>
</flight_plan>
```

C.4   Paparazzi Control Loops

The following control loop overview was sourced from [56].

General Information

All the possible combinations of control loops might not be fully detailed. This is especially the case when using extra features such as **AGR_CLIMB**, **STRONG_WIND**, etc.

In the following diagrams, the block **s** is used for the **derivative** function and **1/s** is used for the **integrator** function.

The variables' names are the one used in the airborne code (written in **C**). Most of this name can the used capitalized in the Airframe Configuration file in order to define the default value of these variables. If in capital letters in the diagrams, the value is fixed and cannot be changed using Settings mechanism.

The best way to determine vehicle behavior is to look at the source code. For determining which control loops are engaged by various flight plan blocks and stages, it may be helpful to look at sw/airborne/subsystems/nav.h and the generated flightplan file in var/<AIRCRAFT_NAME>/generated/flight_plan.h.

Fixed-wing autopilot

Global view
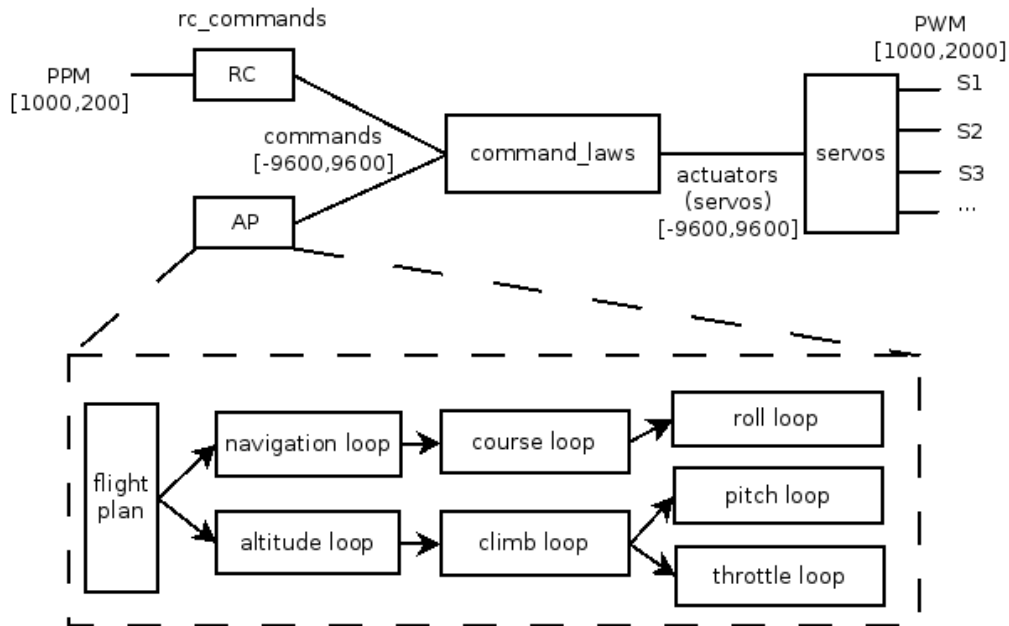
The elements **servos**, **rc_commands**, **commands** and **command_laws** correspond to specific section of the Airframe Configuration file. Most of the code located in these blocks is generated from the xml of th configuration file.

The value **+/-9600** correspond to **+/-MAX_PPRZ**. This **pprz** unit is used as a normalized internal unit for input and output values of the **control_laws** block.

Navigation loop

The navigation loop is located in **sw/airborne/subsystems/nav.***. The navigation routines are called from the Flight Plans. Advanced navigation routines are in**sw/airborne/subsystems/navigation/**.

Course loop
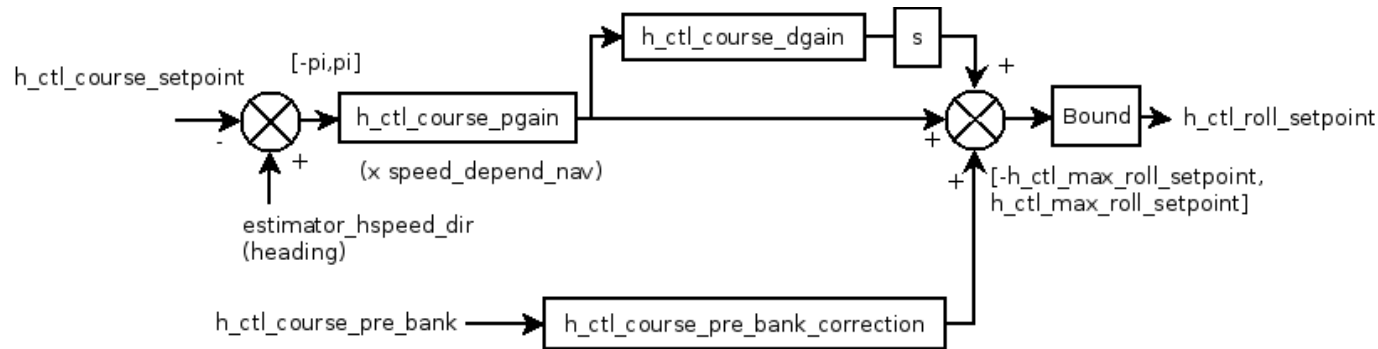
The course loop is the upper stage of the horizontal control. It is located in**sw/airborne/firmwares/fixedwing/stabilization/stabilization_attitude.c** (formerly fw_h_ctl.c).

Roll loop
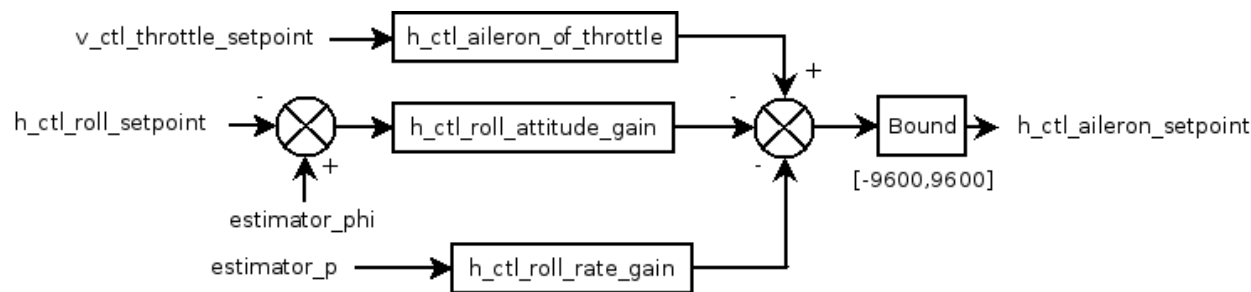
The roll loop is the lower stage of the horizontal control and is used for lateral attitude stabilization. It is located in **stabilization_attitude.c**. If `H_CTL_ROLL_ATTITUDE_GAIN` is undefined, the code will fallback to a attitude-only loop, where `estimator_p` is disregarded and the gain for `estimator_phi` is `H_CTL_ROLL_PGAIN`.

Note; estimator_phi is the measured roll angle, and estimator_p is the measured rate of change in roll angle.

Altitude loop
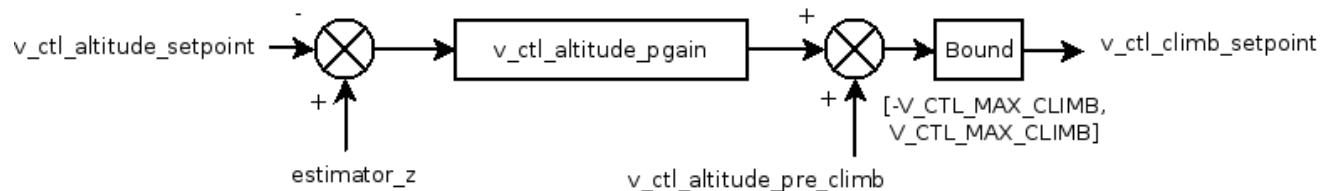
The altitude loop is the upper stage of the vertical control. It is located in**sw/airborne/firmwares/fixedwing/guidance/guidance_v.c** (formerly fw_v_ctl.c) If AGR_CLIMB is defined in the airframe file, the altitude loop also sets the v_ctl_auto_throttle_submode for use in the climb loop.

Auto Throttle and Auto Pitch climb loops

Two climb loops are available. The are called from the flight plan by changing the vertical navigation mode. The default mode is **Auto Throttle**. The **Auto Pitch** loop is only available if**V_CTL_AUTO_PITCH_PGAIN** is defined. Only one loop is active at a time. Note also that if**USE_AIRSPEED** is defined, then the Auto Throttle loop is replaced by the Auto Airspeed loop, see [Control_Loops#Control_loops_using_Airspeed_Sensorlbelow].

Auto throttle loop

v_ctl_climb_mode = V_CTL_CLIMB_MODE_AUTO_THROTTLE
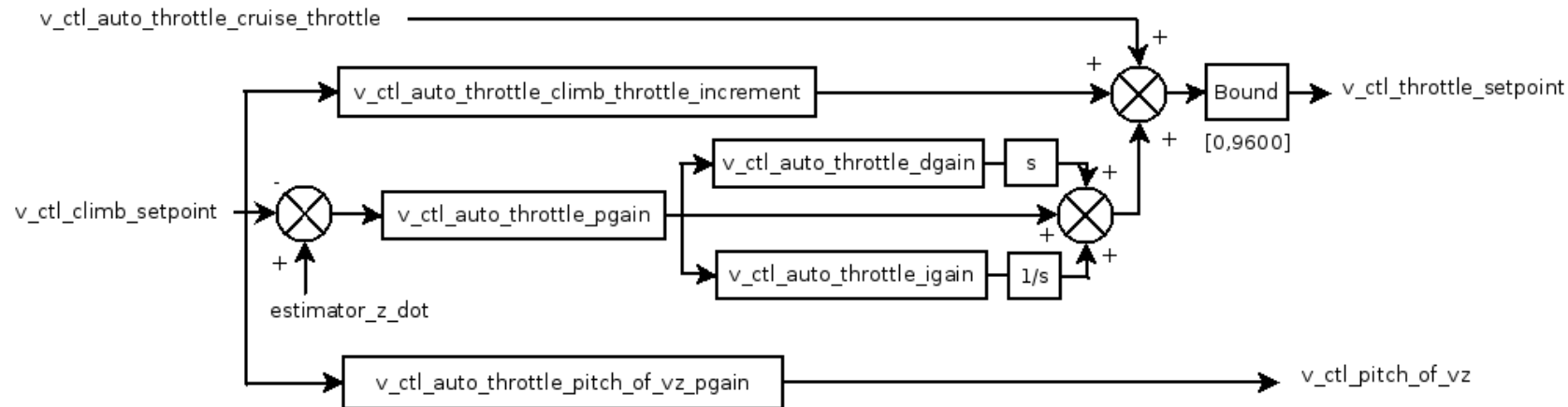
If **AGR_CLIMB** is defined, then the auto throttle submode is used to determine setpoint outputs. This may be the standard control loop outputs, the aggressive outputs (static setpoints defined in airframe file) or a blend of both.

Auto pitch loop

v_ctl_climb_mode = V_CTL_CLIMB_MODE_AUTO_PITCH
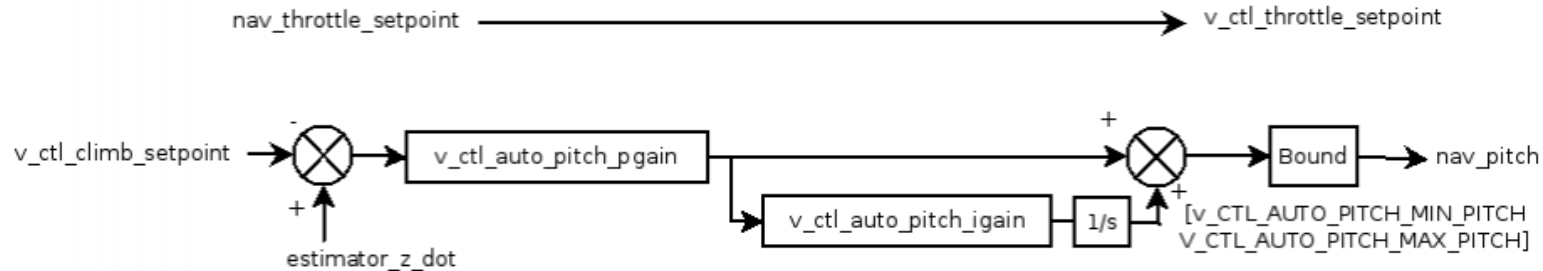
The climb loop is the intermediate stage of the vertical control. It is located in **guidance_v.c**.

Pitch loop
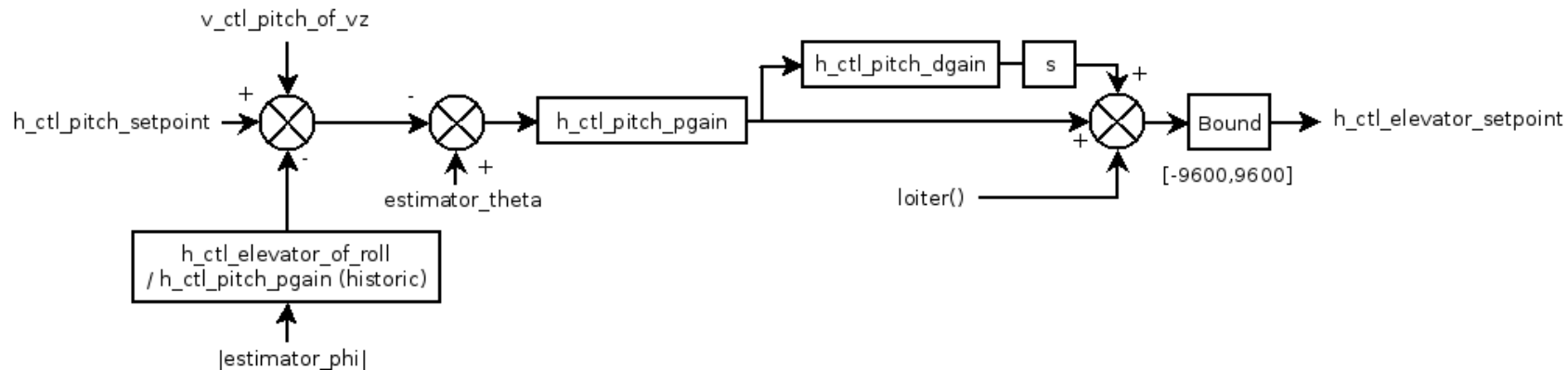
The pitch loop is the lower stage of the vertical control and is used for longitudinal attitude stabilization. It is located in **stabilization_attitude.c**. The first sum block of the diagram is not completely accurate. The input to the pitch stabilization loop is h_ctl_pitch_setpoint, though v_ctl_pitch_of_vz is not a direct input. Rather h_ctl_pitch_setpoint is assigned in the main autopilot loop from nav_pitch, in general (in auto1, it is assigned directly from the pitch r/c input). The nav_pitch value is obtained in a few ways, depending on which control loop(s) are active. If auto throttle is active, nav_pitch is the sum of v_ctl_pitch_of_vz and a fixed setpoint defined using the pitch attribute in the flightplan. If AGR_CLIMB is set, nav_pitch is either the airframe file defined ascent and descent pitch setpoints, the standard sum, or a blend of each. If auto pitch is active, nav_pitch is defined directly from the output of that loop. If airspeed is active, nav_pitch is defined in the auto airspeed pitch loop.

Control loops using Airspeed Sensor

Adding an airspeed sensor measures actual airspeed resulting in better throttle control and aircraft performance especially in windy conditions. The use of an airspeed sensor is described here.

v_ctl_climb_mode = V_CTL_CLIMB_MODE_AUTO_THROTTLE

Pitch Control Loop
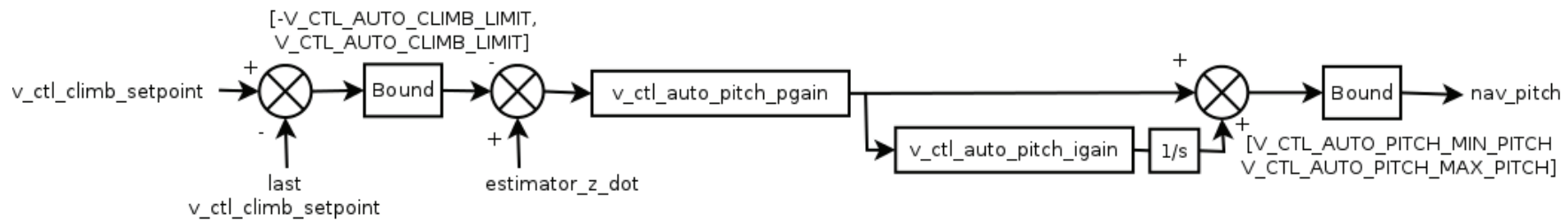
Groundspeed Control Loop
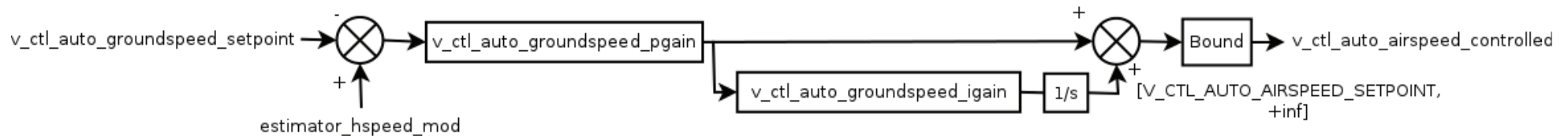
Airpeed Control Loop
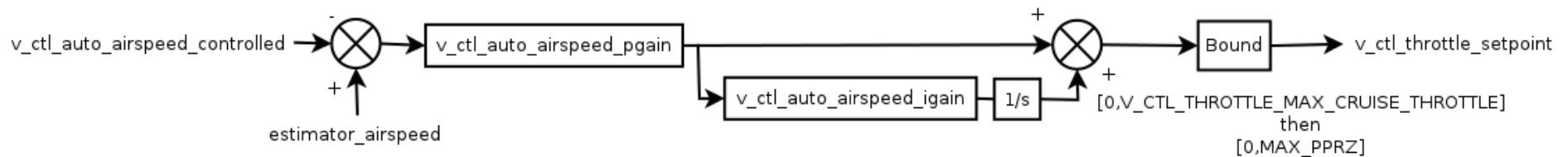
The auto airspeed cascaded control loops control both pitch and throttle. This control loop set replaces the Auto Throttle climb loop; it is engaged in the same manner in the flight plan. It is located in **guidance_v.c**.

Energy Control loops using Airspeed Sensor

Total Energy (speed + height) control for fixed wing vehicles developed by the MAVLab of the Technical University of Delft. An airspeed sensor is mandatory. The energy control loops control both pitch and throttle. This control loop set replaces the Auto Throttle climb loop and is located in **energy_ctrl.c**.

v_ctl_altitude_loop
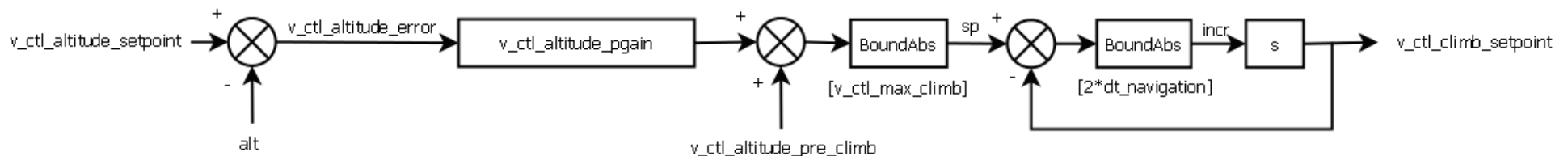
v_ctl_climb_loop
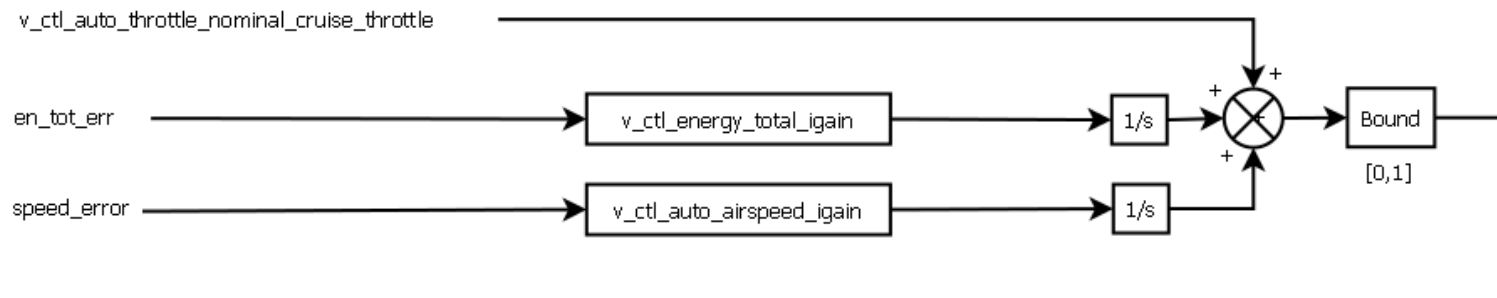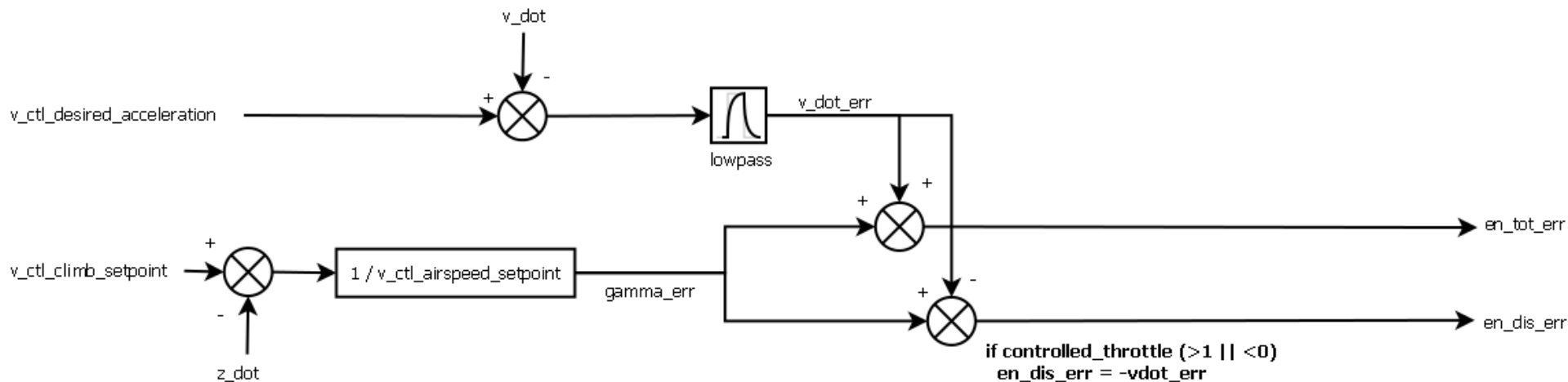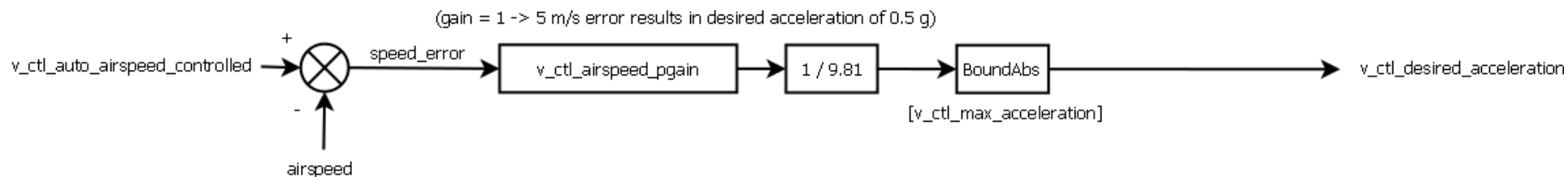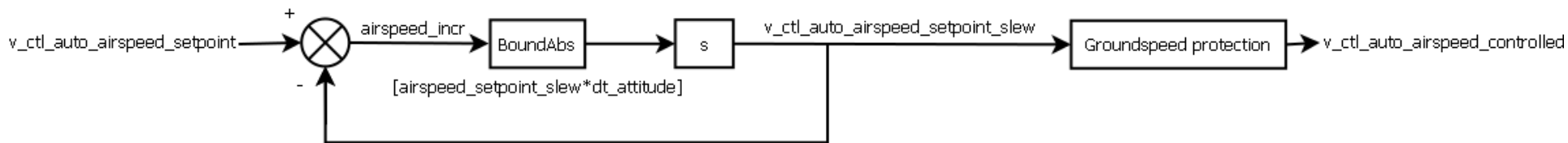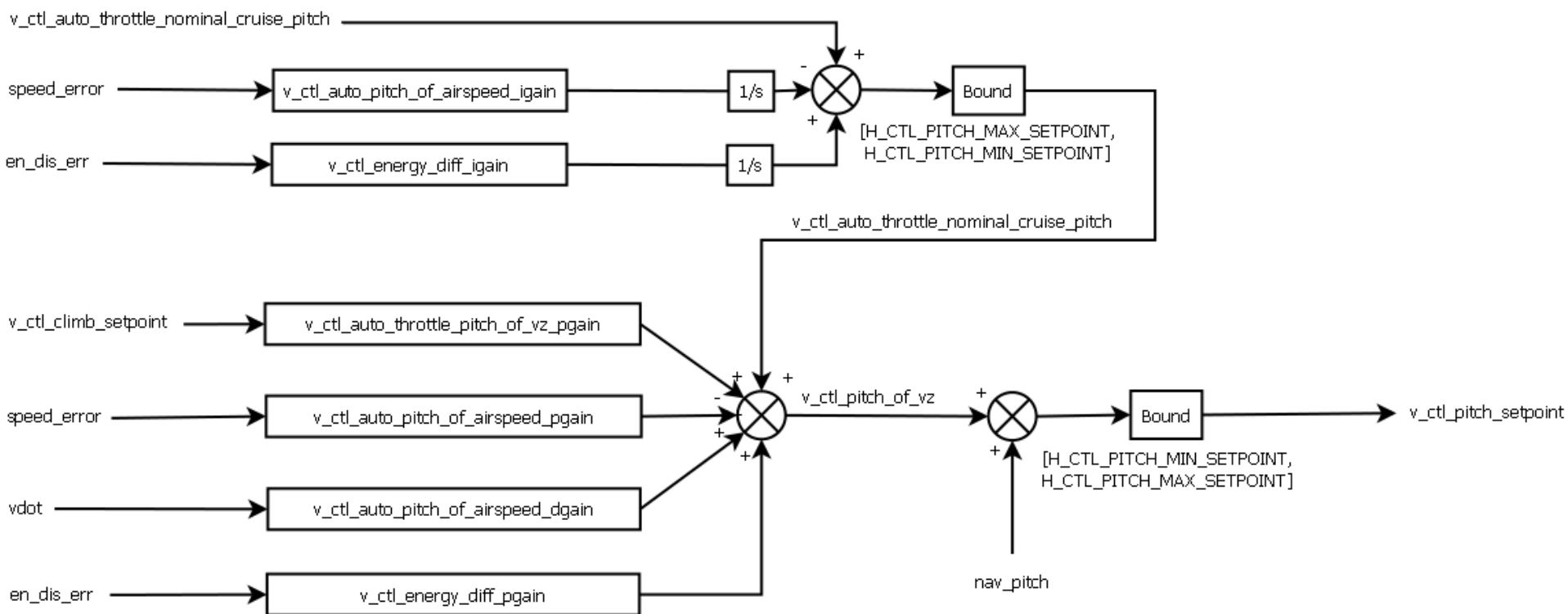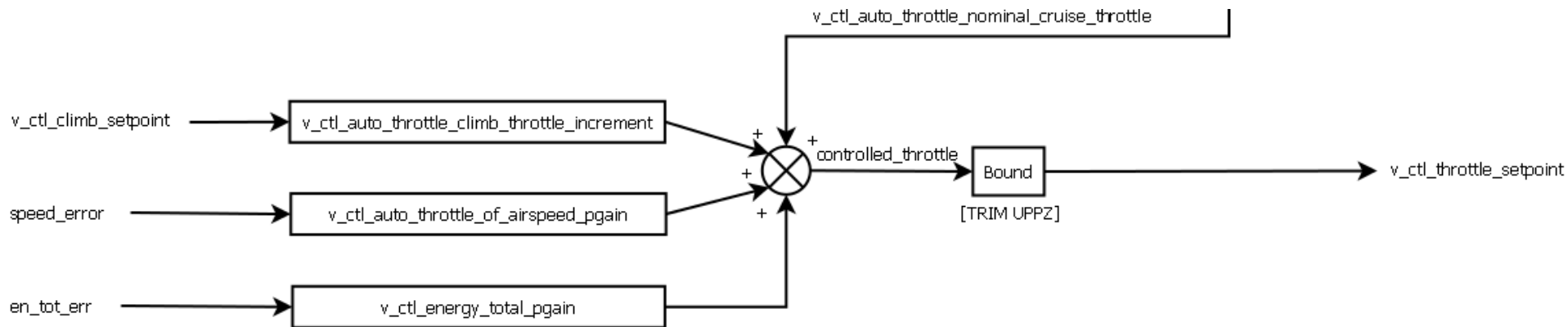
Appendix D

Special Flight Operations Certificate

Note: personal contact information has been removed for compliance with Theses Canada.

344 Edmonton Street
Winnipeg, MB
R3C 0P6

February 7, 2013   5812-11-12012
                                          RDIMS: 8176818

Dr. Michael Lipsett
Office 5-8J
Mechanical Engineering Building
University of Alberta
Edmonton AB T6G 2G8

Dear: Dr. Lipsett:

Pursuant to section 603.67 of the *Canadian Aviation Regulations*, this constitutes your **Special
Flight Operations Certificate (SFOC)** for the operation of the **Hobby Lobby Senior
Telemaster, Hobby Lobby Senior Telemaster Plus and the Multiplex Mentor Unmanned Air
Vehicle (UAV),** as described in your SFOC application dated **January 27, 2013,** for flight testing,
product research and development. Issued under the authority of the Minister pursuant to the
Aeronautics Act, this document certifies that the Certificate holder is adequately equipped and
able to conduct a safe operation, subject to the observance and performance by the Certificate
holder of the conditions set out in this Certificate, or any part thereof:

1. This Certificate:

a) is issued to **Dr. Michael Lipsett / University of Alberta UAS Group.**

   b) may be suspended or cancelled at any time by the Minister for cause, including failure on
       the part of the Certificate holder, its servants or agents to comply with the provisions of
       the *Aeronautics Act* and the *Canadian Aviation Regulations* (CARs);

   c) is not transferable and is valid **February 5, 2013 to December 31, 2013** unless
       suspended or cancelled;

   d) is valid for the operation of the **Hobby Lobby Senior Telemaster, Hobby Lobby Senior
   Telemaster Plus and the Multiplex Mentor** UAVs at the **ERSC Bremner Field,
       UAlberta EMEND Forest Research Site and the University Ellerslie Farm** sites as
       described in the SFOC applications dated **January 27, 2013**.

2. Nothing in this Certificate shall be held to relieve the Certificate holder from the requirement
    to comply with the provisions of such Canadian Aviation Documents as may have been
    issued to him pursuant to the *Aeronautics Act* or the *Canadian Aviation Regulations* (CARs).

3. This Certificate is issued for the operation of **Hobby Lobby Senior Telemaster, Hobby
    Lobby Senior Telemaster Plus and the Multiplex Mentor** UAVs without, transponder,
    aircraft markings, aircraft registration or a flight authority.

4. The Certificate holder shall maintain an adequate management organization that is capable
    of exercising supervision and operational control over persons participating in the UAV
    operations.

Canadä■✦■

5. The management organization, the facilities, the normal operations plan, the emergency operating procedures, the operating limitations, the flying areas to be used, the Security and Emergency contingency plans for the **Hobby Lobby Senior Telemaster, Hobby Lobby Senior Telemaster Plus and the Multiplex Mentor UAVs**, shall be in accordance with data provided in the SFOC application dated **January 27, 2013** or as otherwise agreed upon between Dr. Michael Lipsett University of Alberta UAS Group and Transport Canada.

6. The Certificate holder shall conduct the operation of the **Hobby Lobby Senior Telemaster, Hobby Lobby Senior Telemaster Plus or the Multiplex Mentor** UAVs in a safe manner.

7. Only one (1) **Hobby Lobby Senior Telemaster, Hobby Lobby Senior Telemaster Plus, or Multiplex Mentor UAV** shall be operated in-flight, by an operator at any one time.

8. All **Hobby Lobby Senior Telemaster, Hobby Lobby Senior Telemaster Plus and Multiplex Mentor** UAV operations shall be limited to a maximum altitude of 800 ft. above ground level (AGL).

9. The **Hobby Lobby Senior Telemaster, Hobby Lobby Senior Telemaster Plus and the Multiplex Mentor** UAVs shall give way to manned aircraft.

10. The **Hobby Lobby Senior Telemaster, Hobby Lobby Senior Telemaster Plus and the Multiplex Mentor** UAVs shall be operated or supervised by personnel who are fully trained in all aspects of its flight planning, operation and recovery.

11. Throughout the flight operation, the Certificate holder shall ensure that the **Hobby Lobby Senior Telemaster, Hobby Lobby Senior Telemaster Plus and the Multiplex Mentor** UAV are flown over areas that would permit a safe landing on the surface without hazard to persons or property in the event of any emergency or system failure requiring or resulting in an immediate descent.

12. The **Hobby Lobby Senior Telemaster, Hobby Lobby Senior Telemaster Plus and the Multiplex Mentor** UAVs shall only be operated during daylight hours.

13. For any **Hobby Lobby Senior Telemaster, Hobby Lobby Senior Telemaster Plus and Multiplex Mentor** UAVs operated under the authority of this SFOC, **Dr. Michael Lipsett / University of Alberta UAS Group** shall have subscribed for liability insurance covering risks of public liability in the amount described in subsection 606.02(8) of the *Canadian Aviation Regulations*.

14. The **Hobby Lobby Senior Telemaster, Hobby Lobby Senior Telemaster Plus and the Multiplex Mentor** UAVs shall only be operated when weather conditions in the area of operation are: Cloud cover, not less than 1500 feet above ground level (AGL) for operations between 500 and 800 feet AGL. Cloud cover, not less than 1000 feet AGL for operations up to 500 Feet AGL. Visibility shall exceed 3 statute miles.

15. The **Hobby Lobby Senior Telemaster, Hobby Lobby Senior Telemaster Plus and the Multiplex Mentor** UAVs must remain clear of cloud and within the operator's visual line of sight during flight operations.

16. The Certificate holder is responsible for ensuring that owners of property, over which flights of **Hobby Lobby Senior Telemaster, Hobby Lobby Senior Telemaster Plus and the Multiplex Mentor** UAVs will take place, have been advised of the proposed operation and have no objections.

17. The Certificate holder shall locate an observer, in the area. This observer must advise the **Hobby Lobby Senior Telemaster, Hobby Lobby Senior Telemaster Plus and the Multiplex Mentor** UAV operator if it appears that the UAV is violating any conditions of this SFOC.

18. The Certificate holder shall ensure that the **Hobby Lobby Senior Telemaster, Hobby Lobby Senior Telemaster Plus and the Multiplex Mentor** UAVs are operated at a distance of not less than 100 feet away from members of the public and inhabited structures such as buildings and vehicles without the owner's consent.

19. Flight over persons not directly involved with the operation is prohibited.

20. Certificate holder shall report to Transport Canada, General Aviation on the first working day following any of the following occurrences, with details of any of the occurrences:

   a) The **Hobby Lobby Senior Telemaster, Hobby Lobby Senior Telemaster Plus or the Multiplex Mentor** UAV flys outside of planned bounds of operation; or

   b) Any person being injured as a result of the operation; or

   c) Any unintended contact between the **Hobby Lobby Senior Telemaster, Hobby Lobby Senior Telemaster Plus, or the Multiplex Mentor** UAV and person(s), livestock, vehicle(s) or structure(s).

21. The Certificate holder shall not operate the **Hobby Lobby Senior Telemaster, Hobby Lobby Senior Telemaster Plus or the Multiplex Mentor** UAV following any of the occurrences listed in condition 20. (a) (b) or (c), until Transport Canada, General Aviation, approves its further operation in writing.

22. All persons involved with these operations (flight crew, ground station crew, and spotters) shall be familiar with the contents of this SFOC, and the contents of the application dated **January 27, 2013.**

22. A copy of this SFOC and a copy of the application dated **January 27, 2013** shall be on site any time the **Hobby Lobby Senior Telemaster, Hobby Lobby Senior Telemaster Plus or the Multiplex Mentor** UAV is in operation.

23. The Certificate holder shall:

   a) Document their flight planning and procedures for each location and flight.
   b) Document a post flight report on performance and any deviations from the plan.
   c) Documentation shall be kept and made available for inspection for 2 calendar years.
   d) Dr. Michael Lipsett/University of Alberta UAS Group shall submit Quarterly reports to Transport Canada (see Appendix #1 for content and format).

Yours truly,

Tim Kalushka
Technical Team Lead Winnipeg Operations
Civil Aviation Winnipeg
Prairie and Northern Region
For Minister of Transport

APPENDIX A

University of Alberta, Quarterly reports to Transport Canada,
Due after the last day of March, June, September, & December.

Date of Flight	Operator / Observer	Flight time (0.1, 0.2, 0.3 hrs)	Location, Address or Co-ordinates	Verification of Weather, Visibility Ceilings Winds	Altitude Flown & General Observations, Comments

Add pages as necessary

Submitted by: _____
Scan and E-Mail to: **PNRspecialflightops@tc.gc.ca**

Subject: SFOC Application 2013
Air Vehicle Name(s): UAP1, UAP2, UAP3
By: J. D. Yuen, S. C. Dwyer
Date: 27 January 2013

Application for a Special Flight Operations Certificate

The following constitutes an application for a Special Flight Operations Certificate for the purpose of operations of 3 unmanned aircraft used as Unmanned Aerial Platforms (UAPs). All aircraft are of similar design with slight variations. These aircraft shall be used to test the flight control system and sensor payloads that are part of a research programme for the Unmanned Aircraft Systems Group (UAS Group) at the University of Alberta.

(a)   the name, address, and where applicable, the telephone number and facsimile number of the applicant;

Dr. Michael Lipsett Office: 5-8J Mechanical Engineering Building University of Alberta Edmonton, AB T6G 2G8 Canada. █████████		

(b)   the name, address, and where applicable the telephone number and facsimile number of the person designated by the applicant to have operational control over the operation (Operation Manager);

Operation Manager: Stephen Dwyer Lab: 1-38 Mechanical Engineering Building University of Alberta Edmonton, AB T6G 2G8	Deputy Operation Manager (1): Jamie Yuen Lab: 1-38 Mechanical Engineering Building University of Alberta Edmonton, AB T6G 2G8	

U of A UAS Group

Canada. Phone: ▇▇▇▇▇▇▇	Canada. Phone: ▇▇▇▇▇▇▇	

(c)   Method of Direct Contact During Flight

Either the operations manager or a deputy operations manager will be able to get in touch with the operating personnel at the field during operations.

(d)   Type & Purpose of Operations

The purposes of these flight operations are to conduct flight testing of an integrated autopilot system and sensory payload mounted in medium-size (maximum 94 inch / 2.4 m wingspan) model aircraft to collect data on the performance of the autopilot system and payload. The autopilot systems will be tested using the Unmanned Aerial Platform (UAP) aircraft described below. These flight operations will serve as a stepping-stone for future development of the Unmanned Aircraft Systems (UAS) programme at the University of Alberta.

Operations will be carried out in day/VFR conditions. The weather criteria to determine whether the flight-testing may proceed are:
- average wind velocity no greater than 15 kts (17 mph, 28 km/h)
- no precipitation
- minimum visibility of 3 miles
- minimum ceiling of 1000 ft AGL or better (for flights up to 500 ft AGL)
- minimum ceiling of 1500 ft AGL or better (for flights up to 800 ft AGL)

Only one aircraft at a time will be operated during the flying sessions – there will be no multi-vehicle flight operations. The intention of bringing multiple aircraft to the field is to simplify logistics and maximize data collection opportunities.

(e)   Date and Duration of Operation

Each flight session will take approximately 4 to 8 hours. Each flight session will consist of a series of individual flights lasting 15-60 minutes. As many sessions as needed for testing will be carried out beginning 1 February 2013 or at the earliest receipt of SFOC approval and ending 31 December 2013. Operations will be held over the course of the day when conditions are appropriate.

(f) Description

UAP 1 Aircraft
- Aircraft designation: "UAP1"

U of A UAS Group

- Type of aircraft: Hobby Lobby Senior Telemaster almost-ready-to-fly model aircraft
- Type of engine: 2-stroke 26cc, "Evolution 26GX"
- Type of fuel: gasoline/oil mixture
- Dimensions: wing span 2.4 m (94 inches); fuselage 1.6 m (64 inches)

- Avionics systems and methods of control:
- Spektrum DX8 radio-control (R/C) system (also used to switch autopilot on and off)
- Paparazzi autopilot

UAP 2 Aircraft
- Aircraft designation: "UAP2"
- Type of aircraft: Hobby Lobby Senior Telemaster Plus almost-ready-to-fly model aircraft
- Type of engine: 2-stroke 26cc, "Evolution 26GX"
- Type of fuel: gasoline/oil mixture
- Dimensions: wing span 2.4 m (94 inches); fuselage 1.6 m (64 inches)

- Avionics systems and methods of control:
- Spektrum DX8 radio-control (R/C) system (also used to switch autopilot on and off)
- Paparazzi autopilot

UAP 3 Aircraft
- Aircraft designation: "UAP3"
- Type of aircraft: Multiplex Mentor model aircraft (EPO foam construction)
- Type of engine: electric, "Himax 3528-1000 Brushless Motor"
- Type of fuel: Lithium Polymer (LiPo) batteries
- Dimensions: wing span 1.7 m (65 inches); fuselage 1.2 m (47 inches)

- Avionics systems and methods of control:
- Spektrum DX8 radio-control (R/C) system (also used to switch autopilot on and off)
- Paparazzi autopilot

UAP 1 & 2 Flight Performance Data
As UAP 1 & 2 are based on the same aircraft; they have the same flight performance.
- Maximum speed: 110 km/h (68 mph)
- Maximum descent rate: 150 m/min (500 ft/min)
- Maximum climb rate: 120 m/min (400 ft/min)
- Maximum payload weight: 6 kg (13 lbs)
- Maximum gross takeoff weight: 12 kg (26 lbs)
- Maximum flight endurance: 60 min (@nominal fuel capacity)
- Maximum fuel capacity: 700 ml (24 oz. fl.) nominal

UAP 3 Flight Performance Data
- Maximum speed: 90 km/h (56 mph)
- Maximum descent rate: 360 m/min (1180 ft/min)

U of A UAS Group

- Maximum climb rate: 240 m/min (790 ft/min)
- Maximum payload weight: 2.0 kg (4.4 lbs)
- Maximum gross takeoff weight: 2.7 kg (5.9lbs)
- Maximum flight endurance: 20 min (@nominal battery capacity)
- Maximum fuel capacity: ~50Whr battery capacity nominal

All of the aircraft are white and red to ensure maximum visibility. There are no lights on the aircraft.

Ground Control Station

The Ground Control Station (GCS) is a laptop computer using the Paparazzi software that allows the autopilot to be programmed for flight. There will also be a telemetry system installed on the aircraft and the ground control station will be in constant communication with the autopilot to enable real time monitoring of the flight and status of the aircraft. The GCS can be used to replay data recorded by the autopilot during flight such as GPS location, heading, airspeed, altitude, etc.

(g)   Security Plan

The UAP will be kept within visual contact of the pilot on the ground at all times. This is an overriding criterion whether the Paparazzi or the pilot is controlling the UAP. The pilot can take over control of the UAP at any time during the flight (including during emergency recovery) using his radio control transmitter. Both the Paparazzi and the radio control system incorporate a "fail-safe" mode of operation which puts the UAP into a predetermined emergency recovery pattern (including eventual engine shutdown) in the event of signal loss or radio interference. The autopilot fail-safe mode includes predefined hard and soft flight boundaries. If the soft flight boundary is exceeded under autopilot control, the autopilot returns the aircraft to a standby holding point. If the hard flight boundary is exceeded under autopilot control, the autopilot shuts down the engine and places the aircraft in a low-energy descent.

All safety guidelines and regulations of the Model Aeronautics Association of Canada (MAAC) will be followed during flight operations. All rules specific to the club where flight operations are being performed will be followed. The Bremner field of the Edmonton Radio Control Society (ERCS) and the University Ellerslie Farm, described in more detail below, have been selected for this flight test series. Two fields have been selected to allow an alternate flight location in the event one field is comprised by a public event or other operation. The Ellerslie farm also has the advantage of several points that have been georeferenced to sub-centimeter accuracy and can be used for the calibration of sensor payloads.

One additional field, the UAlberta EMEND, is a forest research site that has been selected to test UAP data collection with the goal of aiding active research. This site is described in more detail below.

U of A UAS Group

MAAC guidelines are written such that they can be applied at any field. They define where spectators may stand, parking areas, etc. They are applicable to all airfields chosen by the team, and will be followed at all times. Since MAAC insurance is only applicable to recreational radio control aircraft flights, insurance coverage of $5M general liability has been secured through the University of Alberta's institutional insurance provider for the UAP flights.

A minimum of 2 members of the University of Alberta UAS Group including an experienced radio control pilot will be involved in the flight operations. The minimum team composition will be:
- 1 pilot (responsible for watching for conflicting traffic)
- 1 GCS operator

The team may be enhanced as required by further personnel such as data recorders, payload operators and spotters. In the event of more complex ground scenarios, for example with invited spectators, at least 1 additional Group member will be present to assist with tasks such as crowd control and spotting. As per standard MAAC flight operations, the pilot has multiple roles of piloting and watching for conflicting traffic. In complex scenarios, the pilot (in conjunction with the Operation Manager) will evaluate his/her ability to safely complete both tasks, and request a dedicated spotter if required.

ERCS Bremner Field
Casual spectators may be expected at the ERCS Bremner field since it is open to spectators whenever operations are in progress. The University may invite a small group of persons having a legitimate technical or operational interest in the University of Alberta UAS Group. The UAP will not be flown at any time when ERCS has specifically invited the public to an event at Bremner.

Spectators at the Bremner field are restricted to the area behind the spectator line shown on the diagram appended to this application. The spectator barrier is signed. This barrier is the requisite 30 metres from the edge of the runway and flying area as required by the "Model Aeronautics Association of Canada Safety Code", Version 003, 25 September 2004 (see attached sketch).

The University of Alberta UAS Group has obtained permission from the ERCS to use their airfield for these tests. The airfield is located on the northeast side of Edmonton, north of Township road 540 between Range Road 231 and 232 (see map appended).

The geographic position at the access road (see sketch appended) is:

53°38'15.97"N   113°17'13.02"W

Operations will be within the envelope of normal club operations at this field as outlined on the appended sketch. The aircraft will be operated within sight of the pilot at all times.

U of A UAS Group

Ellerslie Farm

Casual spectators are not expected at the Ellerslie farm since it is not open to the general public. There may be various farm related activities ongoing throughout the year, and all flight operations will be coordinated with the farm manager. The university may invite a small group of persons having a legitimate technical or operational interest in the University of Alberta UAS Group. All spectators will be restricted to the area behind the spectator line shown on the diagram appended to this application. The spectator barrier is temporary, but is signed and is the requisite 30 metres from the edge of the runway and flying area as required by the "Model Aeronautics Association of Canada Safety Code", Version 003, 25 September 2004 (see attached sketch).

The University of Alberta UAS Group has obtained permission from the University of Alberta to use the Ellerslie farm for these tests. The airfield is located on the southwest side of Edmonton, between 9 Ave and 41 Ave SW, and 127 St and 141 St SW (see map appended).

The geographic position as shown in the appended sketch is:

        53°25'7.55"N   113°33'10.18"W

Operations will be within the envelope of operations at this field as outlined on the appended sketch. The aircraft will be operated within sight of the pilot at all times.

Since the Ellerslie Farm site lies within airspace controlled by the Edmonton International airport, the IFR Shift Manager at the Edmonton Area Control Center ███████████ was contacted to confirm that the flight operations outlined in this SFOC will not interfere with IFR operations. Todd Trischuk, the Edmonton International Control Tower Manager ████████ ██████ was contacted to confirm flight clearance and emergency procedures. The team will work closely with air traffic control for the area to ensure there is no interference with regular or emergency manned aircraft operations, and follow any recommendations or requirements given.

UAlberta EMEND Forest Research Site

The EMEND location is in northern Alberta, approximately 85km northwest of Peace River. Due to the remote location of the EMEND site, casual spectators are not expected. All personnel on site will be present to perform a pre-determined role in support of flight operations. The ground operations layout is shown in Appendix A.

The University of Alberta UAS Group has obtained permission from all stakeholders to use the EMEND lease and surrounding land for these flights. This includes the EMEND group at the University of Alberta and DMI Ltd., an integrated forest products company. As the EMEND lease as well as the surrounding region is an area of active research interest, a number of additional protocols are in place through EMEND and DMI regarding site access, site safety and emergency procedures. A copy of these protocols are available to the team and will be followed. In general, these protocols do not directly impact flight operations.

U of A UAS Group

The geographic position as shown in the appended sketch is approximately:

56° 44' 37.94" N 118° 20' 38.80" W

Operations will be within the envelope of operations at this field as outlined on the appended sketch. The aircraft will be operated within sight of the pilot at all times.

It is noted that while the location is relatively remote, it has been verified that there is cellular coverage available.

The three closest airports to the flight location are the Peace River Airport (YPE), approximately 79 km southeast of the flight location, the Manning Municipal Airport, approximately 48 km northwest of the flight location, and the Grimshaw Airport, approximately 76 km southeast of the flight location.

(h) Emergency Contingency Plan

The operations manager and/or deputy operations manager are required to have an active cellular telephone with reception at the field during all flight operations.

In the event of a loss of the communications link with the UAP, the aircraft will automatically return to its home position which will be a GPS coordinate above the runway. Should the R/C link be lost, the UAP will continue its flight plan and can be recalled at anytime. If at any point in flight the UAP crosses the flight boundaries, a return to home command will be automatically executed. If a communications and R/C failure occur simultaneously, the UAP will return to home. In the event of an autopilot failure, all servos will move to pre-progammed failsafe positions that will bring the UAP to the ground in a minimum radius. The safety pilot can command an emergency engine kill at any time using the R/C link. If the UAP becomes unresponsive and leaves flight boundaries, an engine kill will be commanded. If the UAP exits the flight boundaries and cannot be recalled or killed, the UAP runaway contingency plan will be invoked.

UAP Runaway Contingency Plan: The nearest control tower will be immediately notified by the operations manager using his cellular phone that we have a runaway UAV with its weight, wingspan, colouring and last known location, bearing, altitude and speed.
- From Bremner this is the Edmonton City Centre control tower at their emergency only telephone line (780-413-5501).
- From Ellerslie this is the Edmonton International control tower emergency only telephone line (780-890-4733).
- From EMEND this is the Peace River airport manager (780-624-2867).
- The NAV CANADA Flight Information Center (FIC) will be notified if the above towers cannot be contacted. All locations above are in the Edmonton FIC area.
- Edmonton FIC: 1-866-541-4102

U of A UAS Group

- National FIC: 1-866-WX-BRIEF (1-866-992-7433)

The operations manager will stay on the line with the tower until receiving confirmation from the ground crew that the UAP is either under control inside of flight boundaries or on the ground. The remainder of the ground crew will make every effort to maintain visual contact and regain communication and control of the UAP.

In the event of a medical emergency during operations at the field, the University of Alberta UAS Group will contact the appropriate authorities by cellular phone. The first to be contacted would be the emergency services at 911. Then, if necessary, the Edmonton Police Service at (780) 423-4567, or, for the EMEND location, the Peace River RCMP detachment would be contacted at (780) 624-6677.

If emergency services can not respond, recourse would be taking an injured person to the nearest hospital with emergency facilities.
- From Ellerslie this is the Grey Nuns Community Hospital (1100 Youville Drive NW, Edmonton, 780-735-7000), approximately 20 min away by car.
- From Bremner this is the Fort Saskatchewan Health Center (9430 95 Street, Fort Saskatchewan, 780-998-2256), approximately 15 min away by car.
- From EMEND this is one of:
  - Peace River Community Health Centre (0101 68 Street, Peace River, 780-624-7500), approximately 40 min away by car.
  - Manning Community Health Centre (600 2nd Street NE, Manning, Alberta, 780-836-3391), approximately 40 min away by car.
  - Grimshaw/Berwyn & District Community Health Centre (5621 50 Avenue, Grimshaw, Alberta, 780-332-6500), approximately 40 min away by car.

There will always be at least one vehicle on site capable of performing this transportation.

A fire extinguisher and a first-aid kit will be on hand during all flight operations. All operators will have available and use appropriate personal protective equipment (PPE) for specific operating scenarios.

(i) Ground Supervisor

The ground supervisor during operations with no spectators will be one of the specified Operation Managers. In the event of complex ground scenarios, for example if there are spectators, an additional UAS Group member (approved and properly briefed by an Operation Manager) will be acting ground supervisor. The ground supervisor will coordinate surface logistics in the area of UAP operations.

It is noted that the pilot will have overriding control of flight decisions during any mission. Any concerns of flight conditions, vehicle airworthiness or other safety considerations that may jeopardize the flight in the opinion of the pilot will be grounds for aborting a specific mission until the concerns can be resolved. Other UAS Group members will be responsible for notifying the pilot of concerns.

U of A UAS Group

(j) Flight Operations Plan

The following are the operational details of flight-testing. Please note that altitudes specified are above ground level.

UAP 1, 2 & 3 Aircraft

The Senior Telemaster and Senior Telemaster Plus type of aircraft have been flown as a radio control model several times by the pilots. The pilots are familiar with the handling characteristics of this type of aircraft, which are conventional and docile. Two University of Alberta UAS Group members who will be involved in flight operations have 3 years of experience flying model aircraft equipped with autopilots as a recreational activity at ERCS fields. Initial test flights will consist of:
- R/C: taxi
- R/C: takeoff at approximately 40 km/h (25 mph) IAS ISA sea level condition
- R/C or autopilot: climb to an altitude of no more than 150 m (500 ft) or 250 m (800 ft), depending on weather conditions
- R/C or autopilot: straight and level flight at approximately 65 km/h (40 mph); left and right turns; climbs and descents; all manoeuvres within the airfield boundaries
- R/C: circuit and landing

Once the performance of the aircraft and autopilot system has been verified, flights may consist of autopilot takeoff and landing under the observation of an R/C pilot with the ability to regain manual control at any time.
The aircraft shall be operated within the area shown in the appended sketches. This area is private property and closed to general public access. UAP operations will not require the erection of any obstacles in the operating area.

(k) Pilot Information

Three pilots have been identified, Messrs. P. Cary, J. Yuen and possibly a student if he/she is found to have sufficient experience and approved by either Mr. Cary or Mr. Yuen.

Mr. James Yuen has 5 years experience flying model aircraft, has flown in international competition for the University of Alberta Aerial Robotics Group, and is a MAAC member with valid insurance.

Mr. Peter Cary has over 30 years experience flying model aircraft, is a member of MAAC and has MAAC insurance. He has been involved with many R/C and autopilot projects with the University of Alberta and the Canadian Armed Forces.

The student pilot must be enrolled at the University of Alberta and be participating in the UAS project. He/she must have R/C piloting experience and be approved by one of the other

U of A UAS Group

previously approved pilots prior to operating any of the UAP aircraft. This approval will include supervised flight time with the previously approved pilots, including emergency recovery procedures.

(k)   Prior Flight Experience in the last 12 Months

The University of Alberta UAS Group held an SFOC from October 2012 to December 2012 (SFOC #5812-11-9612) for the same UAP1, UAP2, and UAP3 aircraft described in this document. Under this SFOC 4.25 hours of flight were logged over several days, the majority of which was under autopilot control. This included testing and tuning flights as well as survey flights of the EMEND research site. All flights remained within the specified boundaries.

The University of Alberta UAS Group also held an SFOC from September 2011 to December 2011 (SFOC #5812-11-3211) and January 2012 to December 2012 (SFOC #5812-11-4611), and for testing of the same UAP1 and UAP2 aircraft described in this document. Several successful flights were made over several days. This included manual controlled flights as well as testing and tuning under autopilot control. All flights remained within the specified boundaries. Members of the group have also successfully flown similar aircraft (a SIG Rascal 110 and Senior Telemaster) under R/C and autopilot control in a recreational setting.

Appendix A

Location of ERCS Field, Sketch of Field, and Sketch of Spectator Area

Note that the satellite imagery is out of date and does not show the Bremner field. Field location and flight boundaries are overlaid on the image.

U of A UAS Group
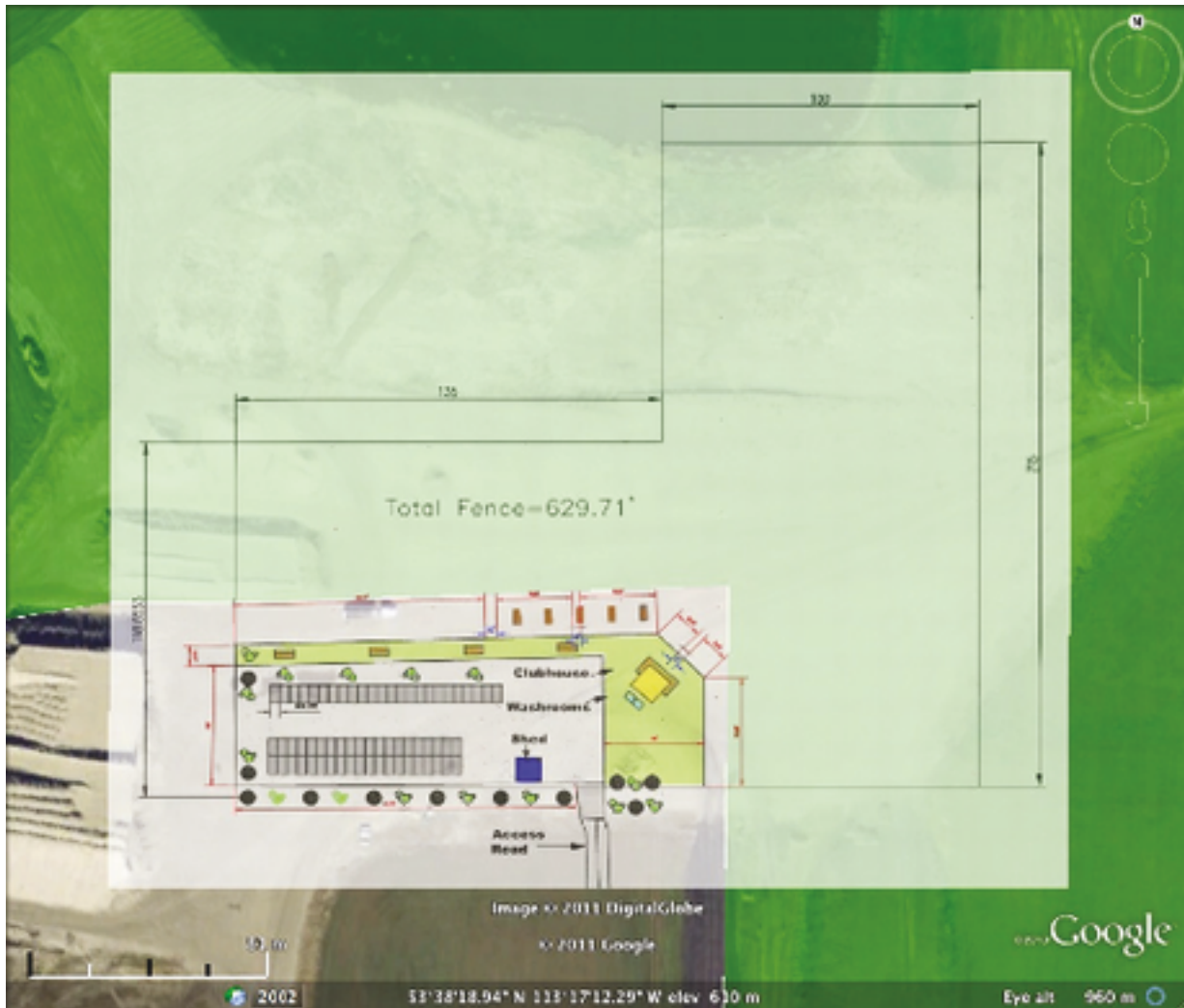
Location of spectator area and runways. Runway dimensions are shown in meters.

U of A UAS Group

PLAN SHOWING
NISBET LEASE DETAIL
ERCS

Detail of spectator area showing dimensions in feet. There is a chain link barrier fence between the spectator area and runways. Geographic location at the access road is 53°38'15.97"N 113°17'13.02"W.

U of A UAS Group

Location of Ellerslie Farm
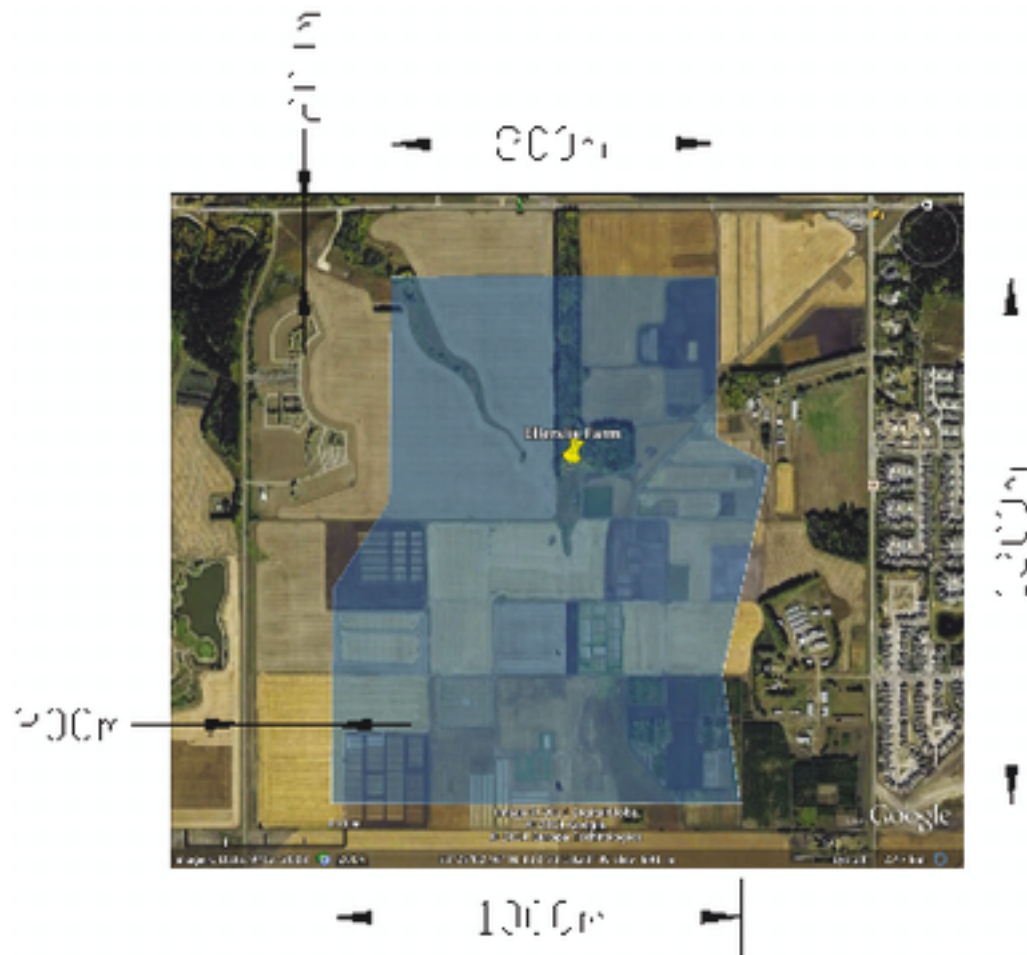
Location of flight area at the Ellerslie farm. Exact location of the ground station may vary, but will be laid out as shown below. Pin location is: 53°25'7.55"N 113°33'10.18"W

Location of EMEND Lease
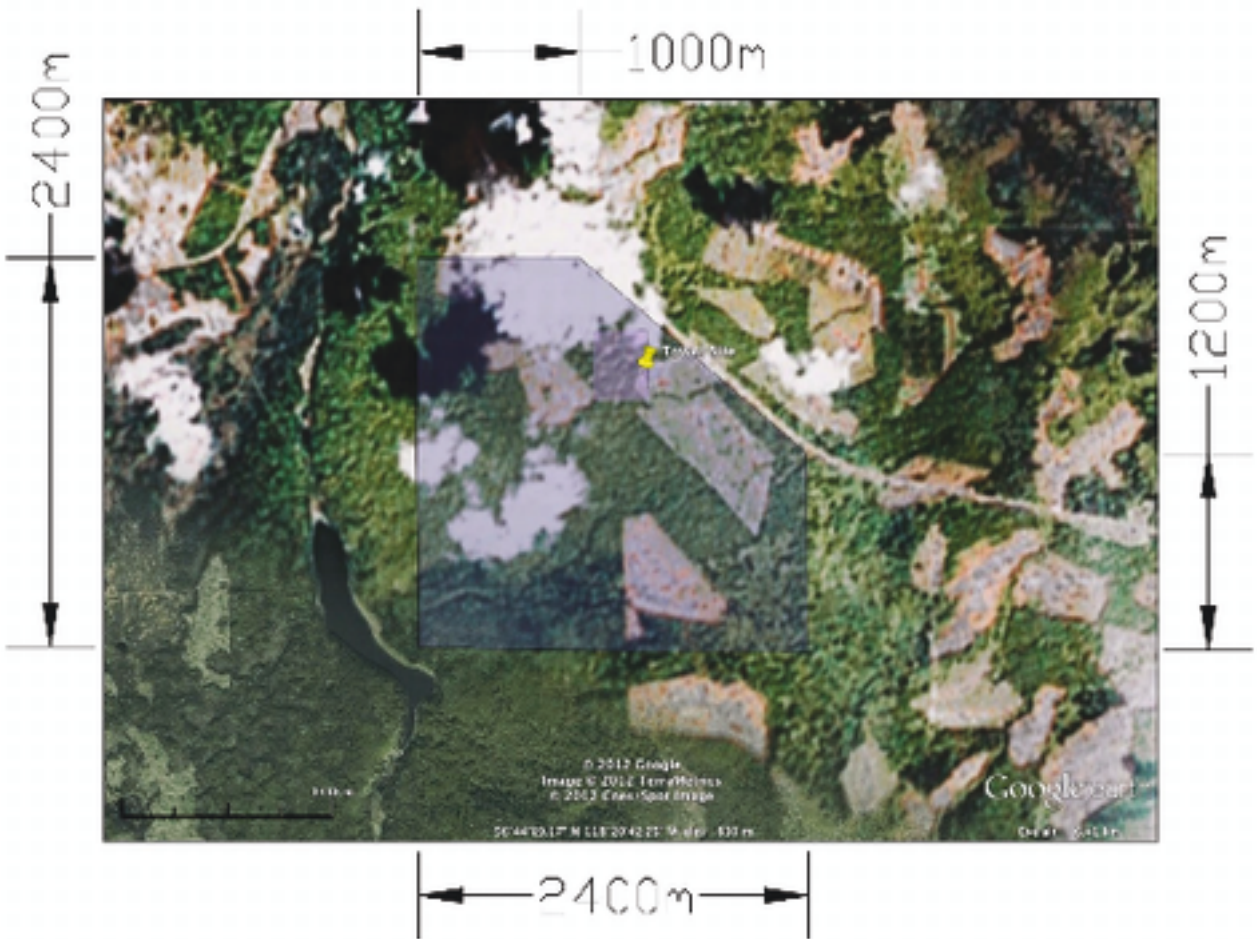
Location of EMEND flight area. Small central box is EMEND lease, surrounding land is DMI Ltd. lease. Operations and spectator area set up at approximately pin location. Top of image oriented north. Pin location is: 56° 44' 37.94" N 118° 20' 38.80" W

Sketch of Ellerslie and EMEND Operations and Spectator Area
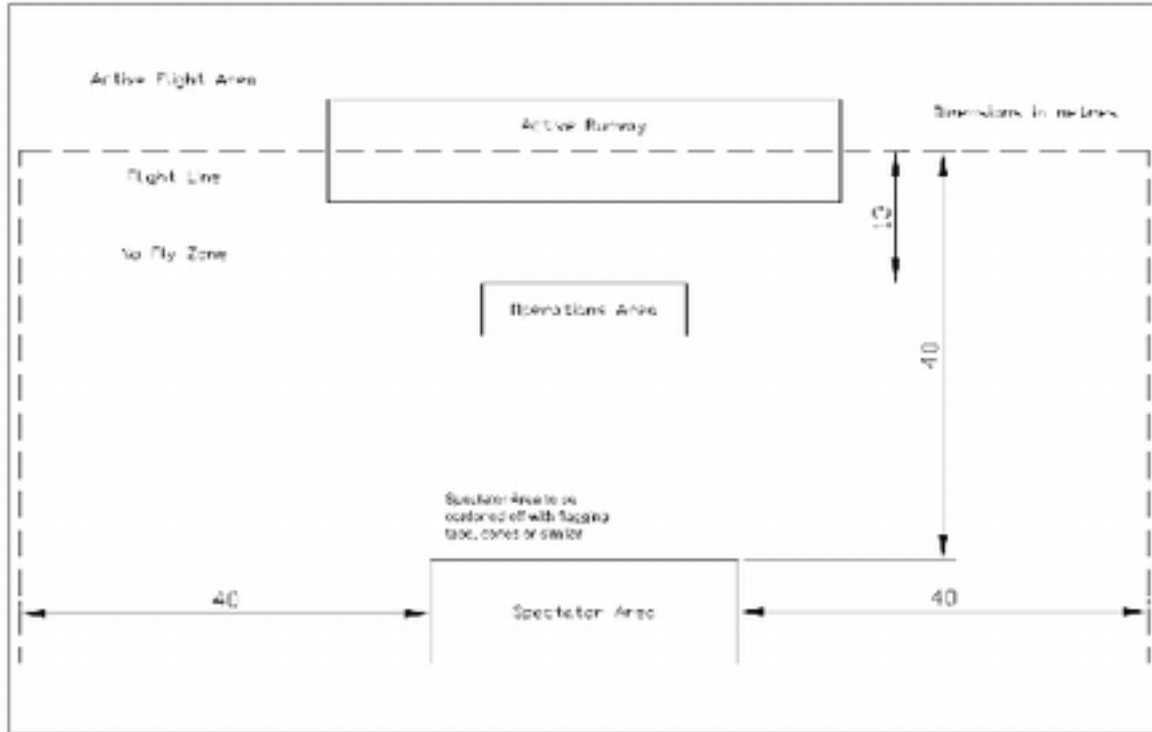
Ground station and spectator layout for use at Ellerslie Farm and EMEND. Dimensions are according to MAAC regulations for fields without permanent barriers.

References

[1] C. Scott Allen and Mark P. S. Krekeler. Reflectance spectra of crude oils and refined petroleum products on a variety of common substrates. *SPIE Active and Passive Signatures*, 7687:76870L, 2010.

[2] C. Scott Allen and Mark P. S. Krekeler. Crude oil, petroleum product, and water discrimination on terrestrial substrates with airborne imaging spectroscopy. *SPIE Active and Passive Signatures II*, 8040:80400L, 2011.

[3] C. Scott Allen and Melvin B. Satterwhite. Reflectance spectra of three liquid hydrocarbons on a common sand type. *SPIE Algorithms and Technologies for Multispectral, Hyperspectral, and Ultraspectral Imagery XII*, 6233:62331M, 2006.

[4] Chris Anderson. A diy drones milestone: 1,000 members! `http://diydrones.com/profiles/blogs/705844:BlogPost:36326`, 2008. Accessed January 23, 2013.

[5] Chris Anderson. Diy drones at 36,000 members. `http://diydrones.com/profiles/blogs/diy-drones-at-36-000-members`, 2013. Accessed January 23, 2013.

[6] Richard C. Anderson. Kite aerial photography for archaeology: An assessment and short guide. *British School at Athens Studies*, 8:167–180, 2001.

[7] ASTM. Standard test methods for laboratory determination of water (moisture) content of soil and rock by mass. Standard D2216, 2010.

[8] J. Berni, P.J. Zarco-Tejada, L. Suarez, and E. Fereres. Thermal and narrowband multispectral remote sensing for vegetation monitoring from an unmanned aerial vehicle. *Geoscience and Remote Sensing, IEEE Transactions on*, 47(3):722 –738, March 2009.

[9] Jean-Yves Bouguet. Camera calibration toolbox for matlab. `http://www.vision.caltech.edu/bouguetj/calib_doc/`, 2010. Accessed May 28, 2013.

[10] R. Bryant, D. Thoma, M.S. Moran, C.D. Holifield, D.C. Goodrich, T.O. Keefer, G. Paige, D. Williamd, and S.M. Skirvin. Evaluation of hyperspectral, infrared temperature and radar measurements for monitoring surface soil moisture. In *Proc. of 1st Interagency Conf. on Research in the Watersheds*, pages 528–533, October 2003.

[11] Paul Burkhardt and Yee Kai Pin. Alaska pipeline crude oil flow rate little changed. *Bloomberg.com*, Jan 18 2011.

[12] CSA. Oil and gas pipeline systems. Standard Z662-07, 2007.

[13] K. Dalamagkidis, K.P. Valavanis, and L.A. Piegl. A survey of unmanned aircraft systems regulation: Status and future perspectives. In *Control and Automation, 2008 16th Mediterranean Conference on*, pages 717 –723, June 2008.

[14] Jonathan P. Dandois and Erle C. Ellis. Remote sensing of vegetation structure using computer vision. *Remote Sensing*, 2(4):1157–1176, 2010.

[15] A. Dean, S. Hughes, W. Gibbons, A. Syed, O. Tsui, C. Renou, D. Dow, A. Mangin, and T. Boivin. Monitoring sustainable development in the oil sands region of alberta, canada, using spot-5 and envisat asar and meris imagery. *European Space Agency, (Special Publication) ESA SP*, SP-636, 2007.

[16] Rozalina Dimitrova and Ernest Yanful. Undrained strength of deposited mine tailings beds: Effect of water content, effective stress and time of consolidation. *Geotechnical and Geological Engineering*, 29:935–951, 2011. 10.1007/s10706-011-9428-7.

[17] Qian Du, Nareenart Raksuntorn, Adnan Orduyilmaz, and Lori M. Bruce. Automatic registration and mosaicking for airborne multispectral image sequences. *Photogrammetric Engineering and Remote Sensing*, 74(2):169 – 181, 2008. Agriculture monitoring;Airborne multispectral image sequences;Automatic algorithms;.

[18] M. Edmonds, R.A. Herd, B. Galle, and C.M. Oppenheimer. Automated, high time-resolution measurements of so2 flux at soufrière hills volcano, montserrat. *Bulletin of Volcanology*, 65:578–586, 2003. 10.1007/s00445-003-0286-x.

[19] Henri Eisenbeiss and Martin Sauerbier. Investigation of uav systems and flight modes for photogrammetric applications. *The Photogrammetric Record*, 26(136):400–421, 2011.

[20] J. Engels, D. Dixon-Hardy, and B. Birch. Thickened and paste tailings facilities—measuring the surface geometry. *Infomine Inc*, June 2006.

[21] I. Entezari, B. Rivard, M. Lipsett, and W. Wilson. Application of hyperspectral remote sensing in estimation of oilsands tailings water content. *5th IEEE GRSS Workshop on Hyperspectral image and signal processing*, Gainesville, Florida, 25-28 June 2013.

[22] Federal Aviation Administration. Faa makes progress with uas integration. `http://www.faa.gov/news/updates/?newsId=68004`, 2013. Accessed March 24, 2013.

[23] Federal Geographic Data Committee. National standard for spatial data accuracy. Standard FGDC-STD-007.3-1998, 1998.

[24] Michael Finn, Mark Lewis, David Bosch, Mario Giraldo, Kristina Yamamoto, Dana Sullivan, Russell Kincaid, Ronaldo Luna, Gopala Allam, Craig Kvien, and Michael Williams. Remote sensing of soil moisture using airborne hyperspectral data. *GIScience & Remote Sensing*, 48(4):522–540, 10 2011.

[25] Waldemar I. Friesen. Qualitative analysis of oil sand slurries using on-line nir spectroscopy. *Applied Spectroscopy*, 50(12):1535 – 1540, 1996.

[26] Holly Gonzalez. Nevada and alberta sign mou to promote unmanned sector. $http://www.$ $auvsi.org/2972013/182013AlbertaNevada$, 2013. Accessed January 3, 2014.

[27] Government of Alberta. Tailings fact sheet. $http://oilsands.alberta.ca/tailings.$ $html$, 2012. Accessed March 23, 2013.

[28] D.P. Groeneveld, W.M. Baugh, J.B. Silverman, D.D. Barz, and M.B. Prescott. Non-imaging airborne spectroscopy for calibrating satellite imagery. ASD Application Notes, HydroBio, 2006.

[29] A. Gurtner, D.G. Greer, R. Glassock, L. Mejias, R.A. Walker, and W.W. Boles. Investigation of fish-eye lenses for small-uav aerial photography. *Geoscience and Remote Sensing, IEEE Transactions on*, 47(3):709 –721, March 2009.

[30] W. N. Hamilton and Pauline H. Babet. Alberta clays and shales - summary of ceramic properties. Economic geology report 3, Alberta Research, 1975.

[31] Perry J. Hardin and Thomas J. Hardin. Small-scale remotely piloted vehicles in environmental research. *Geography Compass*, 4(9):1297–1311, 2010.

[32] Dieter Hausamann, Werner Zirnig, Gunter Schreier, and Peter Strobl. Monitoring of gas pipelines - a civil uav application. *Aircraft Engineering and Aerospace Technology*, 77(5):352 – 360, 2005.

[33] Headwall. Microhyperspec data sheet. $http://www.headwallphotonics.com/Portals/$ $145999/docs/ds\_micro\%20hyperspec\_airborne\_solution.pdf$, 2013. Accessed March 24, 2013.

[34] ThomasC. Henderson, Mohamed Dekhil, RobertR. Kessler, and MartinL. Griss. Sensor fusion. In Bruno Siciliano and KimonP. Valavanis, editors, *Control Problems in Robotics and Automation*, volume 230 of *Lecture Notes in Control and Information Sciences*, pages 193–207. Springer Berlin Heidelberg, 1998.

[35] B. Hörig, F. Kühn, F. Oschütz, and F. Lehmann. Hymap hyperspectral remote sensing to detect hydrocarbons. *International Journal of Remote Sensing*, 22(8):1413 – 1422, 2001.

[36] Keith Horton, Glyn Williams-Jones, Harold Garbeil, Tamar Elias, A. Sutton, Peter Mouginis-Mark, John Porter, and Steven Clegg. Real-time measurement of volcanic so2 emissions: validation of a new uv correlation spectrometer (flyspec). *Bulletin of Volcanology*, 68:323–327, 2006.

[37] Hyvista Corp. Hymap sensor contractor. *http://www.hyvista.com/*, 2010. Accessed November 27, 2010.

[38] ING Robotic Aviation. Reinventing aviation. *http://ingrobotic.com/*, 2014. Accessed August 6, 2014.

[39] G. Konecny. *Geoinformation: Remote Sensing, Photogrammetry and Geographical Information Systems*. Geoinformation: Remote Sensing, Photogrammetry and Geographic Information Systems. Taylor & Francis, 2002.

[40] Andy Yaw Kwarteng. Remote sensing assessment of oil lakes and oil-polluted surfaces at the greater burgan oil field, kuwait. *International Journal of Applied Earth Observation and Geoinformation*, 1(1):36 – 47, 1999.

[41] Talita Lammoglia and Carlos Roberto de Souza Filho. Spectroscopic characterization of oils yielded from brazilian offshore basins: Potential applications of remote sensing. *Remote Sensing of Environment*, 115(10):2525 – 2535, 2011.

[42] Jin Liu, Zhiyong Chen, and Ruifang Guo. A mosaic method for aerial image sequence by r/c model. In *Computer Science and Software Engineering, 2008 International Conference on*, volume 6, pages 58 –61, dec. 2008.

[43] Michael Loose. High accuracy pavement comparison between low level mapping and mobile lidar mapping for an interstate project for the pennsylvania department of transportation (penndot). In *ASPRS 2014 Annual Conference*, Louisville, KY, March 23-28 2014.

[44] David G. Lowe. Distinctive image features from scale-invariant keypoints. *International Journal of Computer Vision*, 60(2):91–110, 2004.

[45] A. J. S. McGonigle, A. Aiuppa, G. Giudice, G. Tamburello, A. J. Hodson, and S. Gurrieri. Unmanned aerial vehicle measurements of volcanic carbon dioxide fluxes. *Geophys. Res. Lett.*, 35(6), 03 2008.

[46] A. J. S. McGonigle, C. Oppenheimer, A. R. Hayes, B. Galle, M. Edmonds, T. Caltabiano, G. Salerno, M. Burton, and T. A. Mather. Sulphur dioxide fluxes from mount etna, vulcano, and stromboli measured with an automated scanning ultraviolet spectrometer. *J. Geophys. Res.*, 108(B9), 09 2003.

[47] M. Minacapilli, M. Iovino, and F. Blanda. High resolution remote estimation of soil surface water content by a thermal inertia approach. *Journal of Hydrology*, 379(3-4):229 – 238, 2009.

[48] G. More and X. Pons. Influence of the nature and number of ground control points to the quality of remote sensing geometric corrections. In *Geoscience and Remote Sensing Symposium (IGARSS), 2012 IEEE International*, pages 2356–2359, July 2012.

[49] M. Nagai, Tianen Chen, R. Shibasaki, H. Kumagai, and A. Ahmed. Uav-borne 3-d mapping system by multisensor integration. *Geoscience and Remote Sensing, IEEE Transactions on*, 47(3):701 –708, March 2009.

[50] Natural Resources Canada. The canada centre for remote sensing celebrates 40 years of excellence and innovation. *http://www.nrcan.gc.ca/earth-sciences/geography-boundary/remote-sensing/poster/1887*, 2011. Accessed March 23, 2013.

[51] Ocean Optics. USB2000+ OEM Data Sheet. *http://www.oceanoptics.com/technical/engineering/OEM%20Data%20Sheet%20--%20USB2000+.pdf*, 2012. Accessed May 22, 2013.

[52] Ocean Optics. STS OEM Microspectrometer. *http://www.oceanoptics.com/products/sts.asp*, 2013. Accessed March 24, 2013.

[53] M. Oczipka, J. Bemmann, H. Piezonka, J. Munkabayar, B. Ahrens, M. Achtelik, and F. Lehmann. Small drones for geo-archaeology in the steppe: locating and documenting the archaeological heritage of the orkhon valley in mongolia. *SPIE Remote Sensing for Environmental Monitoring, GIS Applications, and Geology IX*, 7478:747806, 2009.

[54] A. Orduyilmaz, N. Raksuntorn, Q. Du, L. M. Bruce, V. Anantharaj, and S. Wright. Multisensor fusion for mini uav platforms. *Proc. SPIE 6230, Unmanned Systems Technology VIII*, 62300Z:8, 2006.

[55] Paparazzi Project. Lisa/M v2.0. *http://paparazzi.enac.fr/wiki/Lisa/M_v20*, 2013. Accessed May 7, 2013.

[56] Paparazzi Project. Paparazzi control loops. *http://paparazzi.enac.fr/wiki/Control_Loops*, 2013. Accessed Dec 17, 2013.

[57] Paparazzi Project. Welcome To Paparazzi. *http://paparazzi.enac.fr/*, 2013. Accessed May 2, 2013.

[58] Alexey Pasumansky. Photoscan forum: Using camera external orientation. *http://www.agisoft.ru/forum/index.php?topic=224.msg929#msg929*, 2011. Accessed October 20, 2011.

[59] B. Rivard, J. Feng, V. Bushan, and M. Lipsett. Infrared reflectance hyperspectral features of athabasca oil sand ore and froth. In *Hyperspectral Image and Signal Processing: Evolution in Remote Sensing (WHISPERS), 2011 3rd Workshop on*, pages 1–4, june 2011.

[60] B. Rivard, D. Lyder, J. Feng, A. Gallie, E. Cloutis, P. Dougan, S. Gonzalez, D. Cox, and M.G. Lipsett. Bitumen content estimation of athabasca oil sand from broad band infrared reflectance spectra. *The Canadian Journal of Chemical Engineering*, 88(5):830–838, 2010.

[61] Benoit Rivard. Eas 451 class notes. University of Alberta, Fall 2010.

[62] Andrés Rodríguez, Clark Taylor, Yohannes Aregawi, Ronald Dennis, and Todd Jenkins. On-board system for synchronizing video and telemetry on a small uav. *Proc. SPIE 6961, Intelli-*

gent Computing: Theory and Applications VI, 696109:12, 2008.

[63] Floyd F Sabins. Remote sensing for mineral exploration. *Ore Geology Reviews*, 14(3-4):157 – 183, 1999.

[64] Toni Schenk. Digital aerial triangulation. *International Archives of Photogrammetry and Remote Sensing*, 31:735–745, 1996.

[65] Marc Schwarzbach and Uwe Putze. Stuttgarter adler payload. Email, 2012.

[66] Marc Schwarzbach, Uwe Putze, Ursula Kirchgaessner, and Maria V. Schoenermark. Acquisition of high quality remote sensing data using a uav controlled by an open source autopilot. In *ASME IDETC/CIE 2009*, volume 3, pages 595 – 601, San Diego, CA, United states, 2009.

[67] Dmitry Semyonov. Photoscan forum: Algorithms used in photoscan. *http://www.agisoft.ru/forum/index.php?topic=89.msg323#msg323*, 2011. Accessed August 5, 2014.

[68] David Shaw, Martin Phillips, Ron Baker, Eduardo Munoz, Hamood Rehman, Carol Gibson, and Christine Mayernik. Leak detection study. Technical Report DTPH56-11-D-000001, U.S. Department of Transportation Pipeline and Hazardous Materials Safety Administration, 2012.

[69] Sil Industrial Minerals. Sil blasting sands. *http://www.sil.ab.ca/images/stories/pdf/abrasives/silblastsands.pdf*, 2013. Accessed December 19, 2013.

[70] Nagula N Suthaker and J Don Scott. Thixotropic strength measurement of oil sand fine tailings. *Canadian Geotechnical Journal*, 34(6):974–984, 1997.

[71] T. Suzuki, Y. Amano, J. Takiguchi, T. Hashizume, S. Suzuki, and A. Yamaba. Development of low-cost and flexible vegetation monitoring system using small unmanned aerial vehicle. *ICCAS-SICE, 2009*, pages 4808 –4812, aug. 2009.

[72] Timothy M. Terry. Pipeline leak detection technology 2011 conference report. Technical Report 32-1-17411, Shannon & Wilson Inc, 2012.

[73] Trimble. Trimble uas. *http://uas.trimble.com/trimble-uas*, 2014. Accessed August 6, 2014.

184

[74] Kevin Underhill. Preliminary meeting with enbridge. Meeting Notes, May 30 2011.

[75] M. van der Meijde, H.M.A. van der Werff, P.F. Jansma, F.D. van der Meer, and G.J. Groothuis. A spectral-geophysical approach for detecting pipeline leakage. *International Journal of Applied Earth Observation and Geoinformation*, 11(1):77 – 82, 2009.

[76] G. Verhoeven, M. Doneus, Ch. Briese, and F. Vermeulen. Mapping by matching: a computer vision-based approach to fast and accurate georeferencing of archaeological aerial photographs. *Journal of Archaeological Science*, 2012.

[77] G. Verhoeven, D. Taelman, and F. Vermeulen. Computer vision-based orthophoto mapping of complex archaeological sites: The ancient quarry of pitaranha (portugal–spain). *Archaeometry*, pages no–no, 2012.

[78] W. S. Warner and W. W. Carson. Improving interior orientation for asmall standard camera. *The Photogrammetric Record*, 13(78):909–916, 1991.

[79] Roland E. Weibel and R. John Hansman. Safety considerations for operation of unmanned aerial vehicles in the national airspace system. Technical Report ICAT-2005-1, MIT International Center for Air Transportation, 2005.

[80] James A Winnefel and Frank Kendall. Unmanned Systems Integrated Roadmap FY2011-2036. Technical report, US Department of Defense, 2011.

[81] James Yuen, Stephen Dwyer, Amanda Kotchon, Walied Moussa, and Michael Lipsett. Commissioning and vibration isolation of a low cost uas for industrial and environmental remote sensing applications. *ASCE Earth and Space 2012: Engineering, Science, Construction, and Operations in Challenging Environments*, pages 1380 – 1389, April 2012.

[82] N. Zabcic, B. Rivard, C. Ong, and A. Muller. Using airborne hyperspectral data to characterize the surface ph of pyrite mine tailings. In *Hyperspectral Image and Signal Processing: Evolution in Remote Sensing, 2009. WHISPERS '09. First Workshop on*, pages 1 –4, aug. 2009.